UNIVERSITY OF TWENTE.

Bachelor's thesis

Growth of $PbTiO_3$ and $BiFeO_3$ thin films on flat and three-dimensional $SrRuO_3$ surface morphologies

Authors:
H.J. Albers
S.W. de Bone

Applied Physics
Faculty of Science and Technology
Inorganic Materials Science

Supervisors:
B.F. Smith M.Sc.
Dr. ir. G. Koster

1st August 2012

Abstract

When thin films of $PbTiO_3$ or $BiFeO_3$ are grown on a $DyScO_3$ substrate with three-dimensional $SrRuO_3$ structures, two different surface morphologies are observed. In this research, the hypothesis — that this different topography is caused by a difference in surface diffusion of the two materials on $SrRuO_3$ and on themselves — is not confirmed nor contradicted. The eventual conclusion is that the results indicate that the diffusion coefficient $PbTiO_3$ on $SrRuO_3$ is lower than the diffusion coefficient of $BiFeO_3$ on $SrRuO_3$, but that this cannot be seen as actual proof of the hypothesis. This conclusion was formed after an AFM step-by-step analysis of the growth of the two materials on $SrRuO_3$, and a diffusivity analysis of the two materials on flat $SrRuO_3$ surfaces. A kinetic Monte Carlo model was executed to gain more insight in the growth of the materials on 3D $SrRuO_3$ structures. The results of this simulation show that other factors not included in this research — as the bonding of $PbTiO_3$ and $BiFeO_3$ with the $DyScO_3$ substrate — could also influence this difference in growth behaviour for the two combinations.

Contents

Preface & Acknowledgements

After both attending the bachelor study Applied Physics at the University of Twente for almost three years, this academic phase of our study is almost coming to an end. We consider the bachelor assignment as a perfect way to put all of the theory and skills we have obtained over the years into practice.

It was not easy to find a research topic that the both of us would like to put our heart in. However, after a couple of conversations we found that the Inorganic Material Science (IMS) group suited both our interests. Our research assignment consisted of a single sentence: find out why two ferroelectric materials, $PbTiO_3$ and $BiFeO_3$, behave differently when grown on a $DyScO_3$ substrate with three-dimensional $SrRuO_3$ surface morphologies. With the help of our daily supervisor Brian Smith, a PhD student at the IMS group, we started this task brimming with positive attitude.

During our time at the IMS group, we have learned a lot about the our own research as well as the research that is being done at IMS. The weekly colloquia provided us with a lot of insight in the focus of the group, as well as with a nice lunch. The friendly atmosphere made we considered our working environment as a very suitable place to fully focus on our bachelor assignment. We could not have done this research on our own, and would like to thank a couple of people.

The first person we want to thank is our daily supervisor Brian Smith, who was always ready to help us with any problems we came across. Besides helping us cope with some of the problems we have encountered, he also introduced us to the COMAT system and all the other systems used in this research, which is a feat on its own.

We would also like to thank our second supervisor, Gertjan Koster. He helped us find a suitable research topic at IMS and helped us with some of our problems. Besides this, he was always trying to stimulate us to get the most results out of our data.

In the last, but certainly not least, place we want to thank the rest of the IMS group, with in particular Bouwe Kuiper, who assisted us with a few of our experiments and helped acquiring some literature. Another special 'thanks' goes to our room mates at the student room — although their presence sometimes resulted in distractions, it was really nice to have some form of social interaction when working on a serious project like this one. Finally, we also wanted to point out that we are very grateful to a lot more IMS members not mentioned in person in this section: we have been happy to work alongside some of you!

Hugo Albers & Sébastian de Bone
Enschede, August 1st 2012

The committee for this bachelor's thesis consists of:

Dr. ir. G. Koster	—	chairman
B.F. Smith M.Sc.	—	daily supervisor
Dr. J.W.J. Verschuur	—	exam committee

Introduction

In 2011, Kuiper *et al.* published a paper [1] about the self-organization of $SrRuO_3$ (strontium ruthenate) on a double-terminated $DyScO_3$ (dysprosium scandate) substrate. The $SrRuO_3$ seemed to prefer to grown on the ScO_2 termination, instead of growing on both the ScO_2 and the DyO terminations. The results are conducting single crystalline nanowires. Both a Monte Carlo model and a surface morphology study have shown that the self-organized growth resulted from a difference in surface diffusivities of the terminations.

Using *pulsed laser deposition*, the ferroelectric materials $PbTiO_3$ (lead titanate) and $BiFeO_3$ (bismuth ferrite) can be grown on such a $DyScO_3$ substrate with $SrRuO_3$ nanowires. Normally, when comparing the surfaces after the deposition of these ferroelectric thin films, a different surface topography is observed. The $PbTiO_3$ surface seems to copy the samples surface, while the $BiFeO_3$ one seems to form a flat surface after the growth of similar film thickness. The goal of this bachelor assignment is to determine why the materials $PbTiO_3$ and $BiFeO_3$ behave so differently when grown on a $DyScO_3$ substrate with three-dimensional $SrRuO_3$ structures. Since this is a common approach in this research field, the research focusses on comparing the surface diffusivity of $PbTiO_3$ and $BiFeO_3$ on the different underlying materials during deposition ($SrRuO_3$, $DyScO_3$ and the concerning ferroelectric material, $PbTiO_3$ or $BiFeO_3$, itself). In this research, only the influence of diffusion on the $SrRuO_3$ islands and the deposition material ($PbTiO_3$ or $BiFeO_3$) itself were analysed, since it was expected that the role of diffusion on $DyScO_3$ was not that important for the growth behaviour. The expectation was further that the surface diffusion of $PbTiO_3$ on $SrRuO_3$ is smaller than the surface diffusion of the $BiFeO_3$ on $SrRuO_3$ and the surface diffusion of $PbTiO_3$ on itself is smaller than the surface diffusion of $BiFeO_3$ on itself. The general idea behind this hypothesis is that atoms that are deposited on a surface with a large diffusion coefficient tend to diffuse further than atoms that are deposited on a surface with a small diffusion coefficient. So the chance of atoms to stay on an area with a small surface diffusion coefficient is larger than an atom that is deposited on an area with a large surface diffusion coefficient.

In order to find out the exact growing behaviour, both experiments and a model were used to determine the driving factor of the just introduced phenomenon; the different surface topography when depositing either $PbTiO_3$ or $BiFeO_3$ on a $DyScO_3$ substrate with $SrRuO_3$ nanowires. A Monte Carlo model was executed to determine the dependence on the energy barriers due to bonding to the different substrates ($DyScO_3$, $SrRuO_3$ and $PbTiO_3$ or $BiFeO_3$). The experimental parts focussed on two different aspects. The first series of experiments were conducted in order to determine the growth at different times during the deposition of $PbTiO_3$ or $BiFeO_3$. The different stages in the growth process can be clarified by imaging the surface, using an *atomic force microscope* (AFM) after short periods of growth. The samples on which $PbTiO_3$ and $BiFeO_3$ are grown, are $DyScO_3$ substrates on which $SrRuO_3$ islands has been grown. This topography is chosen, because it is very hard to create a consistent nanowire array. The individual pictures can tell one something about the surface morphology and maybe even explain the different topographies. The second series of experiments focussed on determining the diffusivity coefficients of $PbTiO_3$ and $BiFeO_3$ on $SrRuO_3$ and the diffusivities of $PbTiO_3$ and $BiFeO_3$ on $PbTiO_3$ and $BiFeO_3$ respectively. This is done by creating flat $SrRuO_3$ surfaces and monitoring the reflective *high-energy electron diffraction* (RHEED) intensity during the growth process. A flat surface is chosen to prevent three-dimensional structures from interfering with the diffus-

ing atoms and therefore with the characteristics in the RHEED signal. Using this data, the relaxation times and the diffusivity coefficients can be determined and calculated respectively. Both experiments are done in the COMAT system, which is a set-up that enables the user to grow material using pulsed laser deposition, perform scanning probe microscopy, measure the reflective high-energy electron diffraction intensity and do x-ray diffraction measurements. All of these measurements can be done *in situ*.

Growing ferroelectric materials on $SrRuO_3/DyScO_3$ samples could lead to more insight in the influence of these underlying nanostructures on the ferro- and piezoelectric properties of the ferroelectric film. Properties of a ferroelectric film mainly depend on the domain structure in the film. This means that developing methods to control this domain structure is an important task when ferroelectric thin films are used for specific applications, since the desired ordering of the domain structure will be dependent upon the desired application [2]. Application examples of ferroelectric thin films are nonvolatile memories, microelectronics, electro-optics and electromechanical systems [3].

Chapter 1

Theory

1.1 Thin film growth

1.1.1 Epitaxy

An important role in this research is reserved for a growth technique called *perovskite oxide heteroepitaxy*. In the world of thin films, the word 'epitaxy' is used to indicate the type of growth where the deposited film adopts the surface lattice structure of the underlying substrate. Epitaxial thin film growth takes place when the unit cells of the film are placed exactly on the unit cells of the substrate. This is easy to imagine when the film and the substrate are the same material, since here the unit cells of film and substrate have the same size. (The epitaxy phenomenon in this case, with the same material for substrate and film, is known as *homoepitaxy*.) However, epitaxy is also possible for the growth of different film materials in comparison with the substrate. It can even occur when the lattice parameters of film and substrate differ (and therefore the size of the unit cells). When this happens, epitaxy is obtained by straining the film lattice so it corresponds with the substrate lattice. Epitaxy for different substrate and film materials is known as *heteroepitaxy*.

1.1.2 Growth at thermodynamic equilibrium

The film morphology created in systems at thermodynamic equilibrium (for small or moderate vapour supersaturation) can be determined by analysing the free energies of the film surface (γ_F), the substrate surface (γ_S) and the interface between film and substrate (γ_{FS}). Layer-by-layer growth (Frank-van der Merwe growth) takes place when $\gamma_F + \gamma_{FS} < \gamma_S$, so in the case where there is a strong bonding between film and substrate [4]. Low bonding between film and substrate, on the other hand, means island growth (Volmer-Weber growth) is obtained. In the latter case the free energies of the interfaces are related by $\gamma_F + \gamma_{FS} > \gamma_S$. Besides these two modes, a third growth mode is possible for heteroepitaxial growth; in this mode the lattice mismatch between substrate and film causes accumulating strain energy for every successive film monolayer. A release of this strain energy after a few monolayers causes a transition from layer-by-layer to island growth. This combination of layer-by-layer growth followed by island growth is known as the Stranski-Krastanov mode.

1.1.3 Kinetic effects during deposition

When the supersaturation of the vapour is high, kinetic effects have to be taken into account for describing the growth. This means that the thermodynamic approach is no longer sufficient when dealing with *pulsed laser deposition* (PLD), which is a *physical vapour deposition* technique. High supersaturation goes hand in hand with a high nucleation rate, which limits the surface diffusion. For homoepitaxial growth, different important parameters play a role in modelling the

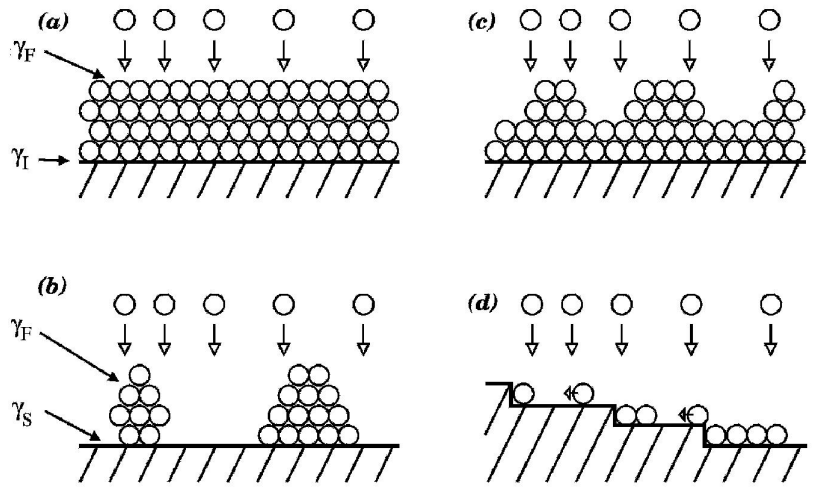

Figure 1.1: Four different growth modes: (a) layer-by-layer or Frank-Van der Merwe, (b) island or Volmer-Weber, (c) Stranski-Krastanov and (d) step flow [6].

deposition: the surface diffusion coefficient (D_S) of the adatoms, the sticking probability of an adatom arriving at the edge of a terrace, and the additional energy barrier (E_S) for adatoms to descent the edge to a lower terrace. De diffusion coefficient determines the surface diffusion length l_D (the average distance an adatom can travel on a flat surface before being trapped), shown in the following relation, where τ is the residence time before re-evaporation:

$$l_D = \sqrt{D_S \tau} \tag{1.1}$$

The surface diffusion coefficient is determined by equation 1.2. Here, E_A is the activation energy for diffusion, ν the attempt frequency and a the characteristic jump distance [7].

$$D_S = \nu a^2 e^{-E_A/(k_B T)} \tag{1.2}$$

These diffusion characteristics play a role in a forth growth mode: step flow growth. This mode takes place on a *vicinal surface*, a surface consisting of descending terraces with a certain length l_T caused by an inevitable miscut of the substrate — an example is shown in figure 1.1(d). Step flow growth occurs when the average diffusion length l_D is sufficiently larger than the terrace width l_T. In this case, the mobility of the adatoms is high enough to reach the step edges, leading to a shift in the positions of the steps. When l_T does not change in this process, the substrate is stable. It can occur, though, that l_T does change (at certain positions) during step flow growth and the substrate step distribution is not reflected in the step flow growth.

1.2 Kinetic growth parameters on a singular surface

RHEED intensities always show a strong correlation with the laser pulses [6]. A typical characteristic in these intensities is the coverage-dependent relaxation time. Layer-by-layer growth on singular surfaces can be analytically described by solving the time-dependent diffusion equation (formula 1.3), after which the step density model of Stoyanov and Michailov could be used to model the RHEED oscillations for given deposition and diffusivity parameters [8]. Using this model the other way around makes it possible to determine diffusivity parameters from RHEED oscillation data, as long as the growth conditions match the growth conditions assumed for the model. The model, for instance, assumes instantaneous nucleation at the start of every monolayer and is based on the growth of a material onto a singular surface, where the start of the second monolayer should not begin before the first monolayer is completely finished. Nucleation

on the surface is modelled describing the nuclei as circular islands with a radius ρ. The model is used to discover surface diffusion coefficients of different growth combinations by determining the relaxation times τ.

$$\frac{\partial^2 n_s}{\partial r^2} + \frac{1}{r}\frac{\partial n_s}{\partial r} = \frac{1}{D_S}\frac{\partial n_s}{\partial t} \tag{1.3}$$

Solving the diffusion equation in equation 1.3, where n_s is the initial condition $n_s(r,0) = n_0$ (n_0 being the density of instantaneously deposited particles due to one laser pule), equations 1.4 and 1.5 are the boundary conditions. Assuming the edge acts as a perfect sink leads to equation 1.6, with τ_m given in equation 1.7.

$$n_s(r = r_0) = n_{SE} \tag{1.4}$$

$$(\frac{\partial n_s}{\partial r})_{r=0} = 0 \tag{1.5}$$

Using these boundary conditions and equation 1.3, a solution can be found. This solution is given in equation 1.6, where A_m are prefactors with a small dependence on r and r_0. This equation becomes more simple when looking at large times. When t is large, only the first terms of equation 1.6 have to be considered.

$$n_s(r,t) = n_0 \sum_{m=1}^{\infty} A_m(r;r_0)e^{-\frac{t}{\tau_m}} \tag{1.6}$$

The variable τ_m is given by equation 1.7. Here, τ represents the relaxation time.

$$\tau_m = \frac{r_0^2}{D_S(\mu_m^{(0)})^2} \tag{1.7}$$

In equation 1.7, the value $\mu_m^{(0)}$ is the root of the m^{th} order Bessel function. Without nucleation on top of the islands, the size of the growing islands depends on the coverage given by equation 1.8, where $\pi\rho_2^2$ is the area of the islands. The variable N_S is the nucleation density, which can be determined experimentally.

$$\pi\rho_2^2(t) = \frac{\theta(t)}{N_S} \tag{1.8}$$

$$\tau_2 = \frac{\theta}{D_S(\mu_1^{(0)})^2\pi N_S} \tag{1.9}$$

$$\pi\rho_1^2(t) = \frac{1-\theta(t)}{N_S} \tag{1.10}$$

$$\tau_1 = \frac{1-\theta}{D_S(\mu_1^{(0)})^2\pi N_S} \tag{1.11}$$

Equations 1.8 to 1.11 all use the subscript one or two on the left side of the equation. This subscript indicates the level of the diffusing particles, the height difference is depicted in figure 1.2. So, subscript 1 means a diffusing particle on the substrate and subscript 2 a diffusing particle on top of the islands. Equations 1.8 and 1.10 describe the area sizes as a function of the coverage θ and the nucleation density N_S. Equations 1.9 and 1.11 both describe the decay time τ_m. These equations can be used to determine the diffusivity D_S of a material when the relaxation time is known. Equation 1.8 gives the area of the islands, while equation 1.10 gives the area between the islands. This means that the coverage used in equation 1.10 should be $(1-\theta)$, instead of θ. Equation 1.12 is a recursive formula that gives the change in coverage as a function of the relaxation times τ_m, time t and the density of deposited particles $1/n_p$.

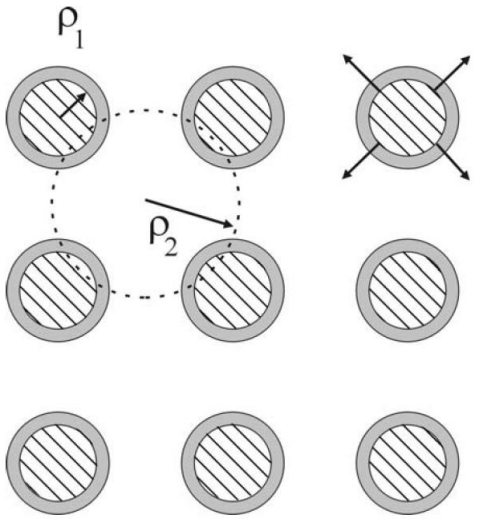

Figure 1.2: A depiction of the islands, with a coverage θ, and the area between the islands. [6].

$$\Delta\theta_n(t) = \frac{\theta_{n-1}}{n_p}(1 - e^{-\frac{t}{\tau_2}}) + \frac{1 - \theta_{n-1}}{n_p}(1 - e^{\frac{t}{\tau_1}}) \tag{1.12}$$

Using equation 1.3, the step density (S) can be determined.

$$I(t) \propto 1 - \frac{S(t)}{S_{max}} \tag{1.13}$$

Equation 1.14 is determined by using equations 1.9 and 1.11 in equation 1.6. When one assumes a direct coupling of the averaged particle density and the diffusive scattered intensity, an exponential increase of the intensity is expected. Equation 1.14 gives this intensity, where I_0 is the intensity just after the deposition.

$$I \sim I_0(1 - e^{-\frac{t}{\tau}}) \tag{1.14}$$

Equation 1.14 can now be used to determine the relaxation time of the material by fitting this equation to the acquired data.

1.3 Materials in this research

In order to grow a material epitaxially, the lattice constants of materials should match; the unit cells of the material should have the same size as the unit cells of the substrate. If the lattice parameters do not match, lattice mismatches can occur. Lattice mismatches lead to strain and will eventually cause three-dimensional structures to appear. This, of course, is unwanted for epitaxial growth. The materials used in this research all have similar (pseudo-cubic) cell parameters. This allows for epitaxial growth, which is why the materials are a suitable subject of this research.

1.3.1 Perovskites

Four materials are extensively used in this research: $PbTiO_3$ (lead titanate), $BiFeO_3$ (bismuth ferrite), $DyScO_3$ (dysprosium scandate) and $SrRuO_3$ (strontium ruthenate). All four materials have crystal lattices arranged in the so-called *perovskite structure* (molecular formula ABO_3). A unit cell of this three elements containing oxide structure is schematically drawn in figure 1.3.

The displayed image shows a unit cell of a cubic perovskite, from which it becomes clear that the structure can be seen as a construction of alternating AO and BO_2 planes placed on one another.

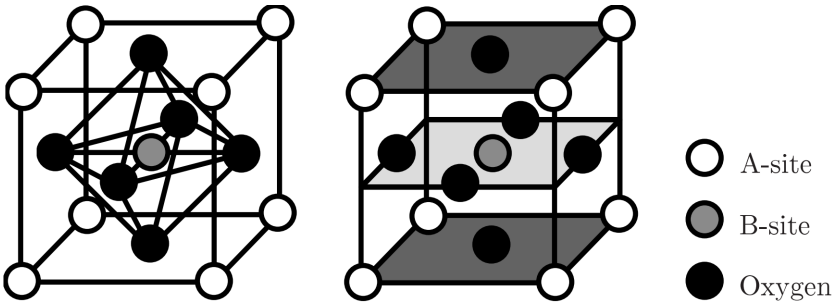

Figure 1.3: The perovskite oxide structure model [25].

1.3.2 Lattice parameters

Unlike the perovskite structure drawn in figure 1.3, the structures of three of the four materials are not cubic under the used experimental conditions. Two of them ($DyScO_3$ and $SrRuO_3$) have unit cells with a substantial longer c-axis compared to the a and b-axis, which at their turn differ only slightly from each other. This corresponds to a *orthorhombic* structure. $PbTiO_3$ does have a cubic unit cell, but undergoes a transition above 720 K to a *tetragonal* perovskite structure ($a = b \neq c$). The other ferroelectric material, $BiFeO_3$, has *rhombohedral* unit cells. This structure is basically a cubic structure (so with $a = b = c$) stretched along the body diagonal. This means that the faces of the rhombohedral cell are not squares, but are all identical parallelograms (with top angels of the three faces $\alpha = \beta = \gamma \neq 90\,^\circ$).

Although only one of the materials has a cubic structure, they all have cell parameter ratios which makes it possible to consider them as *pseudo-cubic* lattices. To be classified as pseudo-cubic, the parameters of the orthorhombic cell should measure up to $a \approx b \approx \sqrt{2}a_0$ and $c \approx 2a_0$ [5]. Here, a_0 is the lattice parameter of the pseudo-cubic perovskite cell, and a, b and c are respectively in the [110], [1$\bar{1}$0] and [001] direction of the pseudo-cubic structure. Figure 1.4 is drawn to clarify the way this cubic structure can be deduced from the orthorhombic unit cell with the given lattice parameters. The consideration of a pseudo-cubic lattice is even more convenient in the rhombohedral case. Since $a = b = c$ for the rhombohedral cell, a pseudo-cube with lattice parameter $a_0 = a/\sqrt{2}$ can be used to describe the lattice structure. Figure 1.5 shows how this works in the specific case of $BiFeO_3$.

An analysis of the lattice parameters known for the four materials in the literature shows that the pseudo-cubic lattice parameter a_0 is approximately equal for all the materials. This makes all the materials very suitable for epitaxial growth on one another. For $DyScO_3$, the lattice constants of the orthorhombic unit cell are $a = 0.5720$ nm, $b = 0.5442$ nm and $c = 0.7890$ nm [26]. This lattice can be described by a pseudo-cubic lattice with cell parameter $a_0 = 1/2\sqrt{a^2 + b^2} \approx \frac{c}{2} = 0.3945$ nm. This value differs only slightly from the pseudo-cubic lattice parameter of $SrRuO_3$, which is $a_0 = 0.393$ nm ($a = 0.555$ nm, $b = 0.556$ nm and $c = 0.786$ nm [27]). The lattice constants of $PbTiO_3$ are experimentally determined to be 0.3969 nm for cubic and 0.3904 nm for tetragonal [28]. The rhombohedral unit cell of $BiFeO_3$ is found to be approximately $a = 0.5635$ nm, corresponding to a pseudo-cubic parameter of $a_0 = a/\sqrt{2} = 0.3985$ nm [9].

1.4 Monte Carlo simulations

When it comes to gaining more insight in growing phenomena expected to be related to diffusivity, computer simulations based on the theory described in section 1.1 ('Thin film growth') is often

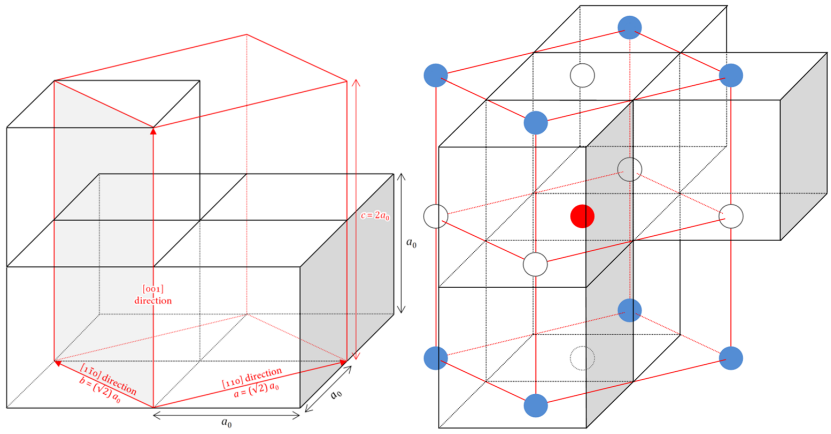

Figure 1.4: The relation between the actual orthorhombic unit cell of the perovskite materials involved in this experiment and the pseudo-cubic unit cell that can be used as an alternative for indicating the existing structure. The orthorhombic unit cell (with $a \approx b$, and $c \approx \sqrt{2}a$) is drawn in red lines, while the cubic representation of this structure (with lattice parameter a_0) is marked black.

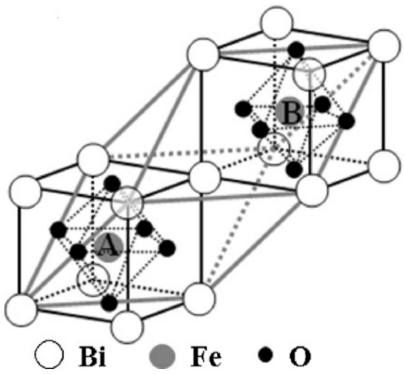

Figure 1.5: The rhombohedral unit cell of $BiFeO_3$ drawn in one picture with the pseudo-cubic alternative [11].

performed. The use such simulations allows for modelling more complex growth types than the one given in section 1.2 ('Kinetic growth parameters on a singular surface'). A widely used computer model in this type of research is the *solid-on-solid* (SOS) model first described by Weeks and Gilmer [10]. In this model, diffusion of deposited particles on a simple cubic lattice is simulated by lattice hopping of single entities on the surface, using a Monte Carlo algorithm.

1.4.1 Kinetic solid-on-solid model

The solid-on-solid model as introduced by Weeks and Gilmer [10] describes the surface of a lattice as columns perpendicular to the (001) plane. These columns have a certain integer height h_i, consisting of piled up cubic entities. The surface is then represented by an array of integers specifying the number of atoms on each column. This means that in this model, only the uppermost entity of the column i gets a change to hop to a neighbouring lattice site j, resulting in an increase by one entity in the h_j value and a decrease by one integer in the h_i value. It also means that each occupied site in a certain column is directly placed on another entity, excluding 'overhangs' and making clear where the name of the model comes from.

The solid-on-solid model is always applied in combination with a Monte Carlo algorithm. This type of algorithms are characterized by making use of random sampling, mostly used for simulations of systems which many couples degrees of freedom. It is therefore an indeterministic method especially useful as more efficient alternative in comparison with deterministic approaches for this type of systems. In the realm of the research presented in this report, kinetic Monte Carlo simulations have been proven to be particularly useful as a tool for describing atomistic principles of thin film growth with both pulsed laser deposition (see section 2.1, 'Pulsed laser deposition') as molecular beam epitaxy (another deposition technique). The basic principle of each thin film growth simulation is kept identical in practically every research. For molecular beam epitaxy, the deposition of an atom or molecule is normally approached by the instantaneous appearance of one entity at a random position of the surface, after which this cluster or adatom can hop over the surface (in accordance with the kinetic theory described in section 1.1) for as long as the calculated total diffusion time allows [12]. Having a higher deposition rate, pulsed laser deposition is, on the other hand, in general simulated by instantly generating much more particles at the same moment at different lattice sites on the surface, after which all the adatoms at the surface get the change to hop in certain directions, one at the time [6, 8, 13, 25]. The site and in which direction the uppermost atom is allowed to move, is selected by a random number generator. In this process, however, adatoms with a higher possibility of moving also have a higher change of doing so.

The entities used in the solid-on-solid model could be single atoms, as well as complete clusters or unit cells. For perovskite growth simulations, an entity usually represents an entire unit cell. This is a convenient assumption for the simulation, since this way all of the deposited objects are the same and thus have the same interaction with each other. There are however examples where single atoms form the entities in the simulation of perovskite structured molecules (cf. [13]). The three different atom types of the deposited ABO_3 perovskite should in that case be generated in the stoichiometric ratio A : B : O = 1 : 1 : 3. This single atom approach is of course more in accordance with the complex growth during the real deposition, but the assumption to treat unit cells as single entities is sufficient most of the times.

1.4.2 Characteristics of the algorithm

The diffusivity in Monte Carlo kinetic simulations is usually described by using an Arrhenius equation like the one in equation 1.2 in section 1.1. This equation is used in the form of equation 1.15 for Monte Carlo algorithm. Equation 1.15 calculates the hopping rate k_i for a certain site i on the surface. This hopping rate depends on multiple components. As shown in equation 1.16, the diffusion barrier E_D^i is composed of the surface diffusion barrier for a free particle on site i due to bonding with the surface (E_S^i) plus the number of nearest-neighbours bonds $n_i = (0, 1, ..., 4)$ of the site multiplied by the energy E_N for each bond formed with a nearest-neighbour. The number of nearest-neighbours is calculated by simply comparing the height of the column under site i with the height of the four closest neighbouring columns. If the height of a neighbouring column h_j is equal to or greater than h_i, an nearest-neighbour is assigned to the particle on site i. Furthermore, in equation 1.15, k_0 represents the attempt frequency for hopping, k_B is the Boltzmann constant and T the sample temperature during the simulated deposition [10]. For simulations of heteroepitaxial growth, the diffusion barrier E_D^i of a site i can change after a first deposited particle is placed on the substrate, due to epitaxial misfit strain or a different atomic termination [14]. A difference in termination is represented by a change in the surface diffusion barrier E_S^i. Taking the misfit strain into accounts also asks for a different E_N value during the growth in the simulation. In this model, ideal sticking of arriving atoms is assumed and no re-evaporation is allowed.

$$k_i = k_0 \, \mathrm{e}^{-E_D^i/k_B T} \tag{1.15}$$

$$E_D^i = E_S^i + n_i \cdot E_N \tag{1.16}$$

From these relations, it becomes clear that the hopping rate is higher for particles with less nearest-neighbours and a relatively low surface diffusion barrier E_S^i, than for particles with many nearest-neighbours and a high diffusion barrier. As stated before, particles with a higher hopping rate have a higher probability of hopping in the model. This is achieved in the model by summing the hopping rates in all four directions ($d = 1, 2, 3, 4$) for all the lattice sites ($i = 1, 2, ..., N$) on the surface, this results in the total hopping probability L (given in formula 1.17), and generating a random number $0 < r < L$ which selects the event (hopping in a certain direction of a certain lattice site) that will be executed [15]. This procedure is explained in more detail in figure 1.6.

$$L = \sum_{i=1}^{N} \sum_{d=1}^{4} k_{i,d} \tag{1.17}$$

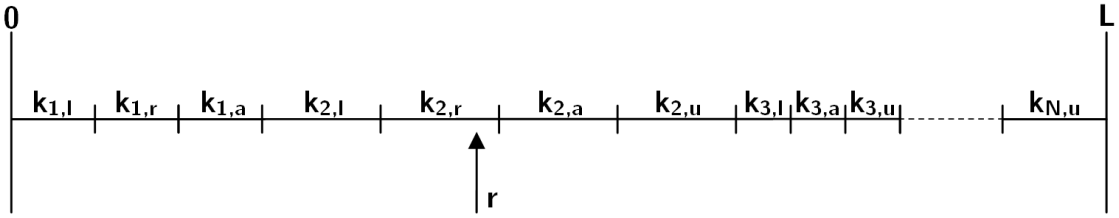

Figure 1.6: A schematic illustration of the procedure used to select hopping events. L is the total hopping probability, calculated in equation 1.17. In the figure, this calculation is depicted in a line segment. Here, $k_{i,d}$ is the hopping rate of site i in direction d. For example, $k_{1,l}$ is the hopping rate of the first lattice site for a move to the lattice site on the left of this site (in these subscripts, r represents hopping to the right, a a move to the lattice site above i, and u a diffusion to the site under i). As can be seen in the line segment, there is no $k_{1,u}$, meaning that a move in this direction is not possible. The hopping rate is in this case set to zero, making sure that such an event is never selected. A random point r ($0 < r < L$) on this line segment is selected. The place of this point on the line determines which event will be executed in the simulation. In this case, the surface particle on site 2 will move to the lattice position on the right.

As described in the previous section (section 1.4.1), the deposition of particles on the surface is simulated by generating new particles at random lattice sites. After these particles are deposited, the hopping rates of all the lattice sites are calculated and the selection execution of hopping events starts. Only one particle moves at the time, after which the hopping rates are updated and a new event is selected. This diffusion process is repeated until a new deposition pulse takes place. The number of hopping events between two laser pulses is determined by solving the elementary probability theory, shown in equation 1.18 [15]. This equation gives the distribution of time intervals τ between events.

$$P(\tau)\ \mathrm{d}\tau = L\ \mathrm{e}^{-L\tau}\ \mathrm{d}\tau \tag{1.18}$$

Now, substituting $u = \exp(-L\tau)$ in the equation leads to the conclusion that u should be a random value, uniformly distributed between 0 and 1. This results in a full expression of the time passed on the simulation clock between successive events in the form of equation 1.19, where r_2 is another random number, this time between 0 and 1.

$$\tau = L^{-1}\ (-\ln\ r_2) \tag{1.19}$$

Chapter 2

Fabrication and Characterization Techniques

2.1 Pulsed laser deposition

Pulsed laser deposition (PLD) is a physical vapour deposition technique, where a thin film is deposited by vaporizing the material from a target onto the substrate [6]. Physical vapour deposition techniques have led to a leap in research capabilities in a lot of fields from superconductivity to ferroelectrics. The physical vapour deposition techniques allow for a huge flexibility in the molecular structure of a bulk material, because of the layer by layer growth.

Physical vapour deposition is the collective term for all deposition techniques that deposit a thin layer of a certain target material onto a substrate. Examples of these physical vapour deposition techniques are sputter deposition, molecular beam epitaxy and chemical vapour deposition. Sputter deposition uses a sputtering gas that has a molecular weight similar to the target material. The inert gas collides with the target material resulting in the ejection of ions. Molecular beam epitaxy uses a heating coil to evaporate the target material, which is directed onto the substrate. Chemical vapour deposition uses a volatile precursor that reacts or decomposes on the substrate, to create a thin layer.

Pulsed laser deposition differs from other physical vapour deposition techniques from the simple fact that the thin layers are deposited by a plasma plume that is created by ablating a material from a target with a high powered laser.

2.1.1 Basics of pulsed laser deposition

A thin film is deposited by focussing a high energy pulsed laser onto a target. This laser causes the material to ablate. The laser pulse creates a dense vapour layer in front of the target, which is ionised because of pressure and temperature increase. This vapour layer forms into a plasma plume that points towards the substrate on which the material needs to be grown. The plasma particles generally reach energies of several hundred electron-volt (eV). The ablation process is at a low pressure and not in vacuum. A deposition in vacuum would cause the particles to scatter all over the system instead of forming a plasma plume. A typical background pressure is 1 to 50 Pa. The presence of a gas mixture allows one to control the interaction of the plasma with the gas, which in turn gives rise to the possibility of controlling the kinetic energy of the plasma particles. Multiple parameters control the instantaneous deposition rate, laser energy density (at the target), pulse energy, distance between the target and the substrate and the ambient gas properties like mass and pressure (used gasses are H_2, O_2 and Ar). This gives rise to one of the biggest advantages of PLD compared to the other physical deposition techniques: the possibility of growing very fast in a controlled way. A very high deposition rate leads to a large degree of supersaturation $\Delta\mu$, as is shown in equation 2.1.

$$\Delta\mu = k_B T \ln \frac{R}{R_0} \tag{2.1}$$

In this equation, $\Delta\mu$ represents the supersaturation of the vapour, k_B is the Boltzmann constant, T is the temperature and R/R_0 is the ratio of the deposition rate (R) and the deposition rate at equilibrium (R_0). Supersaturation causes two-dimensional nucleation of high density clusters. This nucleation takes place after the laser pulse. Some of these clusters are unstable and dissipate over the surface as adatoms.

All of these previously mentioned parameters determine what growth mode is possible. Step flow growth happens if the atoms diffuse to a step edge before they nucleate into a island. This growth mode is obtained by using a high temperature or using a high miscut substrate. In layer-by-layer growth mode, the islands nucleate on the surface until a critical island density is reached. At this point, depositing more material will lead to a fusion of the different islands. The three-dimensional growth mode is a lot like the layer-by-layer growth mode, but the nucleation also takes place on top of the islands. Therefore, a three-dimensional structure is created in this mode.

2.1.2 Setup

The basic parts of the PLD setup are: laser, reaction chambers, ablation target, substrate, substrate heater, and equipment to measure the growth process. The laser used in the setup is a high powered ultra-violet laser. The ablation target is positioned on a rotating holder, so multiple targets can be used in the experiment to create a substrate that consists of multiple materials. The substrate itself is positioned in such a way that the ablation plume is centred on the substrate. The substrate is held by a heater, which has an open backside so a laser can be focussed onto the substrate. This laser heats the substrate to the desired temperature. Besides the actual components of the PLD, the chambers also contain measuring equipment like reflective high energy-electron diffraction (RHEED).

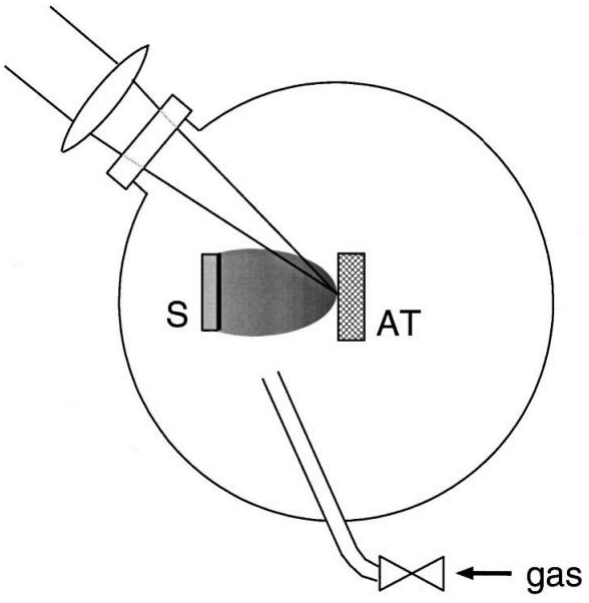

Figure 2.1: A depiction of a pulsed laser deposition setup. The laser beam is focused onto the ablation target (AT), this forms a plume that is directed onto the substrate (S). Multiple valves in the system regulate the gas flow and concentration of gasses in the system [16].

.

2.2 Scanning probe microscopy

Scanning probe microscopy is the collective term for all microscopy techniques that use a physical probe to scan a substrate. This section focusses on two techniques in particular: atomic force microscopy and scanning tunnelling microscopy. Scanning probe microscopy has a big advantage over optical microscopy because it is not limited by a diffraction limit. Some techniques can also be used to modify the surface, or make nanostructures, by using the tip to pick up, push or drag an object.

2.2.1 Atomic force microscopy

Atomic force microscopy (AFM) is a scanning probe microscopy technique capable of imaging surface topography with a nanometer scale resolution. AFM images can provide different information compared to similar images made with a scanning tunneling microscope (STM) or a scanning electron microscope (SEM). This is the case for images of metallic and micro-structures, because of the capability to acquire reliable nanometer scale measurements [17]. The AFM can measure in different modes: contact mode, non-contact mode and tapping mode. Each of these modes has its advantages and disadvantages. This will be explained in the section 'Modes of operation.'

Basic principles and setup

The AFM is build up out of a number of key components that require some explanation: the cantilever, piezoelectric tube, base, laser, photodiode combination and sample holder [2]. The tip is micromachined or etched onto a cantilever, an example of this can be seen in the SEM image in figure 2.2. This tip shape is not the only possible tip shape. To name a few: spheres or tips with carbon nanotubes are also used. A laser is focussed onto the top part of the cantilever. When the z-position of the tip changes, the reflection of the laser is shifted up or down. The reflections of the laser are correlated with certain changes in height of the surface. This can be measured using an a photodiode setup, that consists of four photodiodes positioned in a square. In order to measure height differences in the substrate, the substrate needs to be stabilised. This can be done in different ways. Simple examples are: placing the base onto a large slab of granite or placing the base onto springs to disconnect the base from the rest of the setup.

When engaging the tip to a surface, a force curve can be measured. An example of a force curve is depicted in figure 2.3. When approaching the substrate, the van der Waals force causes the cantilever to bend towards the substrate. When the tip is engaged, this force starts to be cancelled by electrostatic forces. The intersection of the force curve with the x-axis therefore represents the point at which the cantilever is back into it's horizontal position.

Modes of operation

The AFM can run in a couple of operational modes: contact mode, non-contact mode and tapping mode [18]. In figure 2.4 an illustration of the different modes is shown. In contact mode, the tip is lowered onto the surface and scrapes over the surface when measuring. Contact mode can operate in two modes: constant height mode or constant force mode. Constant height mode keeps the tip at the same position by changing the position of the piezoelectric tube or the step motor. In constant force mode, the deflection of the tip stays constant but the z-position of the tip changes. The force set point is usually in the range of 2-4 nN. Advantages of contact mode are high scan speeds, the possibility of atomic resolution and the possibility of scanning surfaces with huge height differences. But this mode also has some disadvantages: capillary forces cause relatively large forces on the tip (this causes some problems *ex situ*) and lateral forces distort the image. The combination of these forces reduces the resolution and can cause damage to the tip.

In non-contact mode the user operates in the attractive force region. In this mode, the tip is near the surface (at a distance of approximately 50 to 150Å) while measuring the change in van

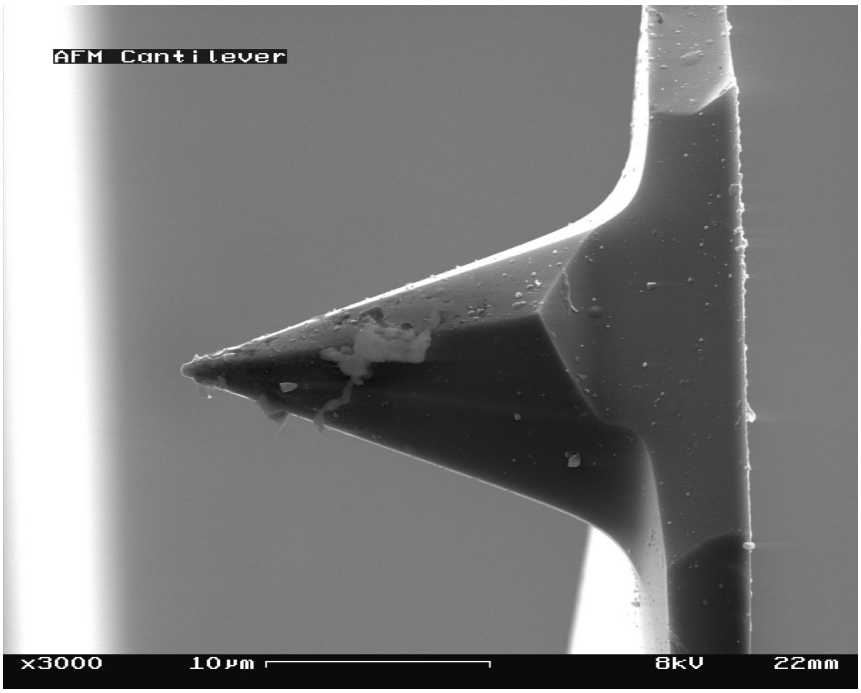

Figure 2.2: A used atomic force microscope cantilever, imaged by a scanning electron microscope, magnification 3000x.

de Waals forces. The advantages of non-contact mode is that the tip exerts a small force on the sample surface. This makes this mode suitable for certain kind of materials, since no damage is caused when using soft samples. The disadvantages of the mode are the lower lateral resolution because of the notable tip-sample separation, a slower scan speed (for avoiding contact with a possible fluid layer) and the fact that it is only applicable for extremely hydrophobic samples with a minimal fluid layer or in a environment with a low humidity and pressure.

In tapping mode the tip is oscillating at or near its harmonic frequency. The tip is lowered onto the substrate until it starts tapping the substrate gently. When scanning the substrate the amplitude is kept constant and a change in amplitude correlates to a change in height. Advantages of tapping mode are a high lateral resolution (1 to 5 nm), almost no lateral forces and low tip-sample force resulting in less damage to soft samples in air. A disadvantage of tapping mode is the slower scan speed than in contact mode [18].

2.2.2 Scanning tunnelling microscope

Scanning tunnelling microscope (STM) is scanning probe microscopy technique that is able to characterize the surface topography of conducting surfaces [20]. A small metal tip is brought very near the surface, at a distance in the order of tens of ångströms [21]. When a voltage bias is applied over the surface and the tip, this is close enough to measure a tunneling current. The tip scans over the surface and changes in surface height and density of states cause changes in the measured current. This gives rise to two different modes of operation: constant current and constant height mode. In constant current mode, the feedback system adjusts the height in order to keep the measured current constant. In constant height mode, on the other hand, the voltage and height are kept constant by varying the current between the tip and the surface. STM can also give information about the electronic structure by applying a sweeping voltage on a single point on the surface. This is called scanning tunnelling spectroscopy.

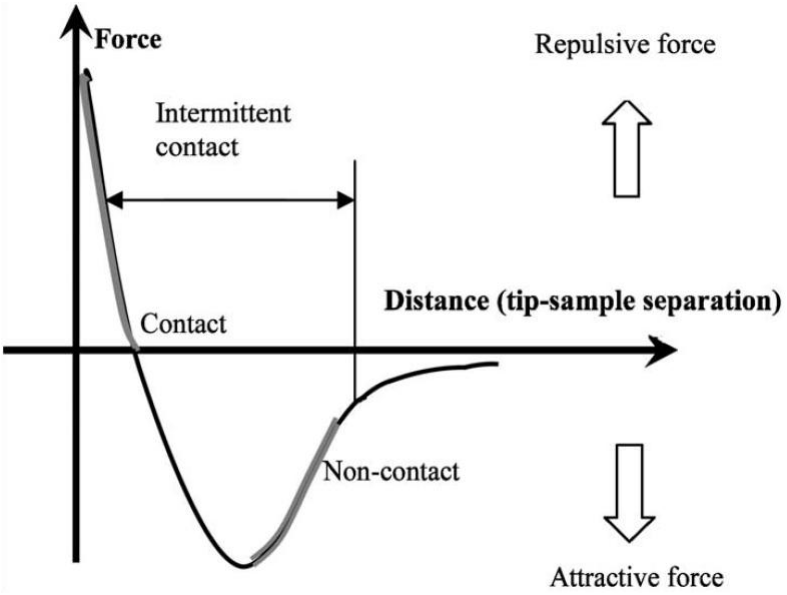

Figure 2.3: A force curve that shows the dependence of the force, experienced by the tip, when the tip-sample distance changes [17].

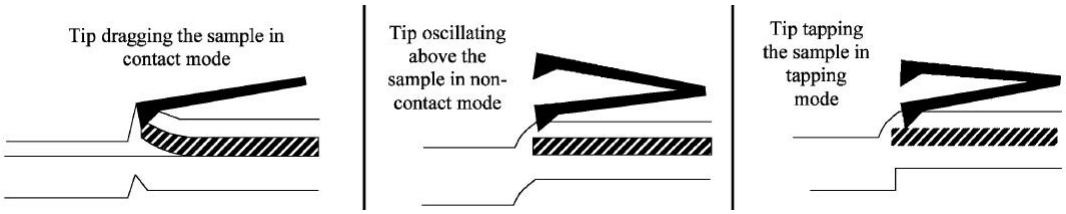

Figure 2.4: A depiction of the different AFM operating modes, from left to right contact mode, non-contact mode and tapping mode [17].

Setup

The STM has a similar setup as the AFM, which is described in the previous section. A vibration free base holds the surface. The tip is attached to a piezotube, that controls the x-, y- and z-motion of the tip over the surface. Finally, a feedback loop determines the corrections that the piezotube needs to apply to keep the height or current constant. The major differences compared to the AFM are the tip and the feedback loops. The tip does not need to be as well defined as the AFM tip: a low budget STM tip can be made by cutting a tungsten wire at a crooked angle. Tungsten or a platinum iridium alloy are commonly used materials for the tip. The STM feedback loop differs from the AFM feedback loop in the simple fact that different quantities need to be kept constant. The resolution of a STM image is, just as for the AFM, bound by the used tip. Obviously, this resolution is never infinitely good, since each tip will always allow some tunnelling in other than a perfect vertical direction.

2.3 Reflection high-energy electron diffraction

Reflection high-energy electron diffraction (RHEED) is a surface characterization technique. An electron beam is directed onto the substrate at glancing angle. The electrons are then diffracted

Figure 2.5: A transmission electron microscope image of an scanning tunnelling microscope tip [22].

by the atoms. At some specific angles the electrons interfere constructively and form a pattern that can be viewed by using a photoluminescent plate. A simple CCD camera is enough for capturing these diffraction spots [24].

2.3.1 Setup

The setup used for RHEED is quite simple. It consists of an electron beam, a photoluminescent plate and a CCD camera [23]. The electron beam is produced by an electron gun. This beam is focused on the substrate surface by using a magnetic and an electric field. The electrons form a diffraction pattern that is visualized by use of a photoluminescent screen. As stated before, a CCD camera can measure the intensity of the spots and the positions.

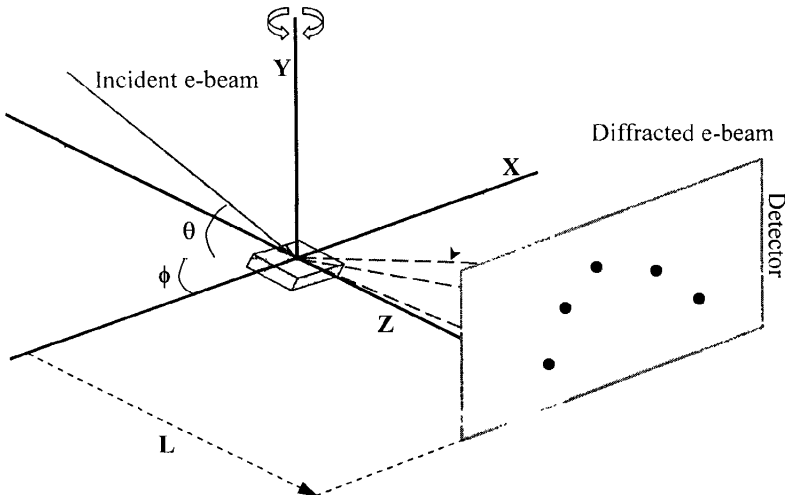

Figure 2.6: A simplified depiction of the RHEED setup [23].

2.3.2 Application

RHEED can be used to determine structural properties of the top layers of a sample. During the growth process the surface is periodically roughened and smoothed by nucleation and growth, which changes the step density and therefore the RHEED intensity [6]. This periodicity can be seen in figure 2.7, where the homoepitaxial growth of $SrTiO_3$ is monitored using RHEED. Figure 2.7 shows two oscillations. The oscillation with the biggest amplitude shows the formation of the monolayers. When the RHEED intensity decreases, the surface roughness increases until a critical surface coverage is reached. From this point on, the surface roughness start decreasing and the monolayer is beginning to form. In figure 2.7 this process is repeated twice. The oscillations with smaller amplitude represent the individual depositions and are strongly correlated to the laser pulses. Each pulse leads to a change in surface roughness: the adatoms diffuse over the substrate until there kinetic energy is depleted. This can clearly be seen in the insets of figure 2.7 (two of these small oscillations have been enlarged in the upper figure). In these two pictures the relaxation time (the time the adatoms need to lose their kinetic energy) can be determined. This can be achieved with the data from the RHEED intensity oscillation by finding the time it takes for the intensity to flatten. The relaxation time determines the diffusivity, so by determining and comparing the relaxation times conclusions about the diffusivity of a certain material substrate combination could be formulated.

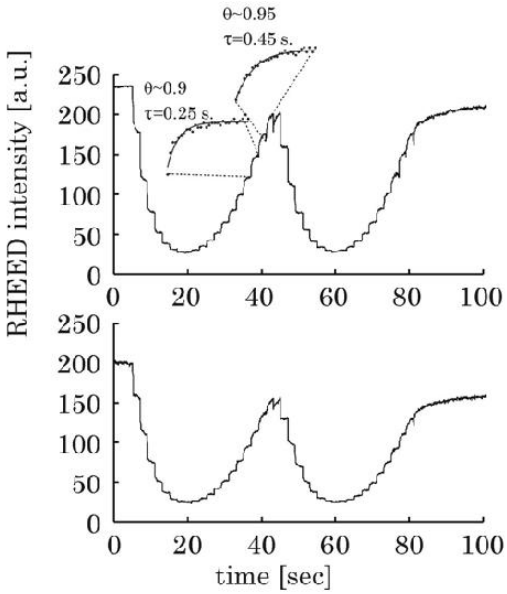

Figure 2.7: A specular RHEED intensity oscillation plot of homoepitaxial growth of $SrTiO_3$ at 3 Pa at 750 °C and 650 °C respectively [6].

Chapter 3

Experimental Settings

In the previous chapter multiple experimental techniques have been introduced. Most of these fabrication and characterization techniques have multiple modes and set-ups that could be used during for doing experiments. This chapter presents the experimental settings and equipment used for this research.

3.1 $SrRuO_3$ growth on double terminated $DyScO_3$ substrates

Since this is the basis of all the samples used in this research, the first step for all the experiments was the thin film growth of $SrRuO_3$ on a $DyScO_3$ substrate. By exploiting the possible presence of both terminations (AO and BO_2 — or in this case DyO and ScO_2) on the surface of a perovskite crystal, one could create a three-dimensional structure by growing $SrRuO_3$ on a $DyScO_3$ substrate. This fabrication of three-dimensional $SrRuO_3$ structures was carried out by using the experimental experience gained by Kuiper *et al.* [25, 1].

The first step in this process is the treatment of the $DyScO_3$ substrate. In order to create double terminated substrates suitable for growing nanowires, Kuiper *et al.* performed an experimental analysis containing the anneal time and sample miscut angle [25]. Unfortunately, no clear relations were found between these variables and the distribution of the terminations, although an experimental method which delivered the most mixed terminated samples was derived. The $DyScO_3(110)$ substrates are all cleaned and annealed for 4 hours at 1000 °C. After the annealing, the surface morphology of the substrates was determined using tapping mode AFM.

The most common form of double termination found in [25] was the unit cell stacking depicted in figure 3.1. As shown in this picture, this stacking mode is characterized by half unit cells up followed by differently terminated one and a half unit cells down at each of the preexisting vicinal steps (caused by a miscut of a certain angle) of the substrate. Whether a substrate is mixed terminated or not could be determined by using AFM. An important AFM output in this respect is the phase image. Phase images are the result of a phase shift in the measured signal compared to the drive signal [25]. A difference in the interaction between the tip and the sample for the different terminations of a perovskite could cause such a phase shift. This makes analysing phase images a convenient method for samples where the termination areas of both DyO and ScO_2 are substantial, since in this case the phase image clearly shows this mixed termination. However, when one of the two termination areas is small and directly followed by a surface step, the amplitude error as a result of the presence of the step could make it impossible to see the mixed termination in the phase image. In that case, a mixed termination could still be visible in height profiles of the AFM images. This might require a thorough analysis, though, since a step of half a unit cell corresponds to an increase of only 0.2 nm in the height profile.

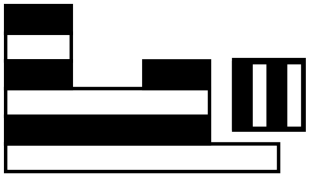

Figure 3.1: Most common form of unit cell stacking in case double termination is found at the substrate. The black boxes represent A-site terminations, while the white boxes are B-site terminations. The inset shows a schematic view of the phase contrast when this type of mixed termination is measured [25].

3.2 Pulsed laser deposition parameters

All the films used for this research are created with pulsed laser deposition (PLD). Multiple parameters and settings for PLD have been introduced in section 2.1, 'Pulsed laser deposition'. Important growth parameters are energy density, heater temperature, gas flow, process pressure, frequency, ablation time, anneal gas, anneal time and anneal pressure. The earlier mentioned growth modes can be obtained by varying some of this parameters. The parameters used in this research are listed in table 3.1 for the depositions done in this research. The values in table 3.1 are based on experience with these materials for many years and can be considered as the optimum growth conditions of the concerning materials on these substrates. Further, the $PbTiO_3$ and $BiFeO_3$ depositions were set in such a way that the adatoms are given enough time to diffuse, so the deposition process itself did not interfere with the research of finding out why the two ferroelectric materials grow differently on $SrRuO_3$ structures.

	$SrRuO_3$ (flat)	$SrRuO_3$ (islands)	$PbTiO_3$	$BiFeO_3$
Energy density (J/cm^2)	2.1	2.1	2.0	1.9
Heater temperature ($^\circ C$)	690	630	640	630
Gas flow O_2/Ar (O_2%)	50	50	100	100
Process pressure (mbar)	0.3	0.3	0.13	0.13
Laser frequency (Hz)	1	1	1	1
Ablation time (min)	36	6	various	various
Mask size (mm^2)	60	60	60	60
Anneal gas	O_2	O_2	O_2	O_2
Anneal time (min)	30	30	120	120
Anneal pressure (mbar)	100	100	100	100

Table 3.1: Pulsed laser deposition growth parameters

3.3 Fabrication of the samples

A total of six $DyScO_3$ substrates is used in this research. These six substrates are divided over the two main research segments. In the first segment, a step by step analysis of the growth of both $PbTiO_3$ and $BiFeO_3$ on $SrRuO_3$ islands is conducted using four substrates. The idea behind this analysis was to gain a better understanding of the growth behaviour. The analysis consisted of measuring the topography of the surface at different stages during the growth. The $SrRuO_3$ islands were created using the PLD setting given in 3.1. Initially, two samples with $SrRuO_3$ were prepared (from this moment on referred to as 'sample 1' for both $PbTiO_3$ and $BiFeO_3$). After this, the $PbTiO_3$ sample was deposited with two ablations of 3 minutes, while the $BiFeO_3$ one was treated with two 12 minutes depositions. The difference in these ablation times on both of

the samples is selected to correct for the different growth rates of the two ferroelectric materials. After each deposition, the surface morphology was determined *in situ* in the COMAT system. In order to gain more detail about the growth, it was then decided to perform another identical analysis, but now look at different growth stages. Again two $DyScO_3$ substrates were deposited with $SrRuO_3$ using the parameters listed in 3.1. This time however, the samples (referred to as the 'second samples' in the rest of the text) were treated with consecutive 1.5 and 3 minutes deposition for $PbTiO_3$ and 6 and 12 minutes for $BiFeO_3$, to make sure AFM images after these ablations gave insight in two new stages for each sample (since these stages were skipped in the first analysis).

The second part of this research consisted of gaining more information about the diffusion parameters for the growth of the two ferroelectric materials on $SrRuO_3$. Using the theoretical model described in section 1.2 ('Kinetic growth parameters on a singular surface'), diffusivity coefficients could be calculated from relaxation times in measured RHEED intensities during the growth. Since the model described growth on singular surfaces, a flat $SrRuO_3$ layer was needed to learn more about the diffusivity of $PbTiO_3$ and $BiFeO_3$ on $SrRuO_3$. This flat layer was created using the PLD parameters shown in 3.1. Apart from a higher temperature (which enhances surface diffusivity and therefore provides in general smoother surfaces), these parameters differ, when compared to the conditions for growing $SrRuO_3$ islands, especially in the ablation time. Short ablations create $SrRuO_3$ islands, but long enough depositions will eventually make the surface flat. After the creating of two flat $SrRuO_3$ samples (again one for each of the two ferroelectric materials), the samples were checked with *in situ* AFM and deposited with $PbTiO_3$ and $BiFeO_3$. The RHEED intensities were recorded during these depositions, since the relaxation behaviour shown in this data contained information about the diffusivity. The ablation times of the last two depositions are not important for this research; since these depositions were only done for determining the diffusivity on a flat $SrRuO_3$ surface, the length of these depositions is only dependant on the amount of RHEED data needed.

3.4 Scanning probe microscopy settings

All parts of the experiment used some form of scanning probe microscopy to determine the surface topography. As explained in the previous chapter, different scanning modes can be used to determine this topography. All modes have their own advantages and disadvantages.

In the *in situ* scanning probe microscope of the COMAT system, both non-contact and contact mode AFM, as well as STM images were made during this research. When using the *in situ* AFM, one does not have to cope with small layers of fluid on the surface, which makes both contact and non-contact mode viable options. According to the theory, the scan speed in contact is normally a lot higher compared to non-contact mode. However, *in situ* non-contact mode operates faster than *ex situ* because it is not hindered by a layer of water. All images between two successive depositions on the same sample are made *in situ*. Since $SrRuO_3$ is a conducting material, doing *in situ* STM was a suitable alternative for imaging $SrRuO_3$ surface topographies. This is why the $SrRuO_3$ islands on the two samples 1 in the first part of the research (the step by step analysis) as well as the flat $SrRuO_3$ surfaces in the second section are both examined using the STM mode in the COMAT scanning probe microscope. The surface topography of the $SrRuO_3$ islands grown on the two samples 2 in the first research segment were determined using contact mode AFM, since this was convenient in combination with doing $PbTiO_3$ and $BiFeO_3$ surface measurements in the same time span — measurements of the same samples after the first deposition of either $PbTiO_3$ or $BiFeO_3$ on each of the samples. On $PbTiO_3$ and $BiFeO_3$ sample 1, the surface morphology after the both of the concerning ferroelectric depositions was found using *in situ* non-contact mode AFM.

Ex situ tapping mode AFM provided AFM images after the last deposition on $PbTiO_3$ and $BiFeO_3$ sample 2. In general, tapping mode provides the best results when measuring outside a vacuum system, since the presence of a small water layer on top of the sample makes non-contact mode useless and contact mode less accurate, as noticed before. In the same AFM in the same

mode, also the images of the $DyScO_3$ substrates were made (after annealing and before the first depositions). On this substrates, the presence of any mixed terminations could be determined by analysing phase images of the AFM pictures (as explained in the beginning of the chapter, 3.1). Tapping mode AFM is one of the AFM modes providing phase information.

3.5 Conditions for determining diffusivity parameters

While the first part of the research consisted of a step by step growth analysis, the second part was focussed on putting the theory about diffusion into practice in order to gain more perception about the diffusivity parameters during $PbTiO_3$ and $BiFeO_3$ growth on $SrRuO_3$ structures. More information about diffusivity parameters involved in these growth combinations is obtained by subjecting the growth to the conditions given in section 1.2 ('Kinetic growth parameters on a singular surface'). In this section, an analytical solution to the time-dependent diffusion equation is provided, based on certain assumptions. When this solution is combined with a widely accepted step density model, diffusivity parameters could be obtained by analysing RHEED oscillations. To use this model for this purpose, the growth conditions should match the growth assumptions for the derivation as much as possible. Therefore — since the model is based on diffusion on a singular surface — $PbTiO_3$ and $BiFeO_3$ were grown on flat $SrRuO_3$ surfaces. The fabrication of this surfaces is described in the beginning of this chapter (section 3.3, 'Fabrication of the samples').

Ultimately, the goal of this research section was to calculate diffusivity coefficients (D_S) from relaxation times extracted from RHEED intensities. The direct relation between these two parameters is given in equation 1.9 (in section 1.2). One should, however, bear a few things in mind before solving this equation for one unknown parameter. The relaxation time τ, for example, depends on the surface morphology. It can be determined by making a best fit of equation 1.14 for any RHEED intensity segment that shows relaxation behaviour, but it should be noticed that a τ used in the theoretical model of section 1.2 is only the relaxation time on one surface level. The model assumes layer-by-layer growth and thus has to deal with two relaxation times, since there are at most two levels during this type of growth: one on top of the nucleation islands and one in between these islands. The τ used in equation 1.9 is the relaxation time on top of the nucleation island. In order to get a useful relaxation time from the RHEED oscillations, one should determine τ at coverages close to unity (this means where the surface roughness is low and the intensities reach the maximum), given that in this case most of the deposited material will come down on top of the islands. For this part of the research, the diffusivity coefficient for growth of the concerning ferroelectric on $SrRuO_3$ is therefore determined after the first few $PbTiO_3$ or $BiFeO_3$ deposition pulses(thus on places where the surface is still almost flat $SrRuO_3$ and the coverage — seen from $PbTiO_3$ or $BiFeO_3$ perspective — is close to zero). The coefficient for the growth of the ferroelectric material on itself, on the other hand, is determined for laser pulses very close to the formation of the first monolayer — this means at coverages close to unity where the RHEED intensity, after going through the first minimum, is (almost) back at the starting position, indicating the growth of one monolayer. In each of the situations, this makes sure that the relaxation behaviour in the RHEED data is especially caused by events on top of islands and the influence of diffusion in between the islands plays a minimal role.

When in possession of the relaxation time of a RHEED recovery signal, the nucleation density N_S should also be determined before the diffusivity coefficient D_S can be calculated using equation 1.9. This density, being the number of nuclei per unit area, could ideally be determined by simply counting the number of islands per unit area when watching the surface with a scanning probe microscope after the deposition of less than half a monolayer. That means, before the RHEED intensity reaches the minimum. In theory, this nuclei density stays the same for the first part of the monolayer growth; the number of nucleation islands does not change and the coverage only determines the radius of the islands. Right when the RHEED intensity reaches the minimum value, the coalescence of the islands starts, which decreases the step density and therefore increases the RHEED intensity. Unfortunately — for practical and time-dependent reasons

— this has not been done for the substrates used in this particular experiment. Therefore a different way of determining the nucleation density had to be devised. This alternative method consist of estimating the N_S ratio for $PbTiO_3$ and $BiFeO_3$ growth by comparing the RHEED intensity drops after each deposition pulse. These drops only provide an indication of the ratio for the growth of the two ferroelectrics. This makes the determination of an absolute value for the diffusivity coefficients impossible, but still allows for a comparison between the coefficients of $PbTiO_3$ and $BiFeO_3$ growth.

3.6 Simulation features and settings

Apart from the two experimental parts, a computer simulation is also used in this research. The algorithm for this simulation is based on the theory described in section 1.4 ('Monte Carlo simulations'), and written in the programming language of the MATLAB program (developed by the MathWorks company). This program is well known for its user-friendliness when it comes to analysing experimental and analytical data. The programming language, 'M-code' or just 'M', allows one to write algorithms in a very simple and straightforward way.

3.6.1 Construction of the algorithm

The model is composed out of the basics mentioned in section 1.4 in combination with some extra components. A few of these components impose some restrictions in the model. For example, the hopping rate k_i is determined by the column height of the concerning nearest-neighbour. When the neighbouring site is two or more steps higher than i, a hop to this site is not allowed and the hopping rate in this direction is set to zero. In the model, a grid of 100×100 lattice points is used. In order to minimize boundary effects, periodic boundary conditions have been assigned to the grid sites of all the four boundaries. These conditions mean that the left grid border is directly attached to the boundary on the right and the upper border to the lower one — a particle moving to the left when positioned on the left border will with these conditions appear at the neighbouring lattice site on the right border.

Because the growth of $PbTiO_3$ and $BiFeO_3$ on three-dimensional $SrRuO_3$ structures should be analysed, the substrate that serves as beginning condition for the growth simulation was prepared to contain islands (simply created by adjusting the height h_i of the concerning columns). Initially, 25 equally divided circular islands with a radius of 11 pixels were created and afterwards deposited on. Later, also some simulations with 9 circular islands with a 21 pixel radius were done. Both type of islands were 23 entities high. To take the surface diffusion barrier into account, three different values should be attached to the model — i.e. the diffusion barrier for the growth of the concerning ferroelectric ($PbTiO_3$ or $BiFeO_3$) on $DyScO_3$ (the substrate material of the grid in between the islands), on $SrRuO_3$ (for particles deposited on the islands and the barrier for homoepitaxial growth of the ferroelectric material on itself. The surface barrier for growth on $DyScO_3$, from now on mentioned by $E_{S,D}$ should be assigned to the lattice sites who have their uppermost particle right on top of the $DyScO_3$ substrate. In case a second particle will land on such a first particle, the surface barrier of the site is updated since the highest particle in column i is now not in direct contact with the substrate any more; $E_{S,F}$, the energy barrier of the ferroelectric particle due to the interaction with a service containing the same ferroelectric material is now activated for site i. The same principle is utilized for deposition on top of a $SrRuO_3$ islands; of course with the difference that the first ferroelectric particle on a $SrRuO_3$ island has to deal with the surface diffusion barrier of the ferroelectric growth on $SrRuO_3$ ($E_{S,S}$). The nearest-neighbour bonding energy E_N is kept constant (at $E_N = 0.25$ eV, a value based on simulations done in previous comparable research, cf. [25]) for the simulations executed, just as the temperature, which was set 300 °C (to decrease simulation time) for each of the simulations. Furthermore, an attempt frequency $k_0 = 10^{13}$ is used.

The number of particles that instantly appear at random lattice sites during the simulation of the deposition, is determined by a parameter n_p, the number of pulses needed for the completion

of one monolayer of the concerning ferroelectric material. For all the simulations done, this parameter was set to $n_p = 20$. After the deposition, the hopping rates are calculated for all the highest particles in each of columns on the lattice. These rates are determined by simply counting the number of nearest-neighbours for each site, discovering what the type of particle the underlying particle is and checking in which direction diffusion is allowed and. Columns with topmost particles who are part of the initial substrate are not allowed to move. When this process is completed, the internal simulation clock is reset (τ is set to zero) and the diffusion starts: the total hopping probability is calculated, a random number is generated and the corresponding event is selected. For this selection, a binary chop algorithm is used. This algorithm, described in detail in [15], constantly divides the events in two groups with the same amount of events. It then checks if the generated value r is in the first group. If this is the case, the first group is divided in two groups and a check whether r is in the first of these groups is performed. If this is not the case, the same procedure is done for the second group. This process is repeated until only one event is left: this is the event represented by r. The actions of the selected event are then executed, which unfortunately changes the hopping rates of the sites involved in this hopping and there nearest-neighbours. Therefore, only these local hopping rates are renewed. As last step, the simulation clock is moved forward by the amount of $\tau = 1/L$, where L is the total hopping probability at the beginning of the last iteration. When all of this is done, the next diffusion event takes place, in which the whole procedure as described above is repeated. This is done until the simulation time τ reaches the value of the selected time (one second for the simulation in this research) between two laser pulses. In that case a new deposition takes place, after which the simulation clock is reset and the millions of diffusion events are again selected and executed.

3.6.2 Simulation parameters

Some of the parameters for the computer model are already mentioned in the previous section. These are however the parameters that are kept constant in all the simulations. The surface diffusion barriers for the different growth combinations have been varied for different runs of the model. As basic values, surface diffusion barriers of $E_S = 0.85$ eV and $E_S = 1.2$ eV were used. It was then examined what variations of one or two of the three important diffusion barriers ($E_{S,D}$, $E_{S,S}$ and $E_{S,F}$) meant for the growth behaviour. The effect of these diffusion barriers on the diffusion is already known and follows very simple from the Arrhenius equation: a higher E_S value means a lower hopping rate and therefore a lower diffusion length. With this in mind, expectations for the growth behaviour have been composed, which have lead to the parameters selected for the simulations. For example, if the $E_{S,S}$ (the surface diffusion barrier for a $PbTiO_3$ or $BiFeO_3$ particle on a directly underlying $SrRuO_3$ unit cell) is relatively low, the morphology will probably need less depositions to become flat then in the case where $E_{S,S}$ is high. This behaviour is expected, because particles have a hight diffusion length when $E_{S,S}$ is small. The particles deposited on the $SrRuO_3$ islands will therefore easier descend to the lower situated region in between the islands, reducing the height difference between the substrate and the islands. Eventually, a layer of the deposited ferroelectric material will be formed on top of the islands, eliminating the influence of $E_{S,S}$, but when that happens, the height difference is already smaller than in cases where a layer of deposited material will be formed earlier on the islands as a result of a relatively high $E_{S,S}$ value. Such an expectation could be logically deduced for each of the surface barrier combinations. By keeping the other parameters constant in the simulation, one is able to get more insight in the influence of each of the different variables and to verify if these expectation match the outcomes of the simulation. The parameters used in the simulations are shown in table 3.2. These values are (apart from the $E_S = 2.5$ eV and $E_S = 0.15$ eV cases) based on typical values used in this research field and have proven to be reliable options for diffusion barriers. The distinct difference between this and the more extreme E_S values is chosen in order to make an effect caused by a change in the particular E_S values as clear as possible.

		$E_{S,D}$ (eV)	$E_{S,S}$ (eV)	$E_{S,F}$ (eV)
(25 islands)	simulation 1	0.85	0.85	0.85
	simulation 2	0.85	0.85	0.55
	simulation 3	1.2	1.2	1.2
	simulation 4	0.85	0.15	0.85
	simulation 5	0.85	2.5	2.5
	simulation 6	0.85	0.15	2.5
	simulation 7	1.2	1.2	0.25
(9 islands)	simulation 8	1.2	1.2	1.2
	simulation 9	0.25	1.2	1.2

Table 3.2: Parameters used in the simulation model for growth on circular $SrRuO_3$ islands.

Chapter 4

Results

In this chapter the experimental results of our research are presented. To observe the growing behaviour in greater detail, a step by step analysis of the surface at different stages during the growth is executed. Further, using RHEED intensity oscillations and the model presented in section 1.2 ('Kinetic growth parameters on a singular surface'), a study concerning the diffusivity of the growth on the various materials was carried out — since a difference in diffusivity was expected to cause the different growth phenomena of the two ferroelectric materials on the $SrRuO_3$ islands. The results of both research sections are discussed in the next chapter.

4.1 Step by step analysis of growth on $SrRuO_3$ island

In this section, AFM pictures at different stages of the $PbTiO_3$ and $BiFeO_3$ growth are presented. For this part of the research four samples are used (two samples for each of the two ferroelectric materials). For each of the samples, the surface morphology is determined at four consecutive stages of the growth: i) after annealing the $DyScO_3$ substrate, ii) after the 6 minute deposition of $SrRuO_3$ and — for both iii) as iv) — after depositing thin layers (of different thickness) of the concerning ferroelectric material.

4.1.1 $PbTiO_3$: a topography respecting material

As stated before, two different $DyScO_3(110)$ substrates are used for the analysis of the $PbTiO_3$ on $SrRuO_3$ growing phenomenon[1]. Tapping mode AFM pictures of the two substrate samples are shown in figures 4.10(a) and (b). Although the substrates do not show any clear mixed termination at first sight, a closer look shows both terminations indeed seem be present at various places on the surface. This is not directly obvious when looking at the phase information of the AFM measurements (which shows only little phase differences between the bright lines caused by the surface steps), but surface profiles like the ones in figures 4.10(c) and (d) reveal the existence of surface steps 0.5 unit cell down followed by 1.5 unit cell up at certain sections of the substrate surface. This step pattern on this substrate indicates the presence of mixed termination, as is shown in previous research done by Kuiper [25]. The particular step composition in this case, with the pattern for mixed termination only shown at some places along the surface steps (not along the entire steps), makes both substrates not ideal for growing $SrRuO_3$ nanowires. Nevertheless, they were still expected to deliver regular islands.

On both substrates, a six minute deposition of $SrRuO_3$ was executed using pulsed laser deposition at a frequency of 1 Hz. The used growth parameters can be found in table 3.1. The results were indeed islands, as becomes clear from both RHEED images and the STM and contact mode AFM pictures that were made *in situ* in the COMAT system (see figures 4.2(a) and (b)

[1] The measurements of sample 1 of both $PbTiO_3$ and $BiFeO_3$ — figures 4.2 and 4.4 — were done by Brian Smith.

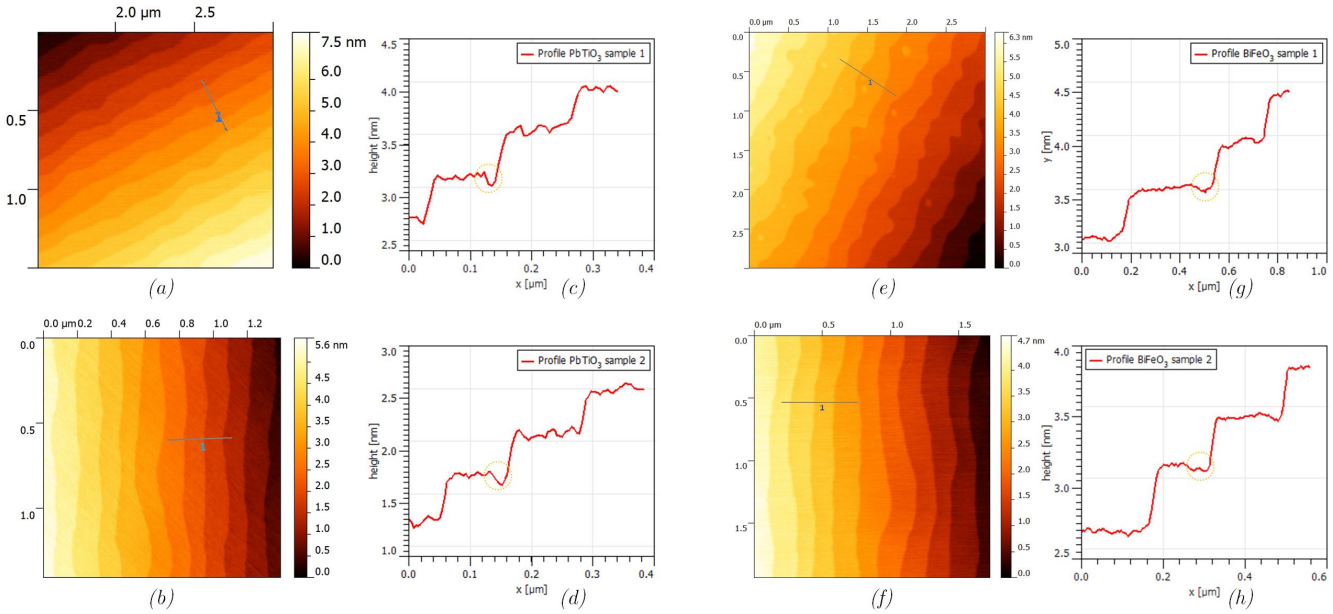

Figure 4.1: Surface sections made with tapping mode AFM after annealing of the four substrates used for both the $PbTiO_3$ as $BiFeO_3$ analysis. $PbTiO_3$ sample 1 is grown on substrate (a), $PbTiO_3$ sample 2 on substrate (b), $BiFeO_3$ sample 1 on substrate (e) and $BiFeO_3$ sample 2 on substrate (f). Figures (c), (d), (g) and (h) show height profiles along the lines drawn in respectively figure (a), (b), (e) and (f). The dotted circles show positions where a mixed termination is probably present — indicated by a drop in the height profile (close to the surface step) of approximately a half unit cell (0.2 nm) followed by an increase in height of 1.5 unit cells (0.6 nm), as explained in section 3.1 ('$SrRuO_3$ growth on double terminated $DyScO_3$ substrates'). AFM phase information of these substrates (not shown here) showed no sign of clear mixed termination along straight lines. This in combination with the observation that the shown height structures for mixed termination were only present at various small areas along the surface (so, with numerous large interruptions along the lines of the surface steps) makes that all of the four substrates were expected to provide regular islands (instead of nanowires), when a thin layer of $SrRuO_3$ was grown on them.

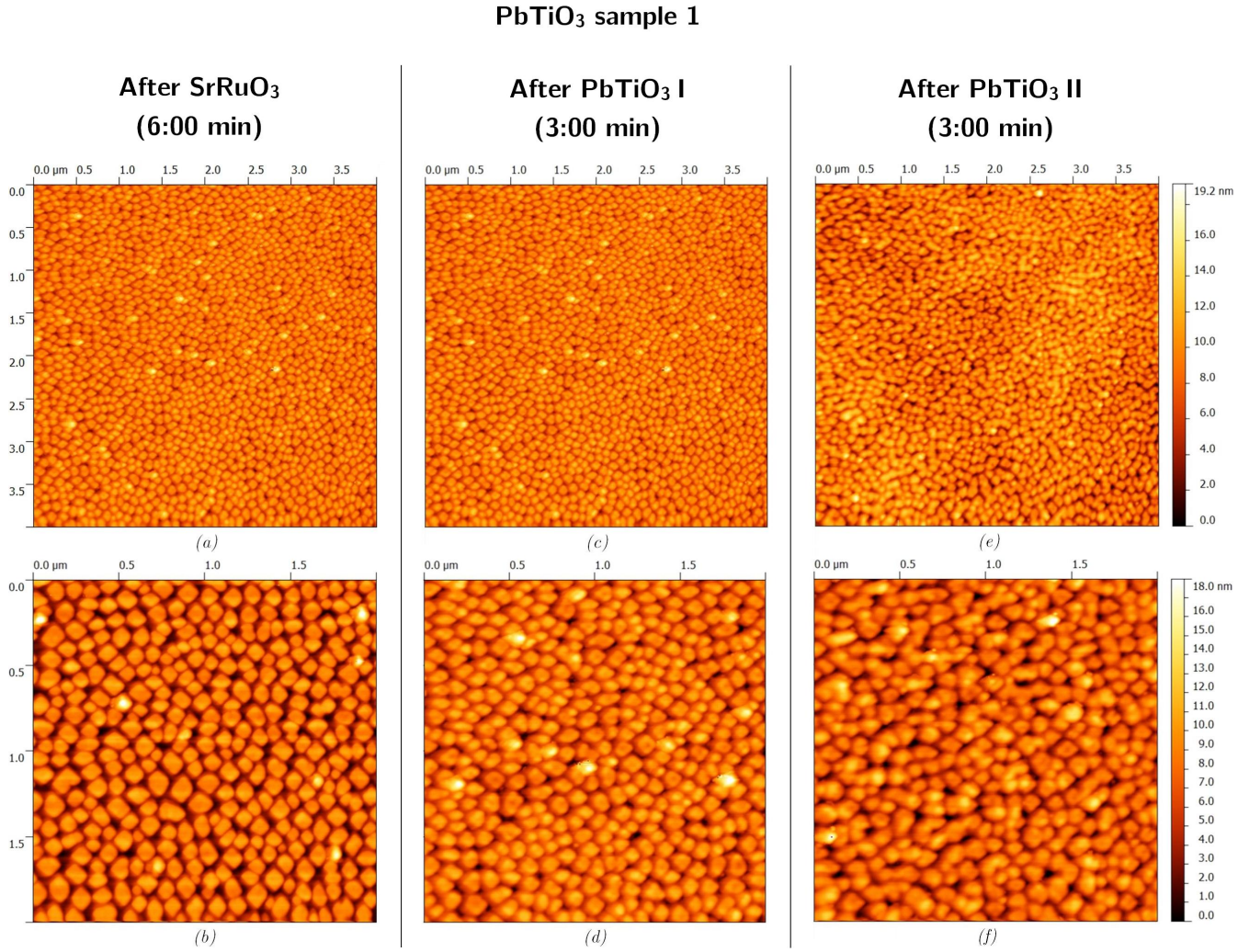

Figure 4.2: $PbTiO_3$ sample 1: STM — (a) and (b) — and non-contact mode AFM — (c), (d), (e) and (f) — pictures of the surface at different stages during the growth. Pictures (a) and (b) are made after the deposition of $SrRuO_3$, (c) and (d) after the first $PbTiO_3$ deposition and (e) and (f) after the second $PbTiO_3$ deposition.

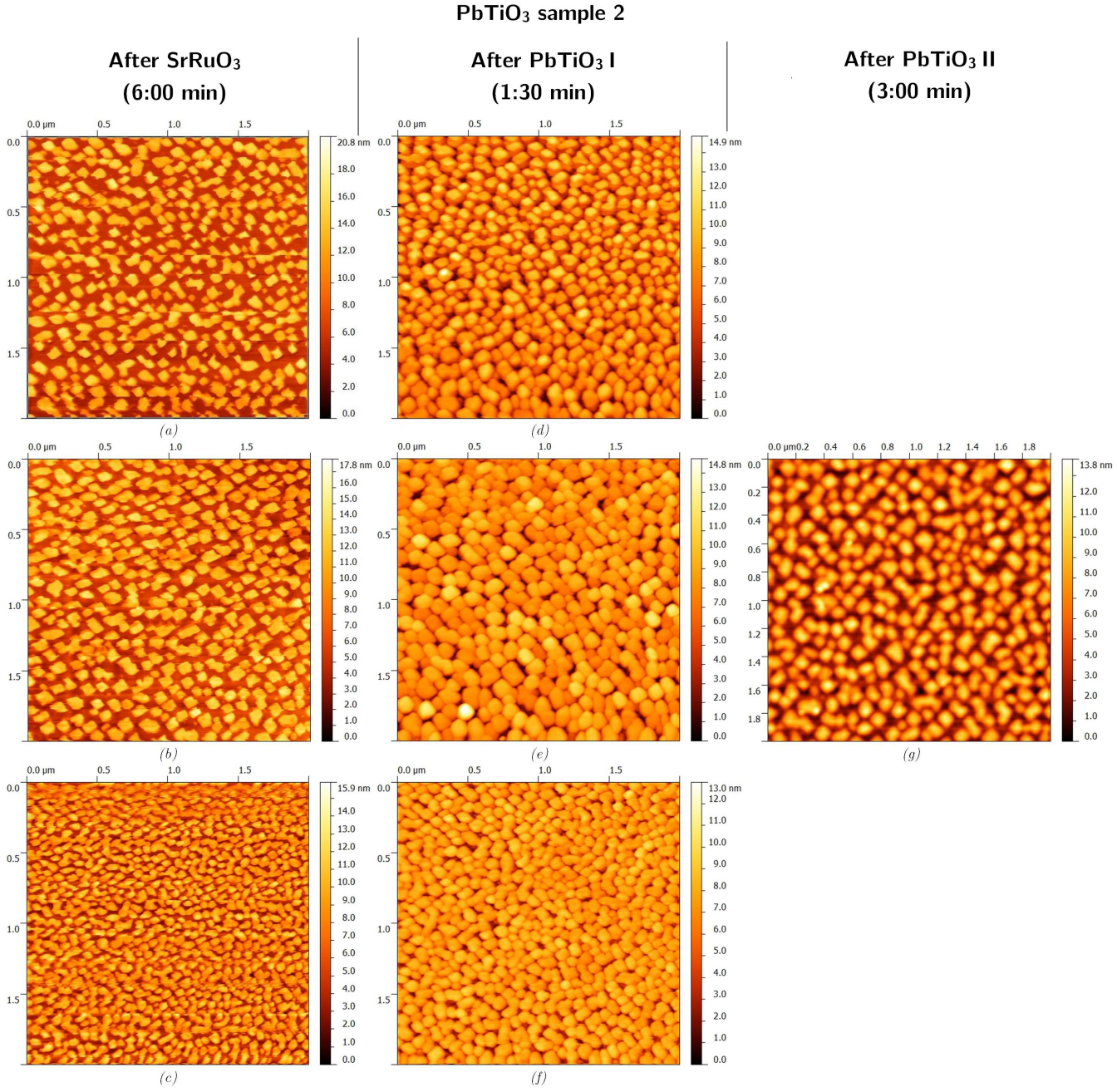

Figure 4.3: $PbTiO_3$ sample 2: Contact mode AFM — (a), (b), (c), (d), (e) and (f) — and tapping mode AFM — (g) — pictures of the surface at different stages during the growth. Pictures (a), (b) and (c) are made after the deposition of $SrRuO_3$, (d), (e) and (f) after the first $PbTiO_3$ deposition and (g) after the second $PbTiO_3$ deposition.

for sample 1 and figures 4.3(a), (b) and (c) for sample 2). Multiple STM (for sample 1) and AFM (for sample 2) pictures were made, to examine the surface roughness at different sections on the sample. In the second sample, the island sizes were different at various places on the surface. This behaviour seems, however, to be in direct relation to the distance of the concerning section from the center of the sample. Figure 4.3(c), for instance, is captured off-centered, as is also indicated by the amount of deposited material on this area of the sample: the shape of the plasma plume causes the deposition of less material in places further away from the center, producing $SrRuO_3$ island with less height difference compared to the islands created near the middle of the plume.

After the creation of the $SrRuO_3$ island, two thin films of $PbTiO_3$ were grown on both the samples. After each deposition, the surface was again examined using atomic force microscopy. On sample 1, shown in figure 4.2, two three minute depositions at a frequency of 1 Hz were done, while the ablations on top of sample 2 (figure 4.3) were made by a one and a half minute growth followed by a three minute growth of $PbTiO_3$. Again, the pictures of the second sample show different island sizes at different regions on the sample — compare for example the islands in figures 4.3(d), (e) and (f). This is in accordance with the images of just the $SrRuO_3$ island; sections further from the middle of the plasma plume again appear to have smaller and lower islands.

The first sample behaved as expected. After the creation of $SrRuO_3$ islands, the first deposition of $PbTiO_3$ (shown in figures 4.2(c) and (d)) hardly changed the surface morphology of the sample. Based on AFM images, the islands kept the same dimensions in both horizontal as vertical directions. The same goes for the islands after the second deposition, although figure 4.2(f) shows there is some island merging going on. All in all, the results of sample 1 are definitely in accordance with the expectations: deposition provided the top of the islands with just as much material as the region between the islands, leaving the topography of the surface almost unchanged after each of the depositions.

The results of sample 2 are not that straightforward. A seemingly striking result in the AFM pictures after the first deposition of $PbTiO_3$, is the apparent growth of the island sizes. In comparison with the images of the $SrRuO_3$ islands in the previous stage, the islands in figures 4.3(d)-(f) seem to have been increased in size. Both the pictures after the deposition of $SrRuO_3$ and after the first $PbTiO_3$ deposition are made *in situ* with the same AFM contact mode tip. A growth in island sizes is — at least at first glance — not in accordance with the expectations, nor with the formulated hypothesis. However, the story becomes even more complicated after the second (now 3 minutes long) $PbTiO_3$ deposition. Brought outside the vacuum system after this last deposition, the island sizes now again seem to have decreased when examining the surface using tapping mode AFM.

A calculation of the average island sizes using autocorrelations of the AFM images does not clearly verifies this observation, as becomes clear in table 4.1. However, this determination produced a relatively large error in the data. Taking this experimental error into account allows the conclusion that the average island size for sample 1 to stay relatively constant. The data also does not contradict with the observation made for sample 2: the autocorrelation shows that the island size after the second $PbTiO_3$ could also be smaller than before the deposition.

stage	average island size (μm)
sample 1 SRO	0.0994 ± 0.0190
sample 1 PTO I	0.0775 ± 0.0169
sample 1 PTO II	0.1014 ± 0.0193
sample 2 SRO	0.0904 ± 0.0194
sample 2 PTO I	0.0852 ± 0.0331
sample 2 PTO II	0.1115 ± 0.0252

Table 4.1: Average island size for sample 1 and sample 2 at different stages in the deposition process.

Comparing the surface roughness at different stages

For determining the roughness of the surface at the different deposition stages, the root mean squared (RMS) values of various AFM measurements on the samples are calculated. Before determining these RMS values, a correction for background height differences and AFM errors in the images is done, to make sure this RMS values gives an indication of the roughness only caused by the islands itself. RMS values after the $SrRuO_3$ deposition for pictures near the middle of the sample were found to be in the range of 2.48 ± 0.21 nm for the first sample (figure 4.2(a) and (b)) and 3.36 ± 0.32 nm for the second (figure 4.3(a), (b) and (c)). For the AFM pictures after the $PbTiO_3$ depositions, the RMS values of sample 1 are in agreement with the expectations of the AFM images of this sample. In these images, both island sizes the island heights appear to remain unchanged after the deposition of the two $PbTiO_3$ layers. This is reflected by the RMS values determined in multiple AFM measurements near the center of the sample: 2.18 ± 0.09 nm after the first and 2.30 ± 0.10 nm after the second $PbTiO_3$ deposition. Unfortunately, the second sample does not reveal this clear results of almost constant RMS values after each deposition. The 3.36 ± 0.32 nm after the creating of the $SrRuO_3$ islands is followed by 1.91 ± 0.22 nm after the first, and 2.53 ± 0.04 nm after the second $PbTiO_3$ deposition.

4.1.2 $BiFeO_3$: a topography undermining material

For $BiFeO_3$, a study similar to the $PbTiO_3$ research described above is conducted. Two $DyScO_3$ substrates were treated in the same way as for $PbTiO_3$. Tapping mode AFM pictures of the annealed substrates are shown in figures 4.10(e) and (f). Again, no clear mixed termination at wide lines along the substrate steps is present. However, just as for the substrates used for the $PbTiO_3$ measurements, the existence of a step down by a certain amount followed by a step up by approximately three times this amount (at certain surface profiles near the steps) shows the apparent presence of both surface terminations at various places on the substrate. The $SrRuO_3$ depositions on both samples indeed produced islands (as can be seen in figures 4.4(a) and (b) and figure 4.5(a)), where the second sample (figure 4.5(a)) even did turn out to have potential for growing nanowires, since the $SrRuO_3$ islands are almost connected in one direction along the surface steps.

Deposition of $SrRuO_3$ and surface determination after this deposition was again followed by two separate ablations of the concerning ferroelectric (in this case $BeFiO_3$) on each of the two samples and examining the sample surface after each deposition. As described in section 3.3 ('Fabrication of the samples'), sample 1 was treated with two depositions of 12 min (approximately 3 nm $BiFeO_3$). Just as for the $PbTiO_3$ analysis, sample 2 provided information about the growth at stages in between the two sample 1 stages, since the first $BeFiO_3$ deposition on sample 2 lasted for 6 min (approximately 1.5 nm) and the second for another 12 minutes. AFM images were made *in situ* (using non-contact mode) for the first sample, and both *in situ* (in contact mode, after the first ablation) and *ex situ* (in tapping mode, after the second) for sample 2. The results are shown in figures 4.4(c)-(h) and 4.5(b)-(g).

The pictures after the first $BiFeO_3$ deposition on sample 1 (figures 4.4(c)-(e)) show a small (but clear) increase in island sizes. This increase is also indicated by the lowering of the islands after the first deposition. The second deposition on this sample almost completely flattened the surface, leaving nearly no clue whether islands have ever existed on this surface. It becomes clear in this pictures that $BiFeO_3$ on $SrRuO_3$ structures has the tendency to first fill the lower situated regions in between the islands, after which layer-by-layer growth takes over. The images of sample 2 show the same growing fashion. Figures 4.5(b)-(e) make clear that the first deposition of 1.5 nm $BiFeO_3$ already provided the islands with growth in both of the lateral directions. Because the distance between the islands on this sample in one direction is different than the distance in the opposite direction, the proportional increase of the island sizes in both lateral directions means the islands grow together faster in one orientation (the direction in which they almost formed nanowires) than in the other one. This is clearly visible in figure 4.5(c) and (e).

The *ex situ* images after the second $BeFiO_3$ deposition are shown in figure 4.5(f) and (g).

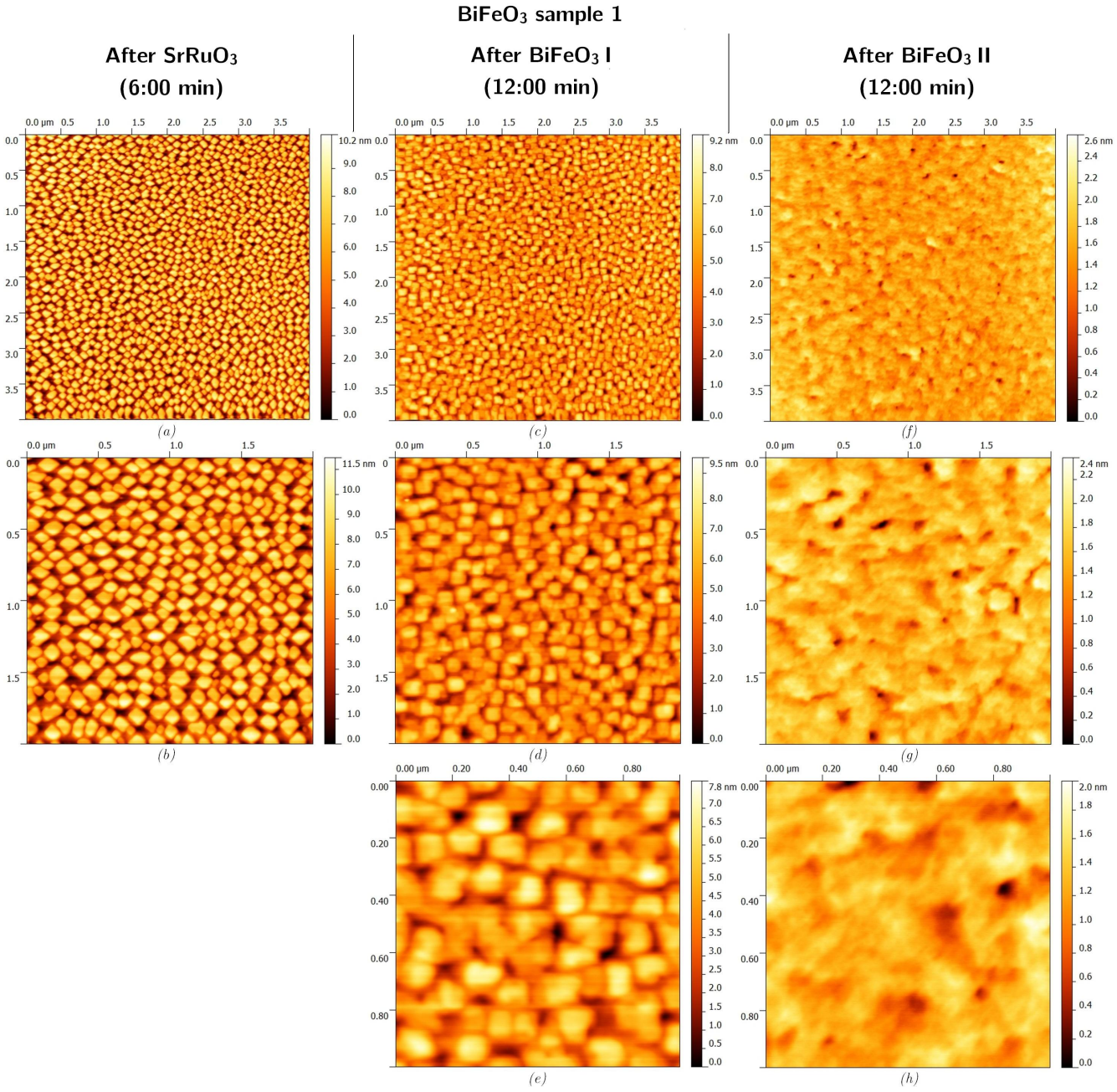

Figure 4.4: $BiFeO_3$ sample 1: STM — (a) and (b) — and non-contact mode AFM — (c), (d), (e), (f), (g) and (h) — pictures of the surface at different stages during the growth. Pictures (a) and (b) are made after the deposition of $SrRuO_3$, (c), (d) and (e) after the first $BiFeO_3$ deposition and (f), (g) and (h) after the second $BiFeO_3$ deposition (of both approximately 3 nm).

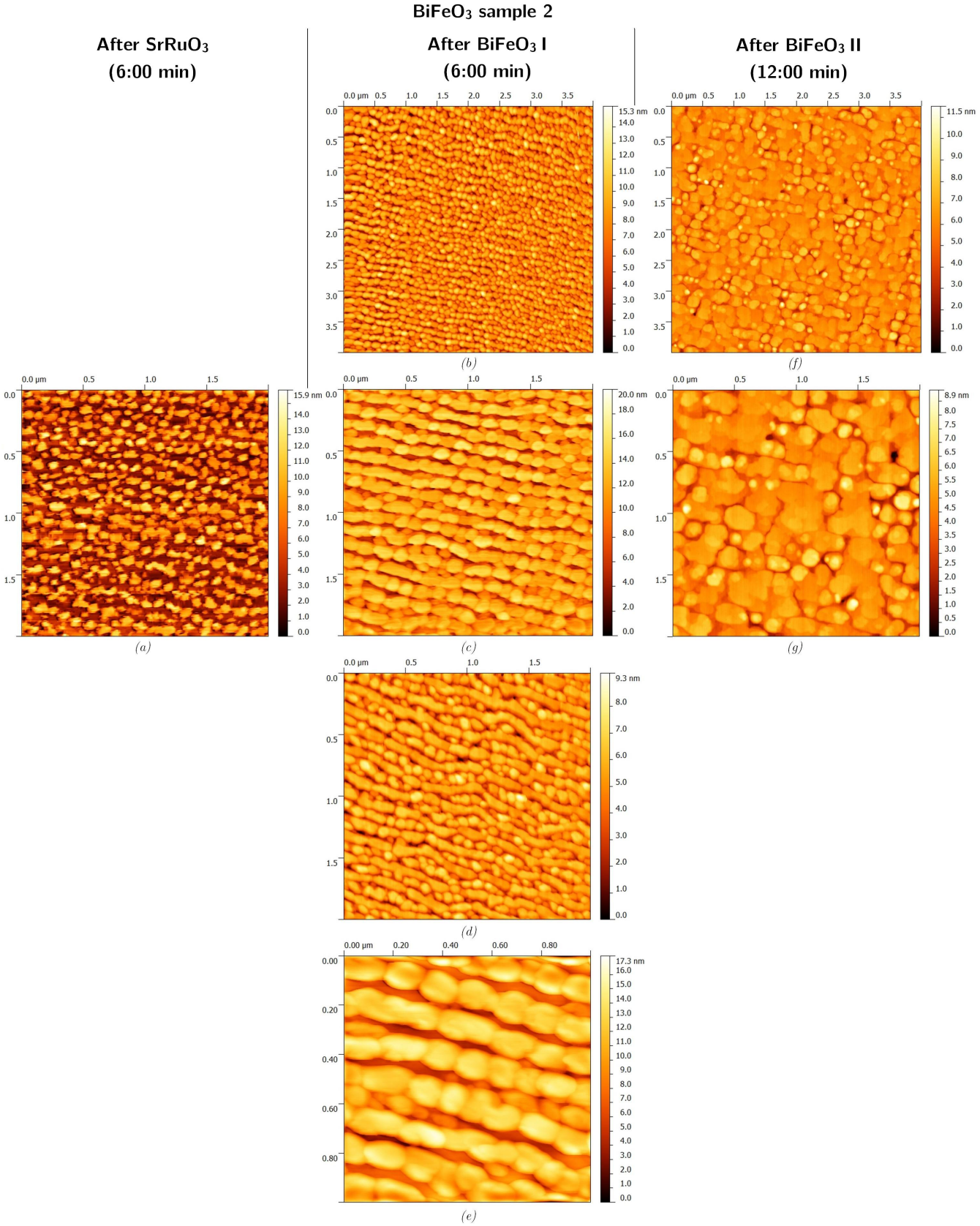

Figure 4.5: $BiFeO_3$ sample 2: Contact mode AFM — (a), (b), (c), (d) and (e) — and tapping mode AFM — (f) and (g) — pictures of the surface at different stages during the growth. Picture (a) is made after the deposition of $SrRuO_3$, (b), (c), (d) and (e) after the first $BiFeO_3$ deposition (approximately 1.5 nm) and (f) and (g) after the second $BiFeO_3$ deposition (3 nm).

Another 3 nm extra on top of the previous deposited material made sure the merging of different islands continued. Remarkable is the height of the island blocks, which is still quite substantial at this stage of the growth. Also striking is the way islands grow together during the last deposition on this sample. Where the growth looked quite straightforward after the previous deposition — it seemed that each island just gradually grew in the horizontal directions, until islands 'interfered' with each other and continued as less-numbered bigger islands — these pictures reveal a more complex way of growing. After the first deposition, it looked like the growth of the islands in both horizontal direction would cause the islands to first fill the regions in the direction of the 'almost nanowires' completely (since along this direction the distances between consecutive islands was smaller than in the distances between islands along the direction in between the 'almost nanowires'), and that further deposition of $BiFeO_3$ just ensured a 'coming together' of different rows of $BiFeO_3$ nanowires until the entire surface became flat. Nevertheless, figures 4.5(f) and (g) now show that this is not what happens. The pictures after the second $BiFeO_3$ show that various regions between islands along the nanowire direction are still not completely filled, while large regions in between the nanowire rows are already part of big island groups.

Comparing the surface roughness at different stages

For both samples, the surface roughness was again determined by calculating RMS values at different positions on the samples. For sample 1, RMS after the $SrRuO_3$ deposition fluctuated in the range of 2.27 ± 0.18 nm. The second sample was rougher at this stage of the analysis: smaller and higher islands caused RMS values of 3.14 ± 0.11 nm for this sample. As expected, growing more $BiFeO_3$ just lowered the RMS value for both. The first sample went down to 1.44 ± 0.17 nm and 0.26 ± 0.07 nm; the RMS values of sample 2 decreased to 2.46 ± 0.47 nm after the first and 0.97 ± 0.02 nm after the second deposition.

4.2 Diffusivity analysis of $PbTiO_3$ and $BiFeO_3$ growth

Along with the step by step images presented in the previous section of this chapter, the second part of this research was focussed on gaining more insight in diffusivity parameters for $PbTiO_3$ and $BiFeO_3$ growth on $SrRuO_3$ structures (since it was believed that a difference in this region was expected to cause the different growth behaviour of the two ferroelectric materials). As mentioned before, a description for the RHEED intensities (for epitaxial growth on a singular surface) between two deposition pulses is given in equation 1.14. The relaxation times in the RHEED data between two successive laser pulses are determined by making a best fit of equation 1.14 for the data, as explained in section 3.5 ('Conditions for determining diffusivity parameters'). An example of such a fit is shown in figure 4.6, which is a detail from a specular RHEED intensity of a $PbTiO_3$ deposition on a $SrRuO_3$ substrate during the formation of the first monolayer. The red line is the fit for the RHEED intensity data, given in blue. The fit provides a relaxation time for recovery behaviour in the RHEED data. In order to calculate D_S for the four different growth combinations — i.e. $PbTiO_3$ on $SrRuO_3$, $BiFeO_3$ on $SrRuO_3$, $PbTiO_3$ on itself and $BiFeO_3$ on itself — relaxation times are determined using this method for the growth of $PbTiO_3$ and $BiFeO_3$ at different coverages during growth on the flat $SrRuO_3$ substrates. Hereby, the condition as described in section 3.5 was applied — that is, determining the relaxation times for coverages as far away from the RHEED minimum during the growth of the first monolayer, to make sure the extracted relaxation time is dominated as much as possible by diffusion at only one surface level. Subsequently, the diffusivity coefficient D_S of this growth combinations can be determined from these τ values, by making use of equation 4.1 (this equation is equivalent with equation 1.9 in section 1.2). As becomes clear from this equation, the diffusivity coefficient depends on the coverage (θ), the relaxation time (τ), the first root of the Bessel function ($\mu_1^{(0)} = 2.40$) and the nucleation density (N_S).

$$D_S = \frac{\theta}{\tau(\mu_1^{(0)})^2 \pi N_S} \tag{4.1}$$

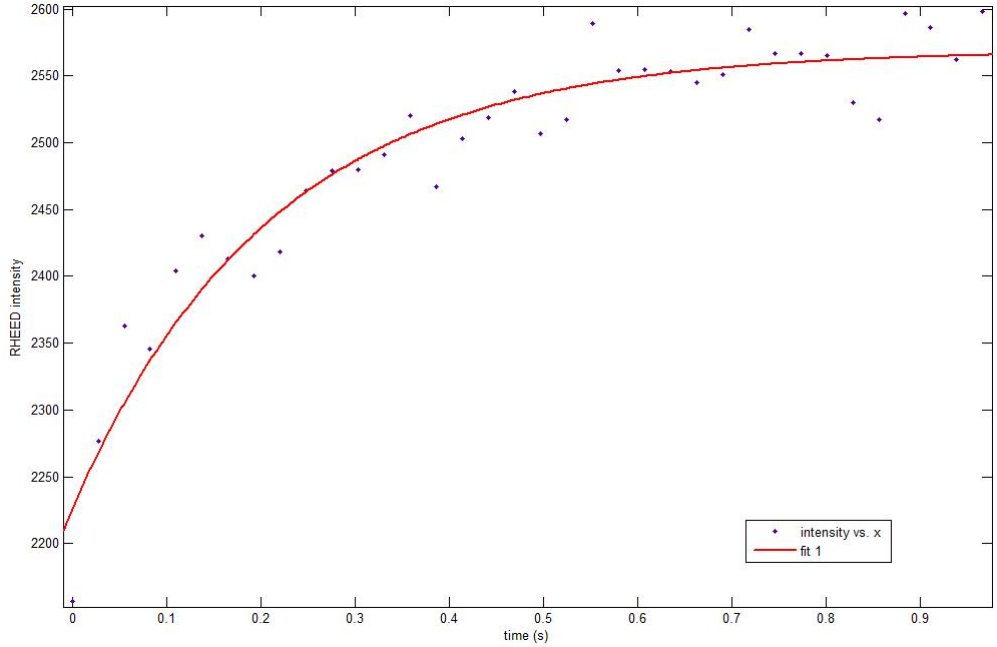

Figure 4.6: A detail from the specular RHEED intensity for the growth of $PbTiO_3$ on a $SrRuO_3$ substrate, focussing on a single diffusion step after the third laser pulse.

In order to determine the diffusivity coefficients using equation 4.1, the nucleation density (N_S) was needed. As described in the previous chapter (section 3.5, 'Conditions for determining diffusivity parameters'), the amount of nucleation during a deposition is estimated by looking at the RHEED intensity recovery. The RHEED spectrum in figure 4.7 shows a steep drop after every laser pulse. This drop is caused by a sudden deposition of randomly positioned atoms, increasing the surface roughness. These atoms then start diffusing towards the step edges of islands, which decreases the roughness and therefore increases the RHEED intensity. The drop and subsequent recovery thus tell something about the nucleation density on the surface. By comparing the recovery of the normalized $PbTiO_3$ RHEED intensity with the recovery of the RHEED intensity for the $BiFeO_3$ deposition, an indication of the amount of nucleation can be given. This should also give an indication of the ratio between the nucleation densities of $PbTiO_3$ and $BiFeO_3$. This comparison has been done for both of the RHEED intensity signals and the indication of the nucleation density ratio is found to be $N_{S,\mathrm{BiFeO_3}}/N_{S,\mathrm{PbTiO_3}} = 0.31$. Using this ratio in equation 4.1 makes finding absolute outcomes for the diffusivity coefficients impossible. However, an indication of the ratio in diffusivity coefficients for the two materials is still possible. These relative diffusivity coefficients are listed in table 4.2 for $PbTiO_3$ and table 4.3 for $BiFeO_3$. The errors in the diffusivity coefficients are mainly caused by the fit parameters for determining the relaxation times in the RHEED data.

θ	$\tau(s)$	$D_{S,rel}(\mu m^2/s)$
4.00	0.1805	1.225 ± 0.0603
8.48	0.1383	3.39 ± 0.17
20.85	0.0900	12.8 ± 0.72
75.38	0.4492	9.3 ± 1.2
87.63	0.3231	15.1 ± 1.2
100	0.2740	20.5 ± 2.1

Table 4.2: Relaxation times and relative diffusivities for $PbTiO_3$ growth on a $SrRuO_3$ substrate

θ	$\tau(s)$	$D_{S,rel}(\mu m^2/s)$
5.17	0.1533	6.1 ± 1.15
10.64	0.0710	27.7 ± 12.2
65.96	0.0831	141.7 ± 53.0

Table 4.3: Relaxation times and relative diffusivities for $BiFeO_3$ growth on a $SrRuO_3$ substrate.

Figure 4.7 and figure 4.8 show the RHEED spectra for the growth of $PbTiO_3$ and $BiFeO_3$ respectively. As expected, both RHEED intensities show a strong correlation with the laser pulses. The deposition of randomly positioned atoms during a pulse almost instantly increases the roughness of the surface. Which leads to an increase in step density that causes a drop in the RHEED intensity. Figure 4.8 seems to recover to 75% of its original intensity. While figure 4.7 only recovers to about 40% of its original intensity. A line has been added in table 4.2 and table 4.3, to distinguish the nature of the substrate on which the deposition takes place. The upper part of the tables is the growth on $SrRuO_3$ the lower part is the growth on the target material itself. During the deposition more and more of the sample changes into the target material itself Therefore the diffusivity value at the beginning of the measurement says something about the growth on $SrRuO_3$ after the minimum in RHEED intensity the diffusivity is the diffusivity of the target material grown on itself.

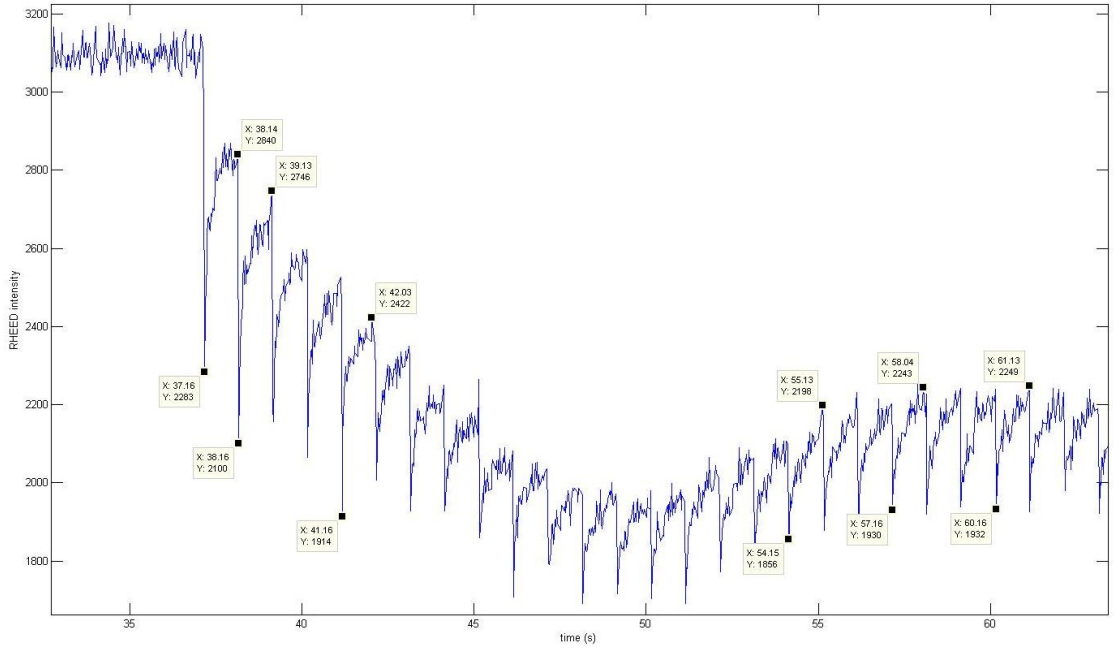

Figure 4.7: A specular RHEED intensity oscillation plot of the growth of $PbTiO_3$ on a flat $SrRuO_3$ substrate.

To find out if the substrates that have been used were actually suitable for this research, AFM images were made. These are displayed in figure 4.10. Figure 4.10 shows that the $PbTiO_3$ substrate was not flat. Earlier in this section a model was used that is based on the epitaxial growth on a singular surface. The $SrRuO_3$ substrate is three-dimensional, so this compromises the validity of the used model for this experiment. In order to determine the difference in 'flatness', two methods have been used. First a mask has been placed on a level of 5 nm below the highest point in the AFM image, which can be seen in figure 4.9, then the mask coverage is determined. With this information the island coverage can be determined. Statistics show that the island coverage is approximately 80%. A more obvious way to determine the surface

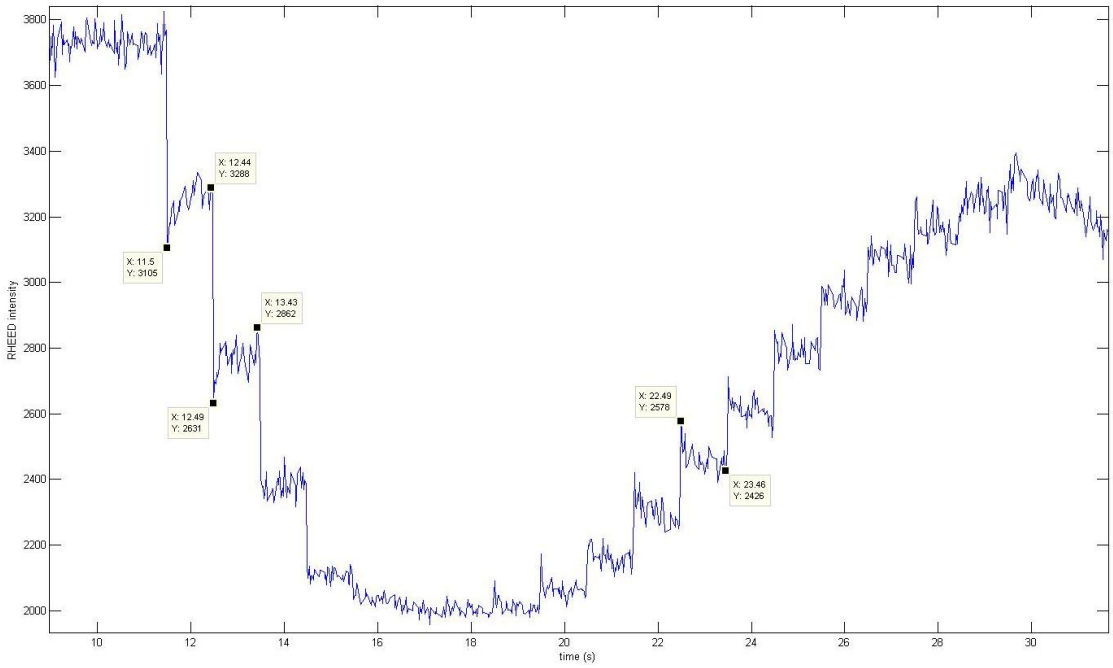

Figure 4.8: A specular RHEED intensity oscillation plot of the growth of $BiFeO_3$ on a flat $SrRuO_3$ substrate.

roughness is to determine the root mean square (RMS) value. Statistics show that the RMS = 1.66 nm. This means that indeed the surface is not flat. For comparison the surface on which the $BiFeO_3$ is grown, which is shown in figure 4.10 on the right, has a RMS = 0.57 nm. From these surface roughness characterization values a conclusion can be drawn, both surfaces aren't perfectly flat. The substrate that is used to grow $BiFeO_3$ on seems to come close to a singular surface, although it seems to have some deep cavities. The surface that is used to grow $PbTiO_3$ on seems to be very rough. The root mean square values tell the same story but also give the opportunity to quantitatively look at the difference. The root mean squares value found for the $BiFeO_3$ AFM image in figure 4.10 is almost three times bigger compared to the root mean square value for the $PbTiO_3$ AFM image in figure 4.10. Although this is true, the analysis using a mask at 5 nm below the top point, shows that the surface seems to be relatively smooth.

The previous section determined the nucleation densities by looking at the nucleation after the first deposition and comparing the normalized change in RHEED intensity. The values used as nucleation densities are actually based on the assumption that the nucleation density is actually dependant on the RHEED intensity after the first pulse. A second method to determine the nucleation densities and therefore the diffusivities is described in the following section.

The fact that the $SrRuO_3$ sample used to grow $PbTiO_3$ on is not flat can actually be used to determine the nucleation density for the growth of $PbTiO_3$. Using the AFM images, like the left one in figure 4.10, a island coverage can be determined. Using this coverage and the average island size, the number of islands per unit area can be determined. Which is the nucleation density for $PbTiO_3$ on the $SrRuO_3$ sample. The island coverage has been determined using a mask at a set level. Unfortunately the height of the mask is quite arbitrary, But 50% of the height scale beneath its highest point, seemed to be a good level for covering the deep crevasses while leaving the islands exposed. An island coverage of 90% was found for the $SrRuO_3$ sample. Using an auto correlation, the average island size can be determined. This was found to be 12.5 nm^2. Using these two values a nucleation density of 72 nm^{-2} is found.

For the $SrRuO_3$ used to grow $BiFeO_3$ on the nucleation density cannot be determined the

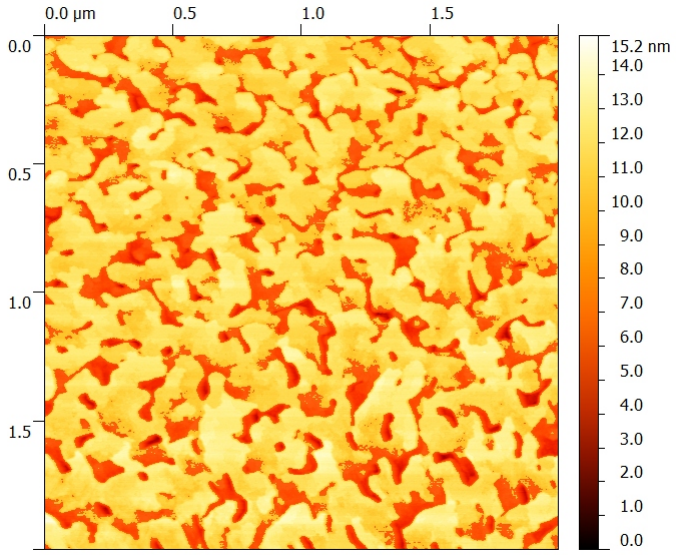

Figure 4.9: A edited AFM image of the substrate used to grow $PbTiO_3$ on.

same way as for the $SrRuO_3$ sample used to grow $PbTiO_3$. Figure 4.10 shows why: the left sample (used for the $PbTiO_3$ growth) is not smooth and the right sample (used for the $BiFeO_3$ growth) is smooth. Because of the lack of islands to begin with, and the lack of an AFM image after the first deposition of $BiFeO_3$ a different way of determining the nucleation density has te be determined. When looking at figure 4.8 it takes 18 pulses before a single monolayer is deposited onto the surface. After the first deposition the RHEED intensity in figure 4.8 does not recover that much. This means that the step density does not increase that much because of atoms diffusing towards step edges. After the second pulse there is almost no recovery, the RHEED intensity after the third pulse does not seem to recover at all. These observations tell something about the nucleation process. If one assumes that 5.56 % (one eighteenth) of the monolayer is deposited every pulse. Now only the island size needs to be determined unfortunately the average island density still needs to be determined to find the nucleation density. So an AFM image still has to be made.

θ	$D_S(\mu m^2/s)$
4.00	0.0170 ± 0.0008.
8.48	0.0471 ± 0.0023
20.85	0.1778 ± 0.0100
75.38	0.1286 ± 0.0163
87.63	0.2102 ± 0.0210
100	0.2843 ± 0.0292

Table 4.4: Diffusivities for $PbTiO_3$ growth on a $SrRuO_3$ substrate.

When looking at figure 4.7, the RHEED intensity only recovers to about 40 % of its original intensity. In figure 4.11 a second part of the RHEED intensity spectrum is visible. It becomes clear that during the deposition the step density increases further and further, as the RHEED intensity decreases during time. The RHEED intensity probably only recovers to 40 % of its original intensity because of the fact that multiple growth modes are present. A layer-by-layer growth mode and a step flow growth. This becomes very clear in figure 4.11, where two flat parts in the RHEED spectrum are visible — from 70 to 80 seconds and 85 to approximately 98

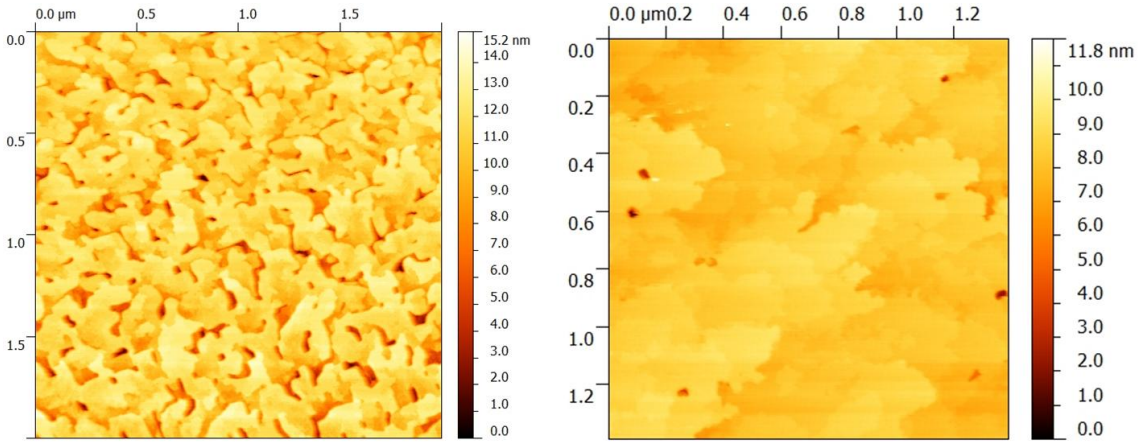

Figure 4.10: An AFM image of the substrates used to grow $PbTiO_3$ (surface on the left) and $BiFeO_3$ (surface on the right).

seconds. A flat RHEED intensity spectrum is characteristic for step density flow. In this limited time span the relaxation time is determined using equation 1.14. The found relaxation time is $\tau = 0.29 \pm 0.01$s.

4.3 Results of the simulations

In this section, a selection of the outcomes of the solid-on-solid Monte Carlo simulations is presented. Since most of the parameter combinations of table 3.2 in section 3.6.2 ('Simulation parameters') delivered quite comparable growth behaviours, not all results of this table will be shown in images. It turned out that it was always possible to flatten the surface. This is agreement with real thin film growth: a long enough deposition will eventually make every three-dimensional morphology approximately flat. Each deposition was continued until the surface became (almost) flat. For some parameter combinations and initial conditions this took over 1500 deposition pulses.

Figure 4.12 shows certain stages of the simulated growth on 25 equally divided islands (each island has a diameter of 11 and a height of 23 entities), for a setting where the surface diffusion barriers of all the three materials involved is 0.85 eV. In this images, it becomes clear that the flattening of the surface is a gradual process, where almost none of the material stays on top of the islands (the islands are not getting much higher until they grow together in the flattening process). The flattening starts with the gathering of material around the circular islands on the lowest level. From here on, a sort of 'stairs' are formed across the islands steps, which become higher and higher (and also wider and wider) as the deposition continues. At a certain point, this 'stairs' reach the island level; from that moment on the islands start increasing in size (radius). Further simulating results in a continuation of the island merging. Gradually the lower holes in between the increased islands are filled. After approximately 500 depositions (25 monolayers) the surface has become more or less flat, although further simulating results in a even flatter surface, with the maximum being reached after approximately 600 depositions (30 monolayers).

The growth behaviour shown in figure 4.12 forms the basis of all of the simulations, since all other configurations show quite similar growth modi. It is not strange that these parameters provide the most common growth behaviour, since the three diffusion barriers all have the same value. Above all, this is also a realistic value. There were quite some combinations in table 3.2 who resulted in practically the same growth behaviour. The first one was the configuration $E_{S,D} = E_{S,S} = E_{S,F} = 1.2$ eV. When comparing this results with the images in figure 4.12, almost no difference was observed. The flattening here took, for example, approximately the

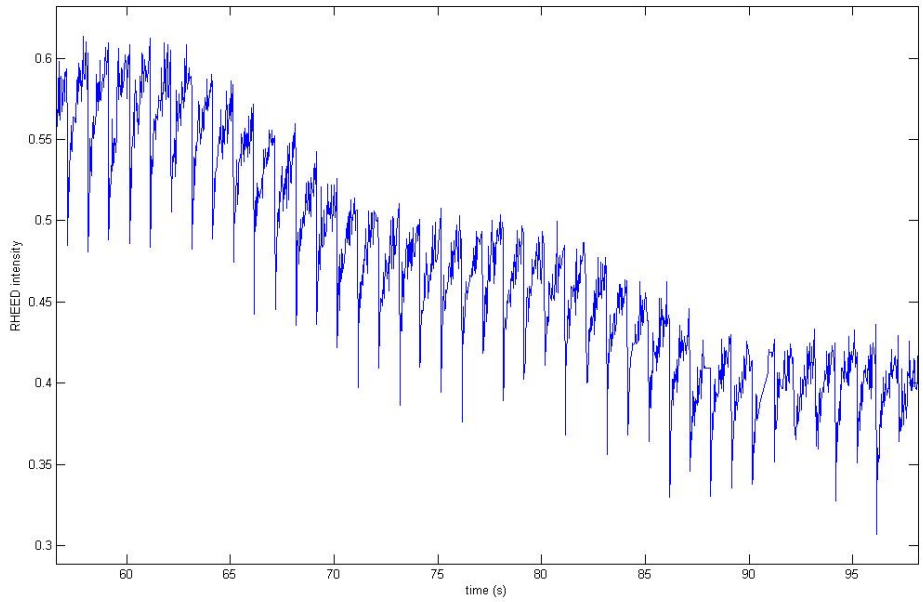

Figure 4.11: A specular RHEED intensity oscillation plot of the growth of $PbTiO_3$ on a flat $SrRuO_3$ substrate.

same number of depositions. More almost identical results were produced in the configurations $E_{S,D} = E_{S,S} = 0.85$ eV, $E_{S,F} = 0.55$ eV and $E_{S,D} = E_{S,S} = 1.2$ eV, $E_{S,F} = 0.25$ eV. Just like in the previous case, for these combinations all the benchmarks of the growth were observed at the same deposition numbers: the 'stairs' reaching the island level, the merging of the islands and the flattening of the surface. In all of this four cases, the island heights do not grow until the merging process starts.

There were, however, also configurations that did turn out the behave differently than the 'standard case' of figure 4.12. Figure 4.13 shows the results for the combination $E_{S,D} = 0.85$ eV, $E_{S,S} = 2.5$ eV and $E_{S,F} = 2.5$ eV. These enlargements in the surface diffusion barrier of the deposited material on $SrRuO_3$ and on itself, make that the deposited particles on an island have only a very small diffusion length. This results in an actual growth in the island height this time, since particles on the islands are now not diffusion towards the lower level. Up until approximately 260 deposition pulses (13 monolayers), the islands more or less manage to keep up with the lower level. It now takes a lot longer before the island tops are reached by the upcoming 'stairs', but the merging of islands and flattening of the surface again take place, albeit after a lot more deposition pulses.

Adjusting the $E_{S,S}$ parameter some more — setting it at $E_{S,S} = 0.15$ eV to another extreme value — delivers the results presented in figure 4.14. A lower surface diffusion barrier for the growth on $SrRuO_3$ apparently means the islands manage to stay out of the hands of the upcoming lower level even longer. It now takes over 700 deposition pulses (35 monolayers) before the surface is flattened. Setting the $E_{S,F}$ value back to $E_{S,F} = 0.85$ eV now decreased the number of pulses needed before flattening, but resulting in another striking growth pattern, as shown in figure 4.15. From the images in this figure, it seems that the island height first increased for a smaller area around the edges of the island level. This increase is probably a result of the 'stairs' reaching the island level, since it happens after this phenomenon is observed (the stairs reach the island level after approximately 300 depositions, the strange growth in island edges takes place between 320 and 360 depositions). After 360 depositions, the ring shaped islands fill in the whole surface

again. This time this happens by enlarging of the rings in both inward and outward direction.

Except for substrates with 25 islands of a 11 pixel diameter, two simulation on a substrate with 9 islands consisting of 21 pixel diameters were performed as well (an example is shown in figure 4.16). As expected, these simulation showed similar behaviour, except for the fact that it took a lot more deposition pulses before the surface became flat. This is completely in accordance with expectation though, since the diffusion length is determined by the parameters used and not by the size of the islands. The diffusion length is thus still approximately equal to the case with 25 islands; larger islands mean that much more particles stay on top of the islands for the same parameters, resulting in a lot longer depositions before the surface flattening is again accomplished. Further, the simulations with larger island did not bring any new insights.

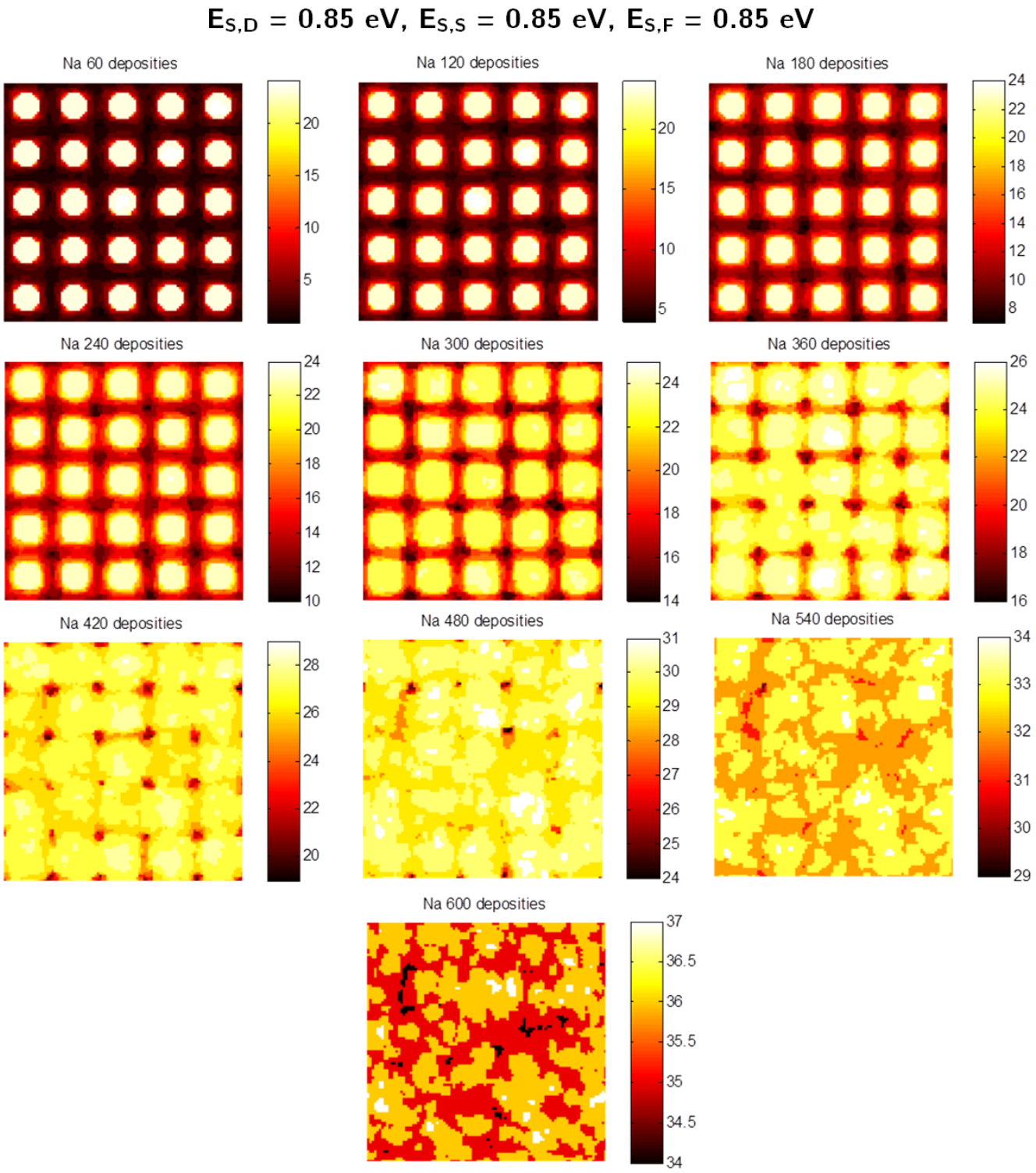

Figure 4.12: Simulation results for a initial substrate of 25 $SrRuO_3$ islands of 11 pixels in diameter and 23 pixels in height. The surface diffusion barriers for the different surface materials are all set the same: $E_{S,D} = E_{S,S} = E_{S,F} = 0.85$ eV. (Here, $E_{S,D}$ is the diffusion barrier for the growth of $PbTiO_3$ or $BiFeO_3$ — the deposited material — on $DyScO_3$, $E_{S,S}$ is the barrier for the growth on $SrRuO_3$ and $E_{S,F}$ is the barrier for the growth of the deposited material on entities of the same material.)

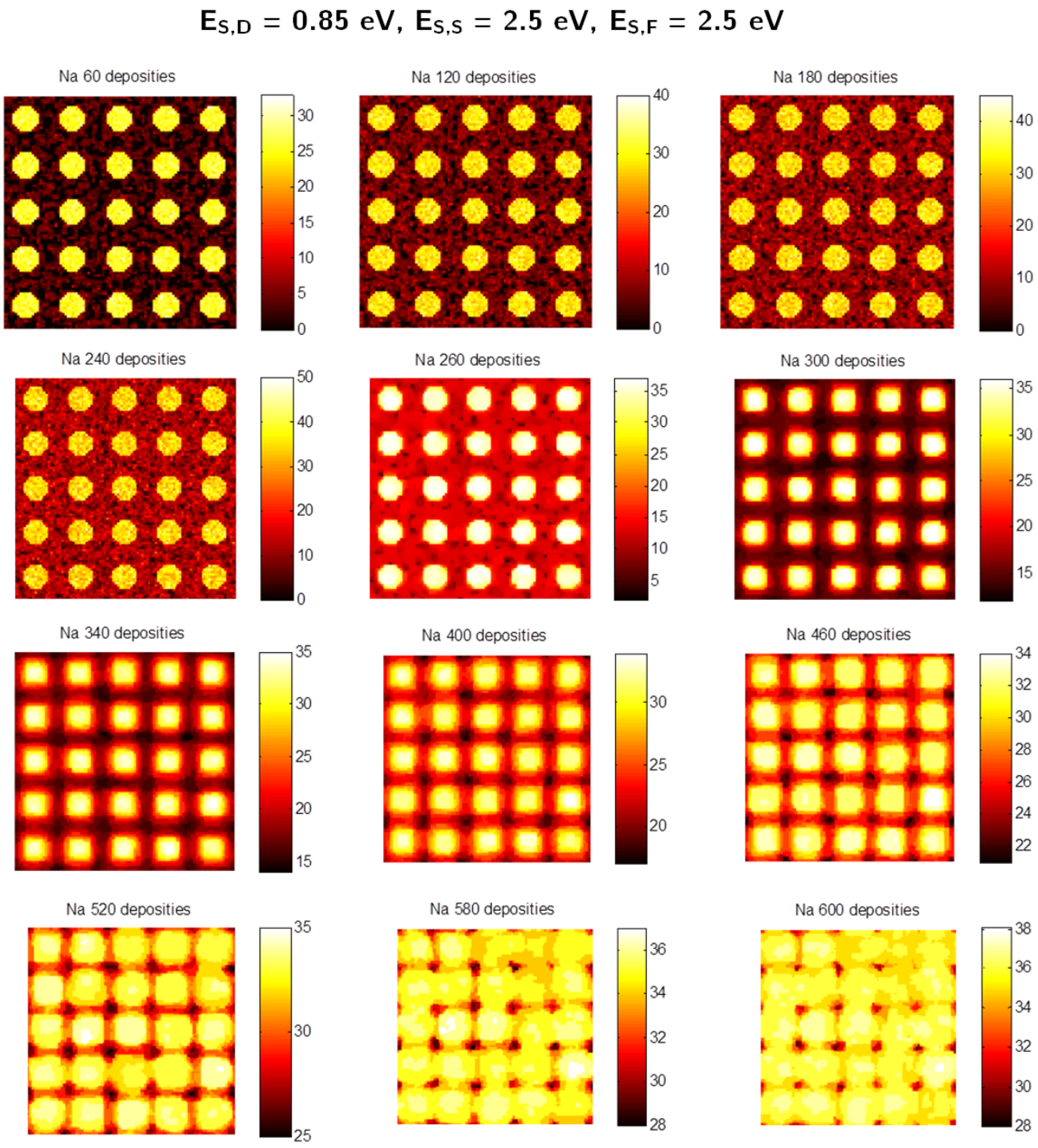

Figure 4.13: Simulation results for a initial substrate of 25 $SrRuO_3$ islands of 11 pixels in diameter and 23 pixels in height. The surface diffusion barriers for the different surface materials set in the following configuration: $E_{S,D} = 0.85$ eV, $E_{S,S} = 2.5$ eV and $E_{S,F} = 2.5$ eV.

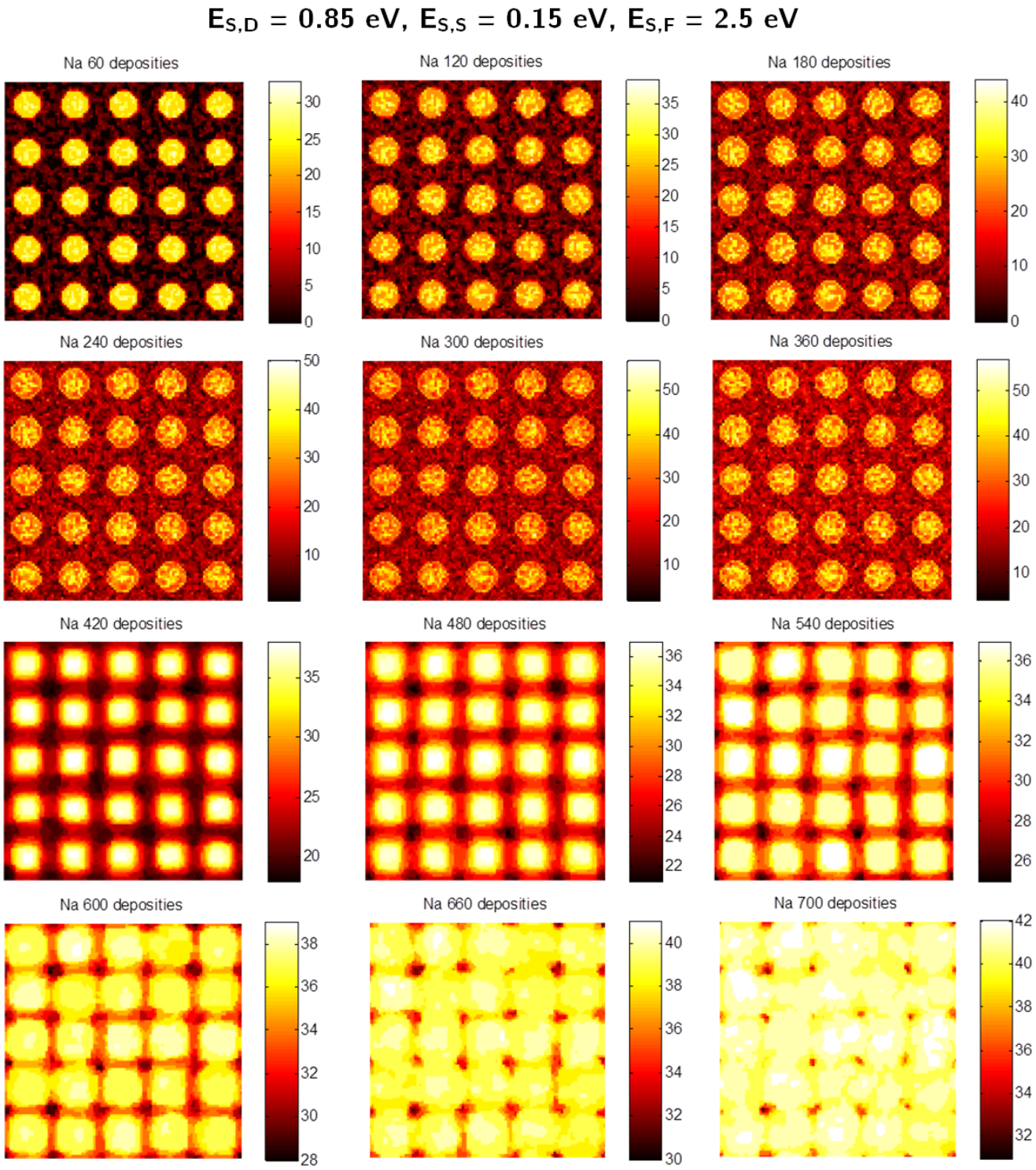

Figure 4.14: Simulation results for a initial substrate of 25 $SrRuO_3$ islands of 11 pixels in diameter and 23 pixels in height. The surface diffusion barriers for the different surface materials set in the following configuration: $E_{S,D} = 0.85$ eV, $E_{S,S} = 0.15$ eV and $E_{S,F} = 2.5$ eV.

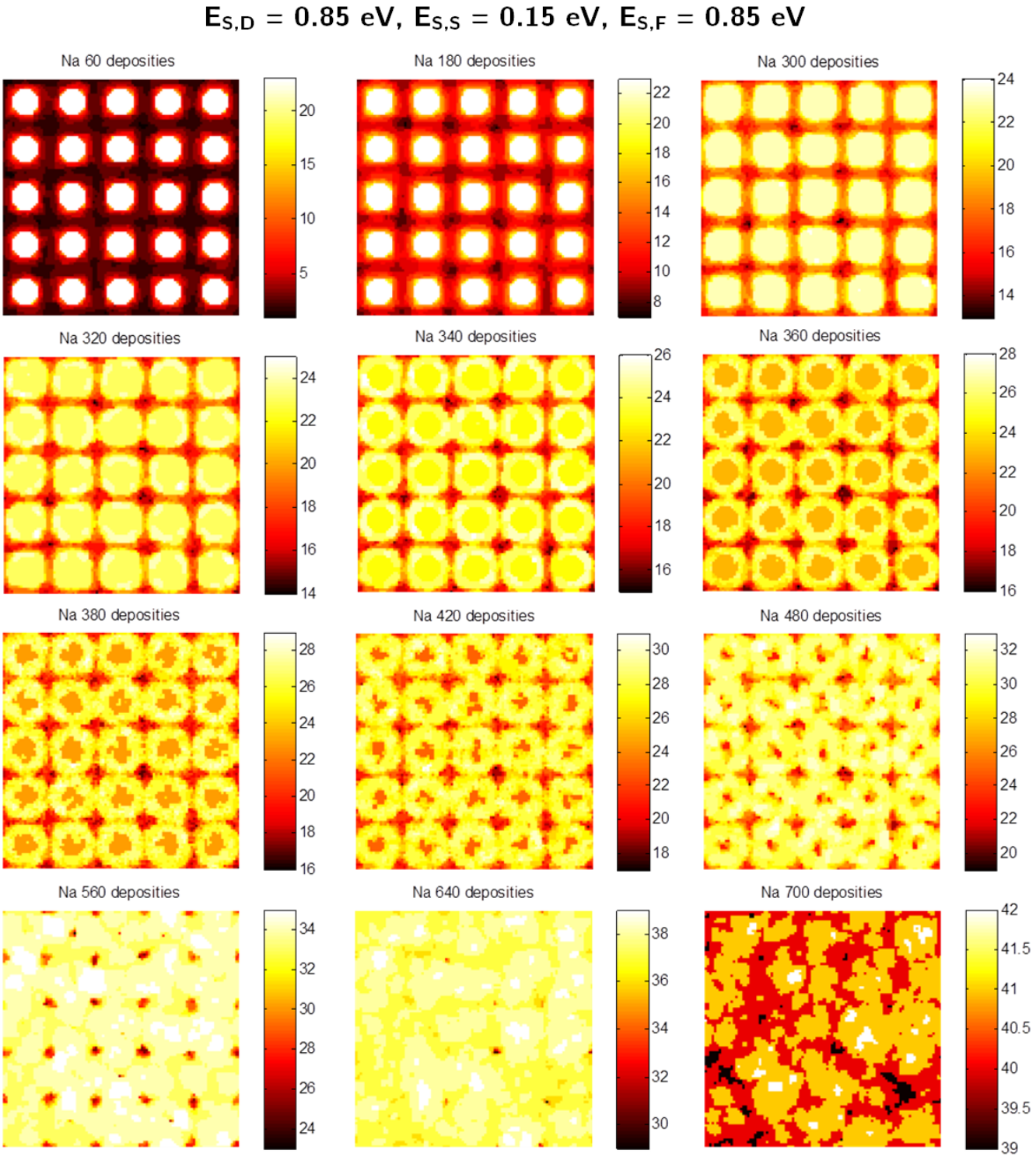

Figure 4.15: Simulation results for a initial substrate of 25 $SrRuO_3$ islands of 11 pixels in diameter and 23 pixels in height. The surface diffusion barriers for the different surface materials set in the following configuration: $E_{S,D} = 0.85$ eV, $E_{S,S} = 0.15$ eV and $E_{S,F} = 0.85$ eV.

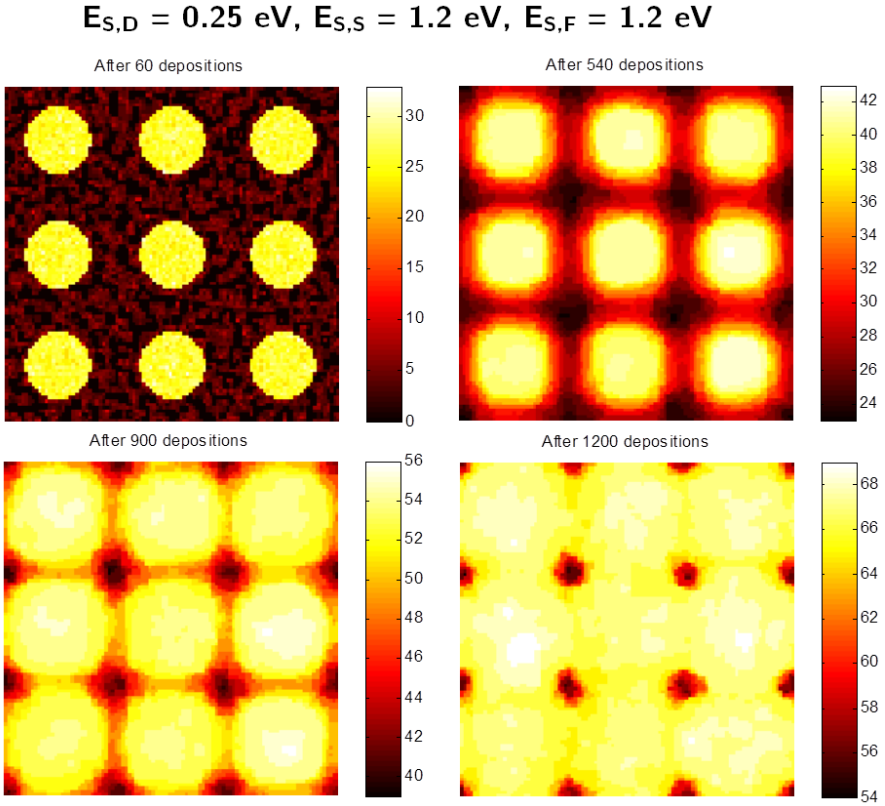

Figure 4.16: Simulation results for a initial substrate of 9 $SrRuO_3$ islands of 11 pixels in diameter and 23 pixels in height. The surface diffusion barriers for the different surface materials set in the following configuration: $E_{S,D} = 0.25$ eV, $E_{S,S} = 1.2$ eV and $E_{S,F} = 1.2$ eV.

Chapter 5

Discussion

5.1 Interpretations of the step by step analysis

In the AFM images of the step by step analysis, numerous phenomena worth discussing were observed. First, some remarks and interpretations about the apparent increase in islands sizes on $PbTiO_3$ sample 2 are reported. After this, the images of the two $BiFeO_3$ samples will be discussed as well.

5.1.1 Apparent growth in $PbTiO_3$ islands sizes

The AFM images of the $PbTiO_3$ step by step analysis showed an apparent growth in lateral island sizes between the start and the end of the first $PbTiO_3$ ablation on the second sample. There are several explanations for this behaviour. It is commonly known that objects can appear bigger (in horizontal directions) in AFM pictures as a result of *tip convolution*. Due to the fact that the tip of an AFM is not ideally sharp, one is never able to retrieve the exact surface morphology. Rather, each AFM image is created in an interaction between tip and sample. This correlation phenomenon does not influence the height of the concerning object on the surface, but it does have an effect on the lateral resolution of the images. When comparing island sizes, AFM pictures could thus be misleading. The *ex situ* tapping mode images after the second $PbTiO_3$ deposition — where the islands again seemed smaller than after the previous deposition — showed that there is indeed something going on in this area. *Ex situ* images of this material, on the other hand, also have some other disadvantages in this case: the formation of a thin layer of water on top of the sample (when taken outside the vacuum system) disturbs the AFM measurement (causing the blur in figure 4.3(g)). The fact that the *ex situ* AFM images are clearly distorted by this water forming on the sample complicates the analysis even further.

All of the previous taken into account, caution is certainly needed when interpreting AFM data. The apparent growth in island sizes in figures 4.3(d)-(f) could very simple be explained as nothing more than an inevitable measurement error caused by tip convolution, leading to no particular conclusion. However, there is also another explanation that is still in agreement with the formulated hypothesis. Theory dictates that the surface diffusion coefficient D_S together with the residence time before reevaporation τ determine a surface diffusion length l_D (formula 1.1). This l_D is especially useful when dealing with epitaxial growth on vicinal surfaces: when l_D exceeds the surface steps terrace width l_T, step flow growth is possible. (In this case, the adatoms diffusion distance is large enough for the atoms to reach the step edges of the substrate.) A similar approach is possible concerning growth on top of islands: if l_D is sufficiently large compared to the size of the islands (for example the diameter when the upper sides of the islands are circular), adatoms get the change to reach the edges of the islands and descend to the lower situated regions between the islands. When the here described situation takes place, the islands sizes will grow in the lateral directions, until l_D is not sufficient any more for the adatoms to reach the edges. From this point on, newly deposited atoms will in theory stay on top of the

islands and the islands sizes will stop growing. Further continuation of the deposition means in general no change in the surface morphology; the extra material both on and in between islands will be the same. This is exactly what could have happened during this particular deposition of $PbTiO_3$. After the deposition of $SrRuO_3$, the created islands possibly had smaller dimensions than the l_D parameter for $PbTiO_3$ growth on $SrRuO_3$ (and probably also for growth on $PbTiO_3$ itself). This could have meant that with the start of the $PbTiO_3$ deposition, the islands were growing in horizontal dimensions till a certain moment where the island sizes were large enough to prevent the adatoms reaching the edges. Going on with the ablation, the topography probably stayed more or less the same until the end of the second $PbTiO_3$ deposition. This interpretation means that, even if the images are not misleading and the islands actually increased in size, this behaviour can still be very well explained by this consideration.

There are several signs in the AFM data in accordance with this line of reasoning. First of all, the statement that tip convolution is to blame for larger looking islands in figures 4.3(d)-(f) seems to be in disagreement with the AFM images after the $SrRuO_3$ deposition in figures 4.3(a)-(c). This images are made with the same AFM tip, which makes a direct comparison between the islands sizes of both samples possible and from which an increase in these dimensions becomes clear. The only difference could be made in the interaction between the tip and the different materials — since the surface in figures 4.3(a)-(c) consist of $SrRuO_3$ and the surfaces in figures 4.3(d)-(f) of $PbTiO_3$ — but it is unlikely that this interaction differs that much.

Another important aspect is the height of the islands in the samples at the different stages of the deposition. Images near the center of the sample after the $SrRuO_3$ deposition (figures 4.3(a) and (b)) show, next to smaller islands in lateral dimensions, also higher objects. This a very strong indication of a real, physical growth of the island sizes: for increasing the lateral dimensions, extra material is used in between the original islands. Material, otherwise used on top of the islands for allowing the islands to grow in height in the same amount as the lower regions in between them.

A third argument is found in the comparison between the $SrRuO_3$ islands on sample 1 and 2 (figures 4.2(a) and (b) compared to figure 4.3(a)-(c), respectively). STM images of the islands after $SrRuO_3$ deposition on sample 1 show much bigger islands than the AFM pictures of the created $SrRuO_3$ islands on sample 2. Since $PbTiO_3$ was grown under the same conditions, the D_S parameter, and therefore also the l_D parameter, should be the same during the subsequent growth of $PbTiO_3$ on both samples. So, a growth of island sizes until the islands dimensions exceed l_D should lead to comparable sizes in the end. The images indeed display a similar end result in both cases, although the eventual islands on sample 2 does seem a little bigger than the eventual islands on sample 1. Nevertheless, there are some similarities present in several images. So are figures 4.2(d) and (f) on sample 1 and figure 4.3(d), e.g., in particular very comparable.

Due to the large error in the measurements, the calculation of the average island sizes using the 2D autocorrelation did not provide the experimental proof of an actual increase in island sizes. This increase is, however, strongly indicated by the development of the RMS value for the different stages. The unexpected results in this value could still be very well explained by previously mentioned phenomena. They could of course be the consequence of misleading images created as a result of tip convolution, but more likely is the consideration of an actual growth of the islands. An actual physical increase does explain the lowering in RMS values after the first $PbTiO_3$ deposition — since the growth of larger islands in lateral dimensions also means lower islands and less surface steps as a result of possible merging of islands — but it has no clarification for the subsequent increase in RMS calculations after the second $PbTiO_3$ ablation. The values after the second deposition may nevertheless be not very reliable, given that the images show clear disturbance as a result of water formation on the sample. This limits the image in both lateral and vertical directions and makes that possibly only the tops of the created islands are captured in the pictures, leaving the lower details of the objects — which matter for both island sizes and heights and therefore decrease the RMS values by a sufficient amount — unnoticed.

5.1.2 Notable observations in $BiFeO_3$ images

As is is showed in figures 4.4(c)-(e), the AFM images of $BiFeO_3$ sample 1 provide in indication that the growth of $BiFeO_3$ on $SrRuO_3$ structures (on a $DyScO_3$ substrate) has the tendency to first fill the lower situated regions in between the islands before layer-by-layer growth takes place. This behaviour can be described completely in line with the explanation of the apparent growth in island sizes on sample 2 of the $PbTiO_3$ analysis. If the previously in detail discussed parameter l_D is larger than the distance between the centres of neighbouring islands, the islands will continue to grow until the entire region between the $SrRuO_3$ is filled with the deposited material. This is what seems to happen with the deposition $BiFeO_3$ on this $SrRuO_3$ structure: the islands slowly grow in lateral dimensions, until they merge and form one uniform layer.

The behaviour shown in the images of the second $BiFeO_3$ sample seemed in line with this simple explanation after the first $BiFeO_3$ deposition. The second deposition suddenly showed a more complex type of growth. Figures 4.5(f) and (g) seemed not to be in agreement with the simple idea that the flattening of the surface is just caused by the gradual increase in island dimensions until they grow together and fill in the remainder of the lower levels. The reason why the growth is more complex according to this AFM image is not immediately clear. The behaviour might, however, be caused by the smaller islands in between the islands in the nanowire direction that were already developing during the first $BiFeO_3$ growth (as can be seen in the images of figures 4.5(c) and (e)). These islands in between the rows all appear to be stretched out in the row direction. One explanation for the growth behaviour in figures 4.5(f) and (g) focusses again on the average diffusion length l_D of this growing combination. It might be that the approximately circular islands as the ones in figures 4.5(c) and (e) (the images near the centre of the sample after the first $BiFeO_3$ deposition) are formed because the l_D value still exceeded the average island diameter, but that during the second deposition the sizes of the circular islands in the nanowire direction became greater than l_D, leading to a stabilization of the islands sizes. Possibly, this critical island size is seen in figures 4.5(f) and (g) in the average circular islands, who have all almost the same size.

At first sight, the here described situation seems invalid, since circular islands in figures 4.5(f) and (g) seem very small compared to large clusters of multiple circular islands grown together, indicating that the average diffusion length is still a lot greater than the size of a regular circular island. But, this merging of circular islands could be caused by the small islands in between the rows, who are (as becomes clear by looking at figures 4.5(c) and (e)) not even approximately circular, but stretched out along the nanowire direction. This in combination with the fact that the distance between the rows in 4.5(c) and (e) are smaller than the width of the rows itself, makes that l_D probably never exceeded the dimension of the small islands in the direction opposite to the row direction and that the presence of the small islands caused the merging of the circular islands. This interpretation explains why the circular islands grew together in some regions in 4.5(f) and (g) and stayed apart in other areas: the existence of a small stretched out island in between two circular islands provided the opportunity to grow together.

Further deposition of $BiFeO_3$ on this substrate will eventually lead to a flat surface, just as happened on sample 1. This is still in agreement with the above described explanation, since growing on islands with the islands sizes exceeding the average diffusion length l_D still causes little enlargement in the islands sizes. This can be understood by remembering that l_D is nothing more than the *average* diffusion length: adatoms deposited near the edges of an island still have the change to reach the edges of the island. This behaviour was also observed on the first $PbTiO_3$ sample (e.g. see figure 4.2(f)) — where the topography remained the same after depositing more and more $PbTiO_3$ on the sample, but some island merging is still observed after the last deposition — and it also the reason why the surfaces of all of the used samples would eventually became flat as long as one does long enough depositions (this was even the way a flat $SrRuO_3$ was created for a diffusivity analysis of both ferroelectric materials). Since the lower situated regions in 4.5(f) and (g) are only very small (so the distances between the various islands are minimal), the transformation of this surface into an atomically flat surface will not need a long extra deposition.

5.2 Limitations in the comparison of the $PbTiO_3$ and $BiFeO_3$ diffusivities

The model for epitaxial growth on a singular surface is based on a couple of assumptions. The model assumes instantaneous nucleation at the start of every monolayer, the step edges act as perfect sinks, no nucleation on top of the islands and a direct coupling between the average particle density and the diffusive scattered intensity.

The used substrates form the first point of discussion. The substrate used for $PbTiO_3$ growth was not flat at all and the substrate used for $BiFeO_3$ looked flat but had holes with small lateral dimensions but very large vertical dimensions. This is contradictory to the used model (which was based on epitaxial growth on a singular surface). The fact that the substrate used for $PbTiO_3$ was not flat could have resulted in a different diffusivity coefficient. The target material that is deposited onto the rough substrate does not get the chance to diffuse the full diffusion distance, as it is likely that the particle will get stuck in a cavity. Besides not being able to diffuse freely, the surface is three-dimensional from the start. This will not enhance two dimensional growth (which is a demand for the used model), since the deposited material will settle on multiple height levels of the substrate.

The second point of discussion is the determination of the nuclei density (N_S). It would have been nice to be able to determine the actual value of this density, by looking at AFM pictures made halfway the deposition of a monolayer of $PbTiO_3$ or $BiFeO_3$. Unfortunately these images were not available, and different methods had to be devised. The first alternative method, described in 'Results' section, is used for determining the ratio between the amount of nuclei of $PbTiO_3$ and $BiFeO_3$. Although the method does not provide the actual nuclei density, it should give a qualitatively indication to what the ratio between the nucleation densities should be. This also means that the values found for the diffusivity coefficients are not the actual coefficients, but a mere indication of the relative diffusivity coefficients. The second alternative method did provide an actual value of the nuclei density, but unfortunately only for $PbTiO_3$. This means that the actual diffusivity coefficients for $PbTiO_3$ on $SrRuO_3$ can be determined, but there is no diffusivity coefficient for the growth of $BiFeO_3$ on $SrRuO_3$ to compare them to.

Another point of discussion is the large signal to noise ratio (SNR). Figure 4.7 and figure 4.8 show RHEED intensity spectra for $PbTiO_3$ and $BiFeO_3$ respectively. In these figures, it is obvious that a high amount of noise is present in the signal. For some reason the $BiFeO_3$ measurement suffers from this noise more than the $PbTiO_3$ measurement. This RHEED data is used to determine the relaxation time, by using equation 1.14, and determining the best fit for a section of the spectrum between two laser pulses. Using data with a large SNR leads to a large error in the possible fitting. This is reflected in the errors that are displayed in table 4.2 and table 4.3. The $PbTiO_3$ errors, above the horizontal line, are in the range of approximately 5% and 32%. The errors below the horizontal line are tremendously bigger. In fact these errors are so big that these diffusivity coefficients can not be used to form any conclusion. The $BiFeO_3$ errors are bigger than the errors in the $PbTiO_3$ values, because of the larger SNR. Only the first relative diffusivity coefficients that are found in the experiment can be compared to each other, but one has to keep in mind that these are not the actual diffusivity coefficients, but represents only the ratio between the two values.

For achieving the goal of the experiment — to determine the difference in the growth behaviour between the two ferroelectric materials — it is not sufficient to only look at the growth of $PbTiO_3$ and $BiFeO_3$ on $SrRuO_3$. The growth of $PbTiO_3$ on itself and $BiFeO_3$ on itself should also be considered. Unfortunately, only an indication could be made of the relative diffusivities of the growth of $PbTiO_3$ on $SrRuO_3$ and the growth of $BiFeO_3$ on $SrRuO_3$. During the growth process the substrate on which the target is deposited changes; the surface used to consist of only $SrRuO_3$ and this slowly changes into $PbTiO_3$ or $BiFeO_3$. This inherently changes the diffusivity of the target material on the substrate. Therefore it would have been interesting to not only find indications of the diffusivity of $PbTiO_3$ on $SrRuO_3$ and $BiFeO_3$ on $SrRuO_3$, but also of $PbTiO_3$ on $PbTiO_3$ and $BiFeO_3$ on $BiFeO_3$. This would allow one to predict the growth of the materials and maybe even for a prediction of critical points in the growth process.

The last point of discussion in this section is based on figures 4.7 and 4.11. These images show that the $PbTiO_3$ did not grow in a single growth mode. This observation is based on the fact that in the minimum of the RHEED intensity plot, the intensity still shows a recovery after every deposition pulse. Besides this, figure 4.11 shows two flat parts in the RHEED intensity spectrum. Both of these observation suggest step flow growth besides the layer-by-layer growth which is also present. This compromises the validity of the initial assumption that the two depositions — $PbTiO_3$ on $SrRuO_3$ and $BiFeO_3$ on $SrRuO_3$ — grow in similar conditions.

5.3 Comparison between experimental results and simulation outcomes

One of the main outcomes of the simulation is the awareness that growing material on three-dimensional structures (like islands) always leads to a certain amount of flattening of the surface. For long enough depositions, each structure will eventually grow flat. This is understood by simple considering that the diffusivity of particles deposited on the structure is always just a characterization technique, giving an indication of average diffusion phenomena when growing thin films in certain combinations. The average diffusion length l_D, which does not depend on the surface morphology when growing one material on another material, is the *average* length an adatom can diffuse on a flat surface before being bond to the surface. This value is always bigger than zero, and this means that the deposition of atoms on an island will always mean atoms will descend to the lower level in between the islands, even if the size of an island is a lot bigger than the l_D value for the growth. Flattening of the surface is thus inevitable but it can be achieved sooner for one growth combination than for another.

This became clear in the simulations: figure 4.13 shows (in comparison with figure 4.12) that an increase in the $E_{S,S}$ and $E_{S,F}$ — which lowers the diffusivity of the deposited particles on $SrRuO_3$ and other deposited particles — leads to a situation where the initial island structure is longer maintained than for lower values of this surface diffusion barrier. Because of the fact that the bonding of the deposited particles with other deposited material is much stronger than the bonding with the substrate material $DyScO_3$ in between the islands, adatoms do not diffuse to the edges of the islands in the first part of the deposition. This means that the formation of such 'stairs' along the edges of the islands is not achieved. The situation changes suddenly changes when there is enough material deposited to entirely cover the $DyScO_3$ surface. In that case, there is only significant diffusion barrier left, and the formation of stairs, followed by the merging of the islands and the flattening of the surface, still takes place. A very interesting result of the model is found in figure 4.14, where it is shown that a very low $E_{S,S}$ value and a very high $E_{S,F}$ value are capable of retaining the island morphology even longer than the previous settings. In this case the deposited particles on top of the islands also have a much stronger bonding with each other than with the $SrRuO_3$ (just as is still the case on the lower level), leading to the formation of smaller extra islands on top of the $SrRuO_3$ islands. These smaller islands can be seen clearly in figure 4.14. A continuation of the deposition leads to the same events as in the previous combination, but the existence of these smaller islands is probably the cause for the fact that the flattening takes more deposition pulses.

Much of the behaviour seen in the AFM images of the step by step analysis (figures 4.2, 4.3, 4.4 and 4.5) is in line with the insight gained in the simulation. The $PbTiO_3$ images, for example, showed that there was indeed some islands merging going on, even for sample 1 after the second $PbTiO_3$ deposition. Sample 2 showed that, at least if the apparent island growth is real, the increase of the islands is in agreement with the simulations: gradual growth in directions perpendicular to the step edges, probably the result of the rising of 'stairs' across these edges. The same growth pattern is seen in the samples of $BiFeO_3$.

The simulations thus show that a gradual flattening of the surface is always going on when depositing a substantial amount of material on three-dimensional structures. The rate at which this flattening takes place depends on the diffusion parameters of the growth combination. According to the results of the simulation, the best way to remain a $SrRuO_3$ three-dimensional

structure as long as possible, is to chose a material for deposition which has a much higher diffusion energy barrier for growing on itself than for growing on both $DyScO_3$ and $SrRu_3$. The results show that the influence of the difference between the deposition material and $DyScO_3$ is a bigger than the influence of the difference between the material and $SrRuO_3$. This is not in accordance with the expectations, since it was expected that the diffusivity of the materials on $DyScO_3$ would not matter that much in the process. Now that it appears that the influence of $DyScO_3$ is bigger than expected, a determination of the diffusivities of $PbTiO_3$ and $BiFeO_3$ on a flat $DyScO_3$ substrate might have also been useful in the analysis of the growth of these two materials on this $SrRuO_3/DyScO_3$ structures.

Although in 'Results' an indication is presented that the diffusivity for $PbTiO_3$ growth on $SrRuO_3$ is higher than for $BiFeO_3$ growth on $SrRuO_3$, this is, according to the results of the simulation, not directly an explanation for the difference in the flattening rate for both materials. This explanation should instead be found in a comparison of the diffusivities for the growth of the two materials on $SrRuO_3$ with the diffusivities for the growth on themselves. These results indicate that diffusivity coefficients of the two ferroelectrics for growing on themselves are much higher than coefficients for growing on $SrRuO_3$. According to the model, high diffusivities for growing the deposition material on itself give rise to a fast flattening of the surface. This could be the explanation why $BiFeO_3$ flattens the surface so quickly: in table 4.3, a very high diffusivity coefficient for $BiFeO_3$ on $BiFeO_3$ growth(compared to the coefficient for $PbTiO_3$ on $PbTiO_3$ growth) was determined. This could, however, only been done by making an assumption not based on any experimental data, as described in the previous section of this discussion.

Besides all of this one should always keep in mind that this results are based on the results of a simulation model. When dealing with models, there is always the possibility that certain effects are just caused by the algorithm itself, instead of describing real physical relations. One of the most important assumptions in this particular model is the restricting that particles are not allowed to move up by one than one step. This assumption seems logical since this research was based on explaining flattening phenomena instead of the creation of 3D structures. It might however influence the growth modes in such a way that the results become misleading.

All in all, combining the different aspects of this research does not lead to one solid explanation for the different growth type of $PbTiO_3$ and $BiFeO_3$ on $SrRuO_3$ structures on $DyScO_3$ substrates. The simulation shows that this difference in growth type is probably nothing more than a distinct 'flattening rate' for both materials. Both the experimental sections give rise to a very strong indication that difference is caused by a divergence in diffusivity for the two growth combinations; $BiFeO_3$ should in that case have a higher diffusion coefficient than $PbTiO_3$ for both the growth on $SrRuO_3$ and the materials themselves. The first experimental section indicates that the average diffusion length for $BiFeO_3$ growth is a lot smaller than the diffusion length for $PbTiO_3$ growth. These values, albeit nothing more than indications, are in agreement with the behaviour showed in the step by step analysis, where a different average diffusion length l_D could be explained as the main reason for the formation of islands with dissimilar sizes. This research can be seen as a first step in solving the exact cause of the different $PbTiO_3$ and $BiFeO_3$ growth on $SrRuO_3/DyScO_3$ surfaces. Further research should make clear whether or not the indications presented in this report are descriptions of the real phenomenon.

Chapter 6

Conclusion

The conducted research consists of two experimental and a simulation part. The results of the simulation, a solid-on-solid kinetic Monte Carlo model, show (under the used restrictions) that eventually every three-dimensional surface will grow flat. The number of deposition pulses applied before a flat surface is achieved, depends on the used diffusion parameters. The outcomes of this simulation part further indicates that the most suitable material for remaining a $SrRuO_3$ three-dimensional structure for as many deposition pulses as possible, is a material which has a much higher diffusion energy barrier (and thus a much lower diffusivity) for growing on itself than for growing on both $DyScO_3$ and $SrRu_3$. A last important result of the Monte Carlo simulations is the observation that the influence of the diffusivity for growth on $DyScO_3$ is higher than the influence for growth on $SrRuO_3$, and therefore that this influence is also higher than expected at the start of this research.

For the experimental parts, most of the behaviour shown in the step by step analysis is in agreement with the expectations. There are, however, some surprises. Possible explanations for the phenomenon seen in the STM and AFM images — such as the enlargement of the island sizes on the second $PbTiO_3$ sample and the complex way of growing that was observed on the second $BeFiO_3$ sample — do not give rise to rejecting the formulated hypothesis, but rather imply some confirmation of this expectation. That is because the developments shown in figures 4.2, 4.3, 4.4 and 4.5 could be explained as a result of a different average diffusion length l_D for both of the materials, as is done in the section 4.1.

Beside this, section 4.2 of 'Results' presents two indications for the relative diffusivities. The main outcome is repeated in table 6.1. For the determination of these value, a model has been used that assumes instantaneous nucleation and layer-by-layer growth on a singular surface. These diffusivity coefficients of $PbTiO_3$ and $BiFeO_3$ are called 'relative diffusivities', because they are related to the coefficient of the other material. This is due to the fact that the nucleation densities for the have not been determined absolutely. Rather, a ratio between the nuclei density of $PbTiO_3$ and $BiFeO_3$ is estimated. The values in the table presented below are therefore only useful when a comparison between the $PbTiO_3$ and $BiFeO_3$ diffusivities is performed. Because the $SrRuO_3$ surface at which the $PbTiO_3$ was deposited turned out to be not flat, an estimation of the absolute value of the nucleation density could be made for just the $PbTiO_3$ case. The resulting diffusivities for this estimation are listed in table 4.4.

	$PbTiO_3$	$BiFeO_3$
Relative diffusivity ($\mu m^2/s$)	1.225 ± 0.0603	6.1 ± 1.15

Table 6.1: Indication of relative diffusivities of $PbTiO_3$ and $BiFeO_3$

Although the research does not provide 'solid proof', the values in table 6.1 indicate that $BiFeO_3$ has a higher diffusivity coefficient than $PbTiO_3$ on a $SrRuO_3$ substrate. This result is in agree-

ment with the original hypothesis. Unfortunately, the obtained data did not allow for a comparison of the diffusivity coefficients of $PbTiO_3$ on $PbTiO_3$ and $BiFeO_3$ on $BiFeO_3$. Combining the fact that this comparison is needed in order to fully understand the exact mechanism with the observation that according to the simulation the effect of growth on $DyScO_3$ should be examined as well, makes that this research does not proof the formulated hypothesis. The results does, however, *suggest* these growing phenomena are caused by a difference in diffusivity coefficients for the growth of both $PbTiO_3$ and $BiFeO_3$ on particular $DyScO_3/SrRuO_3$ structures.

6.1 Recommendations

As stated above, the introduced hypothesis is only partly proven; just an indication of the ratio between the diffusivities of the ferroelectric materials on $SrRuO_3$ has been found. The diffusivity for $PbTiO_3$ on $SrRuO_3$ has been determined, but the matching values for $BiFeO_3$ could not have been determined. In order to compare the actual diffusivity coefficients for both materials on both $SrRuO_3$ and the material itself, more experiments should be conducted.

For determining the diffusivities of $PbTiO_3$ or $BiFeO_3$ on $SrRuO_3$, the experiments should be repeated on actual flat $SrRuO_3$ samples. After the first few deposition of the ferroelectric material both samples should be inspected using a scanning probe microscope to determine the nucleation density. Completing the depositions of a couple of monolayers of the ferroelectric materials, while measuring the RHEED intensity, should give the relaxation times. These relaxation times can then be used, in combination with the found nucleation densities, to find the diffusivities of $PbTiO_3$ and $BiFeO_3$ on $SrRuO_3$.

Another interesting experiment, is to grow the ferroelectric materials on a vicinal surface in step flow growth mode. When growing in step flow growth mode, the diffusion length l_D equals the terrace width l_T. Zhu [29] proposed a model that describes the diffusivity as a function of the relaxation time τ and the diffusion length l_D.

$$D_S \sim \frac{4l_D^2}{\pi^2\tau} = \frac{4l_T^2}{\pi^2\tau} \tag{6.1}$$

The general idea of the experiment is to make a substrate with a miscut not equal to zero. By growing either $PbTiO_3$ or $BiFeO_3$ onto this vicinal surface, while monitoring the RHEED intensity, the relaxation time can be determined. During the growth process the relaxation time should not change, since this is a characteristic of step flow growth. Once the step flow growth is achieved and the RHEED measurement is done, l_T and therefore l_D can be determined by imaging the surface with an AFM. Equation 6.1 shows that the diffusivity is proportional to the diffusion length and the relaxation time. The found diffusivity coefficients are the diffusivities of $PbTiO_3$ on $PbTiO_3$ and $BiFeO_3$ on $BiFeO_3$.

The step by step analysis could, of course, be improved by gaining AFM data at more stages during the growth. To do this efficiently, an experimental set-up should be used where AFM images could be made without having to do all the steps before and after a deposition (as heating, pre-ablation and annealing). Ideas for creating a device which can perform AFM measurements after each few laser pulses, could turn out very useful for really examining this growth behaviour. In this analysis, also samples with multiple $SrRuO_3$ islands sizes could be used. The possible change in island dimensions after growing the ferroelectrics on these samples could provide more information about the role the average diffusion lengths on the different terminations plays in this growth.

Improvements in the kinetic Monte Carlo simulation could, first of all, be made by rewriting the algorithm in a more efficient language than the standard MATLAB language. Programming in MATLAB is user-friendly and does not require a lot of programming experience, which is the reason why it is used for this research. However, executing an MATLAB algorithm requires more simulation time, than (for example) compiling an C++ algorithm. Therefore, writing the algorithm in C++ programming language probably means that more realistic conditions (cf. temperatures higher than 300 °C) can be used for the same simulation time. More improvements

in the simulation code could be made by introducing more physical growth phenomena in the model; the restriction that particles can not hop to sites which are situated at more than one step higher could, for example, be replaced by inserting a physical barrier for hopping in vertical directions.

As mentioned numerous times, the results of the simulation model show that the influence of the diffusivity of the deposited atoms on $DyScO_3$ might be higher than expected. A possible difference in the diffusivity of $PbTiO_3$ and $BiFeO_3$ on $DyScO_3$ could be determined with the same methods as for the determination of diffusivity parameters on a $SrRuO_3$ surface. Discovering whether the influence of $DyScO_3$ is really that sufficient, could perhaps be achieved by making use of other perovskite materials in this lattice parameter group. Proper determination of all diffusivity coefficients (on $DyScO_3$, on $SrRuO_3$ and on itself) for all the materials used for deposition should allow for a more complete analysis of the influence of each of the diffusivities. This bigger research plan also provide more opportunities for using the simulated growth behaviour: growth types observed step by step analyses for each of the materials could be compared to outcomes of the model for a better understanding of what diffusivity parameters really have an influence on the growth.

Bibliography

[1] B. Kuiper, J.L. Blok, H.J.W. Zandvliet, D.H.A. Blank, G. Rijnders and G. Koster (2011), 'Self-organization of $SrRuO_3$ nanowires on ordered oxide surface terminations,' *MRS Communications*, **1** (1), pp. 17-21

[2] B.F. Smith (2009), *Lead Titanate films on Dysprosium Scandate with a Strontium Ruthenate Buffer Layer grown by Pulsed Laser Deposition*, Master's Thesis, Rijksuniversiteit Groningen

[3] K. Lee and S. Baik (2006), 'Ferroelectric domain structure and switching in epitaxial ferroelectric thin films,' *Annual Review of Materials Research*, **36**, pp. 81-116

[4] M. Ohring (2001), *The materials science of thin films: deposition and structure*, second edition, Academic Press

[5] N. Ramadass (1978), 'ABO_3-type oxides — Their structure and properties — A bird's eye view', *Materials Science and Engineering*, **36** (2), pp. 231-239

[6] A.J.H.M. Rijnders (2001), *The Initial Growth of Complex Oxides: Study and Manipulation*, Ph.D. Thesis, Faculty of Science and Technology, University of Twente

[7] G. Rijnders and D.H.A. Blank (2007), 'Growth Kinetics During Pulsed Laser Deposition,' *Pulsed Laser Deposition of Thin Films: Applications-Led Growth of Functional Materials*, John Wiley & Sons, Inc.

[8] G. Koster (1999), *Artificially layered oxides by pulsed laser deposition*, Ph.D. thesis, Faculty of Science and Technology, University of Twente

[9] D. Kothari, V.R. Reddy, V.G. Sathe, A. Gupta, A. Banerjee and A.M. Awasthi (2008), 'Raman scattering study of polycrystalline magnetoelectric $BiFeO_3$,' *Journal of Magnetism and Magnetic Materials*, **320**, pp. 548-552

[10] J.D. Weeks and G.H. Gilmer (1979), 'Dynamics of crystal growth,' *Advances in Chemical Physics*, **40**, pp. 157-228

[11] K. Liu, H. Fan, P. Ren and C. Yang (2011), 'Structural, electronic and optical properties of $BiFeO_3$ studied by first-principles,' *Journal of Alloys and Compounds*, **509** (5) , pp. 1901-1905

[12] Q.L. Zhang, J.L. Zhu, J.Z. Tan, G.L. Yu, J.G. Wu, J.G. Zhu and D.Q. Xiao (2006), 'Monte Carlo simulation of the growth of $SrTiO_3$ thin film with molecular source,' *Vacuum*, **81** (4), pp. 539-544

[13] X.J. Zheng, B. Yang, Z. Zhu, B. Wu and Y.L Mao (2007), 'Kinetic Monte Carlo simulation of growth of $BaTiO_3$ thin film via pulsed laser deposition,' *Transactions of Nonferrous Metals Society of China*, **17** (6), pp. 1441-1446

[14] C. Ratch and A. Zangwill (1993), 'Step-flow growth on strained surfaces,' *Applied Physics Letters*, **63** (17), pp. 2348-2350

[15] P.A. Maksym (1988), 'Fast Monte Carlo simulation of MBE growth,' *Semiconductor Science and Technology*, **3** (6), pp. 594-596

[16] P.R. Willmott and J.R. Huber (2001), 'Pulsed laser vaporization and deposition,' *Reviews of Modern Physics*, **72** (1), pp. 315-328

[17] N. Jalili and K. Laxminarayana (2004), 'A review of atomic force microscopy imaging systems: application to molecular metrology and biological sciences,' *Mechatronics*, **14**, pp. 907-945

[18] A. Vilalta-Clemente and K. Gloystein (2008), *Principles of Atomic Force Microscopy*, Lecture notes Physics of Advanced Materials Winter School, Aristotle University, Thessaloniki (Greece)

[19] Brooklyn College, *Atomic Force Microscopy*, Department of Physics, http://userhome.brooklyn.cuny.edu/mlnakarmi/facility/AFM.html, visited: 15th June 2012

[20] J. Tersoff and D.R. Hamann (1985), 'Theory of the scanning tunnelling microscope,' *Physical Review B*, **31** (2), pp. 805-813

[21] G. Binning and H. Rohrer (1983), 'Surface imaging by scanning tunneling microscopy,' *Ultramicroscopy*, **11** (11), pp. 157-160

[22] R. Reifenberger (2002), *TEM Pictures of STM Tips*, http://www.physics.purdue.edu/nanophys/uhvstm/tip.html, visited: 15th June 2012

[23] I. El-Kholy (2009), *Surface dynamics of silicon low-index surfaces studied by reflection high-energy electron diffraction*, Doctoral Thesis, Electrical and Computer Engineering, Old Dominion University

[24] A. Ichimiya and P.I. Cohen (2004), *Reflection High Energy Electron Diffraction*, first edition, Cambridge University Press, Cambridge

[25] B. Kuiper (2009), *Self-assembled $SrRuO_3$ nanowires through selective growth on $DyScO_3$ surface terminations*, Master's thesis, Faculty of Science and Technology, University of Twente

[26] M.D. Biegalski, J.H. Haeni, S. Trolier-McKinstry, D.G. Schlom, C.D. Brandle and A.J. Ven Graitis (2005), 'Thermal expansion of the new perovskite substrates $DyScO_3$ and $GdScO_3$,' *Journal of Materials Research*, **20** (4), pp. 952-958

[27] X.D. Wu, S.R. Foltyn, R.C. Dye, Y. Coulter and R.E. Muenchausen (1993),'Properties of epitaxial $SrRuO_3$ thin film,' *Applied Physics Letters*, **62**, pp. 2434-2436

[28] H. Landolt and R. Bornstein (1996), *Numerical Data and Functional Relationship in Science and Technology*, Springer, Berlin

[29] X.D. Zhu and E. Nabighian (1998), 'Azimuthal dependence of classical over-barrier hopping diffusion of hydrogen on a vicinal Ni(111) surface,' *Physical Review*, **58** (12)

Appendix A: The MATLAB Algorithm

In this appendix, a version of the MATLAB algorithm used for the simulations is presented. In this m-code the green parts are comments, included to provide explanations about the different parts of the algorithm. The algorithm itself is not as compact as one could ultimately achieve. This is caused by the fact that this algorithm only calculates necessary values: instead of just letting MATLAB calculate all the hopping rates again after a deposition event, this algorithm only computes the new hopping rates of the (few) grid positions that actually change as a result of a hopping event (these positions are calculated and used in the recurring arrays `v1` in the algorithm). This approach makes the code a lot less compact and transparent, but gives rise to a much more efficient execution in terms of simulation time.

For some of the simulations, a few variations and additions in this code have been used as well. Nonetheless, these variations are very straightforward and do not influence the general ideas behind the algorithm. Therefore, this conditional extra parts have not been included in the code below.

```
%% Creation of the substrate
clear all; close all; clc

isl     = imread('island.bmp');          % 'island.bmp' is a picture of the shape of the islands (in this case a circle)
d       = 11;                            % The diameter (in pixels) of the SrRuO3 islands on the substrate (this should
                                           be an odd number)
isl     =~im2bw(isl,graythresh(isl));
isl     = imresize(isl,[d d]);           % This last two commands create a binary matrix with (in this case) islands
                                           with a diameter of d px.
hght    = 23;                            % The height of the SrRuO3 islands

N       = 100*100;                       % The dimensions of the substrate
sqN     = sqrt(N);
sub     = zeros(sqN,sqN);                % The 'substrate' (the starting position), a sqrt(N) x sqrt(N) px surface

border  = zeros(8,sqN);
border(1,:) = 1 : 1 : sqN;               % Determination of the indices on the borders of the grid represented by H
border(2,:) = border(1,:) + sqN;
border(3,:) = (N-sqN+1) : 1 : N;
border(4,:) = border(3,:) - sqN;
border(5,:) = 1 : sqN : (N-sqN+1);
border(6,:) = border(5,:) + 1;
border(7,:) = sqN : sqN : N;
border(8,:) = border(7,:) - 1;

numI    = 5*5;                           % The number of islands on the substrate
sqnumI  = sqrt(numI);
cnt     = sqN/(sqnumI);                  % The index of the center of the first island in the row

for k = 1:sqnumI;
    for m = 1:sqnumI;
        sub(((k-0.5)*cnt-(d-1)/2):((k-0.5)*cnt+(d-1)/2),((m-0.5)*cnt-(d-1)/2):((m-0.5)*cnt)+(d-1)/2) = isl;
    end
end

H       = zeros(1,N);
for k = 1:sqN;              % This loop transforms the substrate matrix into an 1D array. This is because it is easier
                              to work with an array in the rest of the program.
    H((k-1)*sqN+1:k*sqN) = sub(:,k);
end
H       = hght * H;         % The islands are set at the right height
indI    = find(H==hght);    % The array 'indI' tells us wat the indices of the islands in H are. This is useful,
                              because this tells us where the surface barrier of SrRuO3 shoud be used.


%% Simulation pulsed laser deposition of ferroelectric materials PbTiO3 and BiFeO3 on SrRuO3 islands

%% Parameters for the simulation:
np      = 20;               % The number of pulses for the deposition of one monolayer
dnum    = 200;              % The number of pulses in the simulation
```

```
drate   = 1;                % The deposition rate (in s^(-1))
dtime   = 1/drate;          % Time between two deposition pulses (in s)
% The substrate is created in the previous section ('Creation of the substrate')
EsD     = 1.2;              % The energy barrier due to bonding with the DyScO3 substrate (in eV)
EsS     = 1.2;              % The energy barrier due to bonding with SrRuO3 islands (in eV)
EsF     = 0.25;             % The energy barrier due to bonding with the ferroelectric (PbTiO3 or BeFiO3) (in eV)
En      = 0.25;             % The nearest-neighbour bond energy (in eV)
kB      = 8.617332478e-5;   % Bolzmann constant (in eV K^(-1))
k0      = 1e13;             % The hopping rate or hopping frequency (in s^(-1))
T       = 300 + 273.15;     % The temperature (in K)

%% Deposition of the ferroelectric unit cells:
% The number of deposition pulses during this simulation:
Hops = zeros(15,N);
for op = 1:15;
for v = 1:dnum;
    %% Instantaneous deposition of (N/np) molecules
    deppos = zeros(1,(N/np)); % 'deppos' keeps track of the indices of deposited positions during the concerning pulse
    for i = 1:(N/np);
        p = round(rand*N);
        while ismember(p,deppos) == 1;
            p = round(rand*N);
        end
        deppos(i) = p;
        H(p) = H(p) + 1;
    end

    %% Diffusion of molecules
    % Hopping rate calculation:
    tau     = 0;                % Resets the 'time' passed since the last deposition pulse (this value determines the
                                        number of diffusivity events before the deposition of a new bunch of particles)
    events  = zeros(1,4*N);
    Es      = zeros(1,N);
    n       = zeros(1,N);
    for i = 1:N;
        b = zeros(1,8);
        if (H(i) == 0) || (H(i) == hght && ismember(i,indI) == 1);
            events((i*4-3):i*4) = 0;
        else                    % 'else' means here that the concerning gridsite i is not part of the substrate
            if H(i) == 1;
                Es(i) = EsD;
            elseif H(i) == (hght + 1) && ismember(i,indI) == 1;   % If the concerning molecule is the first molecule on
                                        a SrRuO3 island, the energy barrier of the ferroelectric with SrRuO3 is activated.
                Es(i) = EsS;
            else                % 'else' means that the concerning molecule is at least the second one on the substrate
                Es(i) = EsF;
            end

            % Determining whether the gridsite i is on the border of the grid and, if yes, on which border:
            for q = 1:8;
                if ismember(i,border(q,:)) == 1;
                    b(q) = 1;
                end
            end

            % Calculating the number of nearest-neighbours for gridsite i:
            if H(i + b(1)*N - sqN) >= H(i);    % Check for nearest-neighbours on the left of i
                n(i) = n(i) + 1;
            end
            if H(i - b(3)*N + sqN) >= H(i);    % Check for nearest-neighbours on the right of i
                n(i) = n(i) + 1;
            end
            if H(i + b(5)*sqN - 1) >= H(i);    % Check for nearest-neighbours above i
                n(i) = n(i) + 1;
            end
            if H(i - b(7)*sqN + 1) >= H(i);    % Check for nearest-neighbours below i
                n(i) = n(i) + 1;
            end
            k = k0*exp(-(Es(i)+n(i)*En)/(kB*T));

            % Calculating the number of nearest-neighbours when moving to the left of gridsite i:
            if (H(i + b(1)*N - sqN) - H(i)) > 1;
                events(i*4-3) = 0;             % Molecules are not allowed to move up by more than one step
            else
                events(i*4-3) = k;             % Store the hopping rate for hopping to the left
            end

            % Calculating the number of nearest-neighbours when moving to the right of gridsite i:
            if (H(i - b(3)*N + sqN) - H(i)) > 1;
                events(i*4-2) = 0;             % Molecules are not allowed to move up by more than one step
            else
                events(i*4-2) = k;             % Store the hopping rate for hopping to the right
            end

            % Calculating the number of nearest-neighbours when moving one place up gridsite i:
            if (H(i + b(5)*sqN - 1) - H(i)) > 1;
```

```
            events(i*4-1) = 0;              % Molecules are not allowed to move up by more than one step
        else
            events(i*4-1) = k;              % Store the hopping rate for hopping to the position above i
        end

        % Calculating the number of nearest-neighbours when moving one place down gridsite i:
        if (H(i - b(7)*sqN + 1) - H(i)) > 1;
            events(i*4) = 0;                % Molecules are not allowed to move up by more than one step
        else
            events(i*4) = k;            % Store the hopping rate for hopping to the position below i
        end
    end
end

%% Event selecting:
while tau < 1;                          % Number of diffusivity events between two laser pulses
    Rh      = 0;
    De      = 1;
    p       = N*4;
    L       = sum(events);
    r       = L*rand;
    while (p-De) ~= 1;
        te = round(De + (p-De)/2);
        Rhlast = Rh;
        Rh = Rh + sum(events(De:te));
        if r < Rh;
            De = De;
            p = te;
            Rh = Rhlast;
        else
            De = te;
            p = p;
            Rh = Rh;
        end
    end
    i       = ceil(p/4);            % Determines at which gridsite the selected event takes place
    m       = rem(p,4);             % Determines the remainder of p/5. The outcome tells us in which direction the
                                    molecule on gridsite i should move.

    % Determining whether the selected gridsite i is on the border of the grid and, if yes, on which border:
    b = zeros(1,N);
    for q = 1:8;
        if ismember(i,border(q,:)) == 1;
            b(q) = 1;
        end
    end

    if m == 1;                  % If m == 1, the molecule moves one position to the left
        H(i) = H(i) - 1;
        H(i + b(1)*N - sqN) = H(i + b(1)*N - sqN) + 1;

        % Updating the surface material for the site H(i)
        if (H(i) == 0) || (H(i) == hght && ismember(i,indI) == 1);
            events((i*4-3):i*4) = 0;
        else                    % 'else' means here that the concerning gridsite i is not part of the substrate
            if H(i) == 1;
                Es(i) = EsD;
            elseif H(i) == (hght + 1) && ismember(i,indI) == 1;   % If the concerning molecule is the first molecule on
                                a SrRuO3 island, the energy barrier of the ferroelectric with SrRuO3 is activated.
                Es(i) = EsS;
            else            % 'else' means that the concerning molecule is at least the second one on the substrate
                Es(i) = EsF;
            end
        end

        % Updating the surface material for the site (i + b(1)*N - sqN)
        if H(i + b(1)*N - sqN) == 1;
            Es(i + b(1)*N - sqN) = EsD;
        elseif H(i + b(1)*N - sqN) == (hght + 1) && ismember((i + b(1)*N - sqN),indI) == 1;   % If the concerning
                                    molecule is the first molecule on a SrRuO3 island, the energy barrier of the
                                    ferroelectric with SrRuO3 is activated.
            Es(i + b(1)*N - sqN) = EsS;
        else                % 'else' means here that the concerning molecule is at least the second ferroelectric
                                    molecule in its row
            Es(i + b(1)*N - sqN) = EsF;
        end

        v1 = [(i) (i - 2*sqN + (b(2) + b(1))*N)  (i - sqN - 1 + b(1)*N + b(5)*sqN)  (i - sqN + b(1)*N)  (i - sqN +
                                    1 + b(1)*N - b(7)*sqN)  (i - 1 + b(5)*sqN)  (i + 1 - b(7)*sqN)  (i + sqN -
                                    b(3)*N)];

        % Calculating the number of nearest-neighbours for 8 gridsites of v1:
        for j = v1;
            if (H(j) == 0) || (H(j) == hght && ismember(j,indI) == 1);
                events((j*4-3):j*4) = 0;
            else                    % 'else' means here that the concerning gridsite j is not part of the substrate
```

```
            % Calculating the number of nearest-neighbours for gridsite j:
            bj = zeros(1,4);
            for q = 1:4;
                if ismember(j,border((2*q-1),:)) == 1;
                    bj(q) = 1;
                end
            end
            n(j) = 0;
            if H(j + bj(1)*N - sqN) >= H(j);    % Check for nearest-neighbours on the left of j
                n(j) = n(j) + 1;
            end
            if H(j - bj(2)*N + sqN) >= H(j);    % Check for nearest-neighbours on the right of j
                n(j) = n(j) + 1;
            end
            if H(j + bj(3)*sqN - 1) >= H(j);    %  Check for nearest-neighbours above j
                n(j) = n(j) + 1;
            end
            if H(j - bj(4)*sqN + 1) >= H(j);    % Check for nearest-neighbours below j
                n(j) = n(j) + 1;
            end
            k = k0*exp(-(Es(j)+n(j)*En)/(kB*T));

            % Calculating the number of nearest-neighbours when moving to the left of gridsite j:
            if (H(j + bj(1)*N - sqN) - H(j)) > 1;
                events(j*4-3) = 0;          % Molecules are not allowed to move up by more than one step
            else
                events(j*4-3) = k;    % Store the hopping rate for hopping to the left
            end

            % Calculating the number of nearest-neighbours when moving to the right of gridsite j:
            if (H(j - bj(2)*N + sqN) - H(j)) > 1;
                events(j*4-2) = 0;          % Molecules are not allowed to move up by more than one step
            else
                events(j*4-2) = k;    % Store the hopping rate for hopping to the right
            end

            % Calculating the number of nearest-neighbours when moving one place up gridsite j:
            if (H(j + bj(3)*sqN - 1) - H(j)) > 1;
                events(j*4-1) = 0;          % Molecules are not allowed to move up by more than one step
            else
                events(j*4-1) = k;    % Store the hopping rate for hopping to the position above j
            end

            % Calculating the number of nearest-neighbours when moving one place down gridsite j:
            if (H(j - bj(4)*sqN + 1) - H(j)) > 1;
                events(j*4) = 0;            % Molecules are not allowed to move up by more than one step
            else
                events(j*4) = k;    % Store the hopping rate for hopping to the position below j
            end
        end
    end

elseif m == 2;                  % If m == 2, the molecule moves one position to the right
    H(i) = H(i) - 1;
    H(i - b(3)*N + sqN) = H(i - b(3)*N + sqN) + 1;

    % Updating the surface material for the site i
    if (H(i) == 0) || (H(i) == hght && ismember(i,indI) == 1);
        events((i*4-3):i*4) = 0;
    else                    % 'else' means here that the concerning gridsite i is not part of the substrate
        if H(i) == 1;
            Es(i) = EsD;
        elseif H(i) == (hght + 1) && ismember(i,indI) == 1;   % If the concerning molecule is the first
                molecule on a SrRuO3 island, the energy barrier of the ferroelectric with SrRuO3 is activated.
            Es(i) = EsS;
        else      % 'else' means that the concerning molecule is at least the second one on the substrate
            Es(i) = EsF;
        end
    end

    % Updating the surface material for the site (i - b(3)*N + sqN)
    if H(i - b(3)*N + sqN) == 1;
        Es(i - b(3)*N + sqN) = EsD;
    elseif H(i - b(3)*N + sqN) == (hght + 1) && ismember((i - b(3)*N + sqN),indI) == 1;   % If the concerning
                molecule is the first molecule on a SrRuO3 island, the energy barrier of the ferroelectric
                with SrRuO3 is activated.
        Es(i - b(3)*N + sqN) = EsS;
    else % 'else' means here that the concerning molecule is at least the second ferroelectric one in its row
        Es(i - b(3)*N + sqN) = EsF;
    end


    v1 = [(i) (i - sqN  + b(1)*N)  (i - 1 + b(5)*sqN)  (i + 1 - b(7)*sqN)  (i + sqN - 1 - b(3)*N + b(5)*sqN) (i
                                + sqN - b(3)*N)  (i + sqN + 1 - b(3)*N - b(7)*sqN)  (i + 2*sqN - (b(4) +
                                b(3))*N)];
```

```
    % Calculating the number of nearest-neighbours for 8 gridsites of v1:
    for j = v1;
        if (H(j) == 0) || (H(j) == hght && ismember(j,indI) == 1);
            events((j*4-3):j*4) = 0;
        else                    % 'else' means here that the concerning gridsite j is not part of the substrate
            % Calculating the number of nearest-neighbours for gridsite j:
            bj = zeros(1,4);
            for q = 1:4;
                if ismember(j,border(2*q-1,:)) == 1;
                    bj(q) = 1;
                end
            end
            n(j) = 0;
            if H(j + bj(1)*N - sqN) >= H(j);    % Check for nearest-neighbours on the left of j
                n(j) = n(j) + 1;
            end
            if H(j - bj(2)*N + sqN) >= H(j);    % Check for nearest-neighbours on the right of j
                n(j) = n(j) + 1;
            end
            if H(j + bj(3)*sqN - 1) >= H(j);    % Check for nearest-neighbours above j
                n(j) = n(j) + 1;
            end
            if H(j - bj(4)*sqN + 1) >= H(j);    % Check for nearest-neighbours below j
                n(j) = n(j) + 1;
            end
            k = k0*exp(-(Es(j)+n(j)*En)/(kB*T));

            % Calculating the number of nearest-neighbours when moving to the left of gridsite j:
            if (H(j + bj(1)*N - sqN) - H(j)) > 1;
                events(j*4-3) = 0;          % Molecules are not allowed to move up by more than one step
            else
                events(j*4-3) = k;    % Store the hopping rate for hopping to the left
            end

            % Calculating the number of nearest-neighbours when moving to the right of gridsite j:
            if (H(j - bj(2)*N + sqN) - H(j)) > 1;
                events(j*4-2) = 0;          % Molecules are not allowed to move up by more than one step
            else
                events(j*4-2) = k;    % Store the hopping rate for hopping to the right
            end

            % Calculating the number of nearest-neighbours when moving one place up gridsite j:
            if (H(j + bj(3)*sqN - 1) - H(j)) > 1;
                events(j*4-1) = 0;          % Molecules are not allowed to move up by more than one step
            else
                events(j*4-1) = k;    % Store the hopping rate for hopping to the position above j
            end

            % Calculating the number of nearest-neighbours when moving one place down gridsite j:
            if (H(j - bj(4)*sqN + 1) - H(j)) > 1;
                events(j*4) = 0;            % Molecules are not allowed to move up by more than one step
            else
                events(j*4) = k;    % Store the hopping rate for hopping to the position below j
            end
        end
    end


elseif m == 3;                  % If m == 3, the molecule moves one position up
    H(i) = H(i) - 1;
    H(i + b(5)*sqN - 1) = H(i + b(5)*sqN - 1) + 1;

    % Updating the surface material for the site  i
    if (H(i) == 0) || (H(i) == hght && ismember(i,indI) == 1);
        events((i*4-3):i*4) = 0;
    else                    % 'else' means here that the concerning gridsite i is not part of the substrate
        if H(i) == 1;
            Es(i) = EsD;
        elseif H(i) == (hght + 1) && ismember(i,indI) == 1;   % If the concerning molecule is the first
                  molecule on a SrRuO3 island, the energy barrier of the ferroelectric with SrRuO3 is activated.
            Es(i) = EsS;
        else     % 'else' means here that the concerning molecule is at least the second one on the substrate
            Es(i) = EsF;
        end
    end

    % Updating the surface material for the site (i - b(3)*N + sqN)
    if H(i + b(5)*sqN - 1) == 1;
        Es(i + b(5)*sqN - 1) = EsD;
    elseif H(i + b(5)*sqN - 1) == (hght + 1) && ismember((i + b(5)*sqN - 1),indI) == 1;   % If the concerning
              molecule is the first molecule on a SrRuO3 island, the energy barrier of the ferroelectric with
              SrRuO3 is activated.
        Es(i + b(5)*sqN - 1) = EsS;
    else      % 'else' means here that the concerning molecule is at least the second ferroelectric in its row
```

```
            Es(i + b(5)*sqN - 1) = EsF;
        end


        v1 = [(i) (i - sqN - 1 + b(1)*N + b(5)*sqN)  (i - sqN  + b(1)*N)  (i - 2 + (b(6) + b(5))*sqN) (i - 1 +
                                    b(5)*sqN)  (i + 1 - b(7)*sqN)  (i + sqN - 1 - b(3)*N + b(5)*sqN) (i + sqN -
                                    b(3)*N)];

        % Calculating the number of nearest-neighbours for 8 gridsites of v1:
        for j = v1;
            if (H(j) == 0) || (H(j) == hght && ismember(j,indI) == 1);
                events((j*4-3):j*4) = 0;
            else                        % 'else' means here that the concerning gridsite j is not part of the substrate
                % Calculating the number of nearest-neighbours for gridsite j:
                bj = zeros(1,4);
                for q = 1:4;
                    if ismember(j,border(2*q-1,:)) == 1;
                        bj(q) = 1;
                    end
                end
                n(j) = 0;
                if H(j + bj(1)*N - sqN) >= H(j);    % Check for nearest-neighbours on the left of j
                    n(j) = n(j) + 1;
                end
                if H(j - bj(2)*N + sqN) >= H(j);    % Check for nearest-neighbours on the right of j
                    n(j) = n(j) + 1;
                end
                if H(j + bj(3)*sqN - 1) >= H(j);    % Check for nearest-neighbours above j
                    n(j) = n(j) + 1;
                end
                if H(j - bj(4)*sqN + 1) >= H(j);    % Check for nearest-neighbours below j
                    n(j) = n(j) + 1;
                end
                k = k0*exp(-(Es(j)+n(j)*En)/(kB*T));

                % Calculating the number of nearest-neighbours when moving to the left of gridsite j:
                if (H(j + bj(1)*N - sqN) - H(j)) > 1;
                    events(j*4-3) = 0;          % Molecules are not allowed to move up by more than one step
                else
                    events(j*4-3) = k;          % Store the hopping rate for hopping to the left
                end

                % Calculating the number of nearest-neighbours when moving to the right of gridsite j:
                if (H(j - bj(2)*N + sqN) - H(j)) > 1;
                    events(j*4-2) = 0;          % Molecules are not allowed to move up by more than one step
                else
                    events(j*4-2) = k;          % Store the hopping rate for hopping to the right
                end

                % Calculating the number of nearest-neighbours when moving one place up gridsite j:
                if (H(j + bj(3)*sqN - 1) - H(j)) > 1;
                    events(j*4-1) = 0;          % Molecules are not allowed to move up by more than one step
                else
                    events(j*4-1) = k;          % Store the hopping rate for hopping to the position above j
                end

                % Calculating the number of nearest-neighbours when moving one place down gridsite j:
                if (H(j - bj(4)*sqN + 1) - H(j)) > 1;
                    events(j*4) = 0;            % Molecules are not allowed to move up by more than one step
                else
                    events(j*4) = k;            % Store the hopping rate for hopping to the position below j
                end
            end
        end

    else                                    % If m == 0, the molecule moves one position down
        H(i) = H(i) - 1;
        H(i - b(7)*sqN + 1) = H(i - b(7)*sqN + 1) + 1;

        % Updating the surface material for the site i
        if (H(i) == 0) || (H(i) == hght && ismember(i,indI) == 1);
            events((i*4-3):i*4) = 0;
        else                    % 'else' means here that the concerning gridsite i is not part of the substrate
            if H(i) == 1;
                Es(i) = EsD;
            elseif H(i) == (hght + 1) && ismember(i,indI) == 1;   % If the concerning molecule is the first
                    molecule on a SrRuO3 island, the energy barrier of the ferroelectric with SrRuO3 is activated.
                Es(i) = EsS;
            else     % 'else' means here that the concerning molecule is at least the second one on the substrate
                Es(i) = EsF;
            end
        end

        % Determination of the surface material for the site (i - b(7)*sqN + 1)
        if H(i - b(7)*sqN + 1) == 1;
```

```
            Es(i - b(7)*sqN + 1) = EsD;
        elseif H(i - b(7)*sqN + 1) == (hght + 1) && ismember((i - b(7)*sqN + 1),indI) == 1;   % If the concerning
                molecule is the first molecule on a SrRuO3 island, the energy barrier of the ferroelectric with
                SrRuO3 is activated.
            Es(i - b(7)*sqN + 1) = EsS;
        else    % 'else' means here that the concerning molecule is at least the second ferroelectric in its row
            Es(i - b(7)*sqN + 1) = EsF;
        end


        v1 = [(i) (i - sqN  + b(1)*N)  (i - sqN + 1 + b(1)*N - b(7)*sqN)  (i - 1 + b(5)*sqN)  (i + 1 - b(7)*sqN)
                                    (i + 2 - (b(8) + b(7))*sqN) (i + sqN - b(3)*N)  (i + sqN + 1 - b(3)*N -
                                    b(7)*sqN)];

        % Calculating the number of nearest-neighbours for 8 gridsites of v1:
        for j = v1;
            if (H(j) == 0) || (H(j) == hght && ismember(j,indI) == 1);
                events((j*4-3):j*4) = 0;
            else                        % 'else' means here that the concerning gridsite j is not part of the substrate
                % Calculating the number of nearest-neighbours for gridsite j:
                bj = zeros(1,4);
                for q = 1:4;
                    if ismember(j,border(2*q-1,:)) == 1;
                        bj(q) = 1;
                    end
                end
                n(j) = 0;
                if H(j + bj(1)*N - sqN) >= H(j);    % Check for nearest-neighbours on the left of j
                    n(j) = n(j) + 1;
                end
                if H(j - bj(2)*N + sqN) >= H(j);    % Check for nearest-neighbours on the right of j
                    n(j) = n(j) + 1;
                end
                if H(j + bj(3)*sqN - 1) >= H(j);   % Check for nearest-neighbours above j
                    n(j) = n(j) + 1;
                end
                if H(j - bj(4)*sqN + 1) >= H(j);   % Check for nearest-neighbours below j
                    n(j) = n(j) + 1;
                end
                k = k0*exp(-(Es(j)+n(j)*En)/(kB*T));

                % Calculating the number of nearest-neighbours when moving to the left of gridsite j:
                if (H(j + bj(1)*N - sqN) - H(j)) > 1;
                    events(j*4-3) = 0;          % Molecules are not allowed to move up by more than one step
                else
                    events(j*4-3) = k;    % Store the hopping rate for hopping to the left
                end

                % Calculating the number of nearest-neighbours when moving to the right of gridsite j:
                if (H(j - bj(2)*N + sqN) - H(j)) > 1;
                    events(j*4-2) = 0;          % Molecules are not allowed to move up by more than one step
                else
                    events(j*4-2) = k;    % Store the hopping rate for hopping to the right
                end

                % Calculating the number of nearest-neighbours when moving one place up gridsite j:
                if (H(j + bj(3)*sqN - 1) - H(j)) > 1;
                    events(j*4-1) = 0;          % Molecules are not allowed to move up by more than one step
                else
                    events(j*4-1) = k;    % Store the hopping rate for hopping to the position above j
                end

                % Calculating the number of nearest-neighbours when moving one place down gridsite j:
                if (H(j - bj(4)*sqN + 1) - H(j)) > 1;
                    events(j*4) = 0;            % Molecules are not allowed to move up by more than one step
                else
                    events(j*4) = k;    % Store the hopping rate for hopping to the position below j
                end
            end
        end
    end
end
    tau     = tau + (1 / L);   % Update of the 'time' passed since the last deposition pulse
end
```